2022

Performance Analysis in Full-Duplex Relaying Systems withWireless Power Transfer

Jiaman Li

UNIVERSITY
OF WOLLONGONG
AUSTRALIA

Performance Analysis in Full-Duplex Relaying Systems with Wireless Power Transfer

Jiaman Li

This thesis is presented as part of the requirements for the conferral of the degree:

Doctor of Philosophy

Supervisors:
A/Prof. Le Chung Tran

Co-supervisor:
Prof. Farzad Safaei

The University of Wollongong
School of Electrical, Computer and Telecommunications Engineering

February, 2022

This research has been conducted with the support of an Australian Government Research Training Program Scholarship.

Declaration

I, *Jiaman Li*, declare that this thesis is submitted in partial fulfilment of the requirements for the conferral of the degree *Doctor of Philosophy*, from the University of Wollongong, is wholly my own work unless otherwise referenced or acknowledged. This document has not been submitted for qualifications at any other academic institution.

Jiaman Li

February 18, 2022

Abstract

Energy harvesting (EH) technology has become increasingly attractive as an appealing solution to provide long-lasting power for energy-constrained wireless cooperative sensor networks. EH in such networks is particularly important as it can enable information relaying. Different from absorbing energy from intermittent and unpredictable nature, such as solar, wind, and vibration, harvesting from radio frequency (RF) radiated by ambient transmitters has received tremendous attention. The RF signal can convey both information and energy at the same time, which facilitates the development of simultaneous wireless information and power transfer. Besides, ambient RF is widely available from the base station, WIFI, and mobile phone in the current information era. However, some open issues associated with EH are existing in the state-of-art. One of the key challenges is rapid energy loss during the transferring process, especially for long-distance transmission. The other challenge is the design of protocols to optimally coordinate between information and power transmission.

Meanwhile, in-band full-duplex (IBFD) communication have gained considerable attraction by researchers, which has the ability to improve system spectral efficiency. IBFD can receive information and forward information at the same time on the same frequency. Since the RF signal can be superimposed, the antenna of the IBFD system receives the RF signal from both desired transmitter and local transmitter. Due to the short distance of the local transmission signals, the received signal power is much larger than the desired transmission signals, which results in faulty receiving of the desired signals. Therefore, it is of great significance to study the local self-interference cancellation method of the IBFD system. In the recent state-of-art, three main types of self-interference cancellations are researched, which are passive cancellations, digital cancellations, and analog

cancellations. In this thesis, we study polarization-enabled digital self-interference cancellation (PDC) scheme in IBFD EH systems which cancels self-interference by antenna polarization (propagation domain) and digital processing (digital domain).

The theme of this thesis is to address the following two questions: how the self-interference would be canceled in the IBFD EH system and how to optimize key performances of the system to optimal system performances. This thesis makes five research contributions in the important area of IBFD relaying systems with wireless power transfer. Their applications are primarily in the domains of the Internet of Things (IoT) and 5G-and-beyond wireless networks. The overarching objective of the thesis is to construct analytical system models and evaluate system performance (outage probability, throughput, error) in various scenarios. In all five contributions, system models and analytical expressions of the performance metrics are derived, followed by computer simulations for performance analysis

The first contribution (Chapter 3) is an analysis of an IBFD wireless power transfer system, where the relay wirelessly harvests energy from the source and a single-carrier system is assumed. The impact of both EH and self-interference cancellation on the throughput and on the error performance of the system is evaluated. Our simulation results show that the IBFD EH relaying system almost doubles the system throughput, compared to the half-duplex (HD) EH relaying system, at the cost of about 5 dB inferior error performance. We also show that to achieve a high throughput along with a good error performance in the IBFD EH relaying system, a combined selection of a high transmit SNR and a suitable EH duration is required.

The second contribution (Chapter 4) is an analysis of an extended model from Chapter 3 where multi-carrier orthogonal frequency division multiplexing (OFDM) is assumed instead. The impact of the number of OFDM sub-bands and the number of multipath on the system performance of the whole OFDM band is studied. Our simulation results show that the IBFD OFDM energy harvesting relaying system almost doubles the throughput while maintaining the same bit error performance by a modest increase in the signal-to-noise ratio compared to the HD OFDM energy harvesting relaying system. It is also

revealed that the optimal time splitting factor should be less than 0.3 to maximize the IBFD system throughput.

The third contribution (Chapter 5) is an analysis of a model similar to that considered in Chapter 4, but at the OFDM sub-band level. The outage probability and throughput are formulated in two different methods which aim to show the trade-off between accuracy, especially at low signal-to-noise ratios, and the computational simplicity of the two methods. Our analysis and simulation results show that the throughput of the system is greatly improved, approaching twice as the traditional HD system.

The fourth contribution (Chapter 6) considers that the source (rather than the relay) harvests energy and analyzes the performance in terms of outage probability and throughput. This system is practical in some wireless sensor network settings, such as the scenarios mentioned in Section 2.3.3 in Chapter 2. With the assistance of the relay, the source node can consume a small amount of energy to transmit information to a distant destination. We investigate the influences of dissimilarity between the polarization states of the antennas on the PDC cancellation effect. The results show that the system throughput is maximized when the polarization states are orthogonal. Besides, we provide the analysis of outage probability and throughput of an IBFD relaying system and two HD relaying systems. The first HD system has the same EH duration as the IBFD system while the second HD one has the same transmitting power from the source as the IBFD one. The results show that the IBFD system can double the system throughput while having the outage probability as low as that of the first HD system, at a cost of adopting the PDC scheme. Meanwhile, the IBFD system can nearly double the system throughput while having the outage probability superior to that of the second HD system.

The fifth contribution (Chapter 7) considers a self-energy recycling relay system and analyzes the throughput and power consumption of the system. The analytical characterization of throughput in the self-energy recycling system is provided and compared with the non-recycling system. The results reveal that, with energy recycling, the consumed power in the system can be saved by 80% to achieve the same level of throughput within a small-to-medium relay-to-destination distance. Besides, the recycling architecture can

boost the system throughput to 1.61 times higher than that of the non-recycling system using the same amount of total consumption power.

The thesis has a considerable contribution to the research field to understand better the performance of the IBFD EH relaying system in different settings in both flat fading and frequency selective fading scenarios.

Acknowledgments

First, I would like to express my deepest gratitude to my principal supervisor A/Prof. Le Chung Tran, and co-supervisor Prof. Farzad Safaei for their patient guidance, enthusiastic encouragement, and valuable suggestions. I sincerely appreciate their advice and assistance in keeping my progress on schedule. During the four and a half years, I have learned the methodology to carry out the research and to present the research works as clearly as possible, which not only helped me to publish papers but also benefited me in the future. It was a great honor to study under their supervision.

I would like to offer my special thanks to the School of Electrical, Computer and Telecommunications Engineering, University of Wollongong. It awarded me the International Postgraduate Tuition Awards (IPTA) and University Postgraduate Award (UPA). Thanks to the financial support of the University of Wollongong, I can concentrate on my research.

I am particularly grateful for the assistance given by my boyfriend Mr. Yiwei Huang. Without his help in my daily life and encouragement in the study, it would be impossible for me to complete my degree.

Finally, I would like to thank my parents Mr. Linmou Li and Mrs. Yan Song for their support and encouragement throughout my study. It is them giving me an opportunity to study overseas and pursuing what I want.

Contents

List of Figures

List of Tables

List of Abbreviations

16-PSK	16 Phase-Shift Keying
ADC	Analog-to-Digital Converter
AF	Amplify-and-Forward
ALMS	Analog Least Mean Square
AWGN	Addictive White Gaussian Noise
BER	Bit Error Rate
BPSK	Binary Phase-Shift Keying
BS	Base Station
CDF	Cumulative Distribution Function
CP	Cyclic Prefix
CSI	Channel State Information
DAC	Digital-to-Analog Converter
DF	Decode-and-Forward
DOA	Direction-of-Arrival
DOD	Direction-of-Departure
EH	Energy Harvesting
EM	Electromagnetic
FD	Full-Duplex
FFT	Fast Fourier Transform
HD	Half-Duplex

I/Q	In-Phase/Quadrature-Phase
IBFD	In-Band Full-Duplex
ICI	Inter-Carrier Interference
IFD	Ideal Full-Duplex
IFFT	Inverse Fast Fourier Transform
ISI	Inter-Symbol Interference
IT	Information Transmission
LMS	Least Mean Square
LNA	Low Noise Amplifier
LS	Least Squares
MIMO	Multiple Input Multiple Output
MMSE	Minimum Mean Square Error
MRC	Maximum Ratio Combining
NER	Non-Energy Recycling
NLMS	Normalized Least Mean Square
OFDMA	Orthogonal Frequency Division Multiple Access
OFDM	Orthogonal Frequency Division Multiplexing
PA	Power Amplifier
PDC	Polarization-Enabled Digital Self-Interference Cancellation Scheme
PDF	Probability Density Function
PSR	Power-Splitting Based Relaying
QPSK	Quadrature Phase-Shift Keying
R-D	Relay-to-Destination
R-S	Relay-to-Source
RF	Radio Frequency

S-D	Source-to-Destination
S-R	Source-to-Relay
SER	Self-Energy Recycling
SIC	Self-Interference Cancellation
SI	Self-Interference
SNR	Signal-to-Noise Ratio
SWIPT	Simultaneous Wireless Information Transmission and Power Transfer
TSR	Time-Switching Based Relaying
UAV	Unmanned Aerial Vehicle
WPT	Wireless Power Transfer

Chapter 1

Introduction

1.1 Background and Objectives

In the recent era, the volume of data is growing significantly, and data interaction faces severe challenges in terms of speed. Regardless of the transmission of TB-level large files or massive small files, information transmission with low latency and high throughput is increasingly pursued. In a wireless network, to meet this challenge, the following two ways are used in industry. The first approach is to increase the system capacity by increasing the spectrum resources. The second approach is to improve the system throughput by increasing the spectrum efficiency. Considering the scarcity of spectrum resources and the high cost of increasing spectrum resources, it is an effective solution to improve network bandwidth utilization to increase transmission speed. This thesis focuses on researching in-band full-duplex technology to improve system spectral efficiency. For simplicity, in this chapter, we use full-duplex (FD) to represent in-band full-duplex (IBFD).

Cooperative communication is indispensable in wireless communication systems. In a shadowing propagation environment, the source may have to rely on the assistance of other nodes to forward information to the destination. Thus, relaying networks are necessary and their characteristics are important to investigate. Some literature consider the half-duplex (HD) communication system which allows the transceiver to communicate in both directions on the same frequency, but not simultaneously. It means that once a transceiver begins to transmit signals, it cannot receive information from other nodes. Differently, FD communication can improve spectral efficiency by allowing transceivers

to transmit and receive signals at the same time on the same frequency. Therefore, FD systems have attracted significant attention from researchers and have become a hot research field in wireless communication in recent years. However, the challenge of implementing the FD lies in canceling the self-interference (SI) signal. This interference occurs in the FD communication when a transceiver is transmitting and receiving simultaneously. It is because that the double direction communication in FD systems uses the same frequency, thus the transmitting and receiving signals are mixed. Typically, for a transceiver, its own transmitted signal will also be received by itself, which will damage the desired signal from the far end. In this situation, the transmitted signal is regarded as SI for the mentioned transceiver, which usually overwhelms the desired signal received from the far-end. The SI dictates the overall throughput of the FD system. The system throughput significantly degrades, which is even worse than that of the HD system if the interference is not sufficiently canceled. Hence, self-interference cancellation (SIC) techniques are often deployed to enable the FD communication.

Contemporarily, through various information sensors, things are connected, and the application field of the Internet of Things (IoT) system involves all aspects. One of the important issues of IoT is how to charge these wireless devices for their normal operation. The traditional method of replacing the battery is very inconvenient. In some extreme conditions, it is even impossible to replace the battery. In addition, the replacement of the battery is prone to waste of resources and environmental pollution. Therefore, it is of great significance to study wireless energy and power transmission. Wireless energy harvesting (EH) is a hot research topic that has the advantages of extending the lifetime of energy-constrained wireless networks and avoiding frequent battery replacement. Thus, in this project, the FD communication for cooperative wireless networks with wireless power transfer (WPT) is researched to facilitate the development of FD in IoT and 5G-and-beyond wireless networks. The primary research objectives are listed as follows.

- To achieve the FD relaying networks with WPT, the biggest challenge is handling the SI. To cancel the SI, SIC techniques can be applied in the propagation domain, analog domain, and digital domain. This thesis will adopt a digital cancellation

scheme associated with antenna polarizations in the propagation domain to cancel the SI.

- The literature of the FD relaying systems with WPT is far from being mature. Their performance analyses are still insufficiently in-depth. Thus, in this thesis, the throughput and bit error rate (BER) of both single-carrier systems and multi-carrier systems will be investigated. Simulation results and analyses will be illustrated with the objective of understanding thoroughly the potential and maximum ability of the FD-WPT relaying networks.
- The thesis also aims at proposing a new FD relaying system with an EH-enabled source to improve system coverage and throughput. The analytical expressions of the outage probability and throughput are derived to verify the simulation results.
- Energy efficiency is also an important aspect in the EH systems. Thus, the thesis aims to propose a self-energy recycling system to improve the overall energy efficiency of the system.

1.2 Research Approaches

The flow chart of the research approaches is illustrated in Fig. 1.1. The research starts with the review of the related research areas, which includes the HD and FD transmissions, cooperative networks, WPT mechanisms, SIC approaches, and self-energy recycling (SER) mechanisms. Motivated by the literature, we identify open research problems and determine the primary research objectives. The key challenges of EH are rapid energy loss during the transferring process especially for long-distance transmission and the design of protocols to optimally coordinate between information and power transmission. The key challenge of FD transmission is cancelling SI signals. To address these concerns, this thesis focuses on investigating the performance, i.e., outage probability, throughput, and BER, of FD relaying systems with wireless power transfer.

The thesis first considers an FD EH, a single-carrier system for flat fading channels, followed by an orthogonal frequency division multiplexing (OFDM) system for multipath

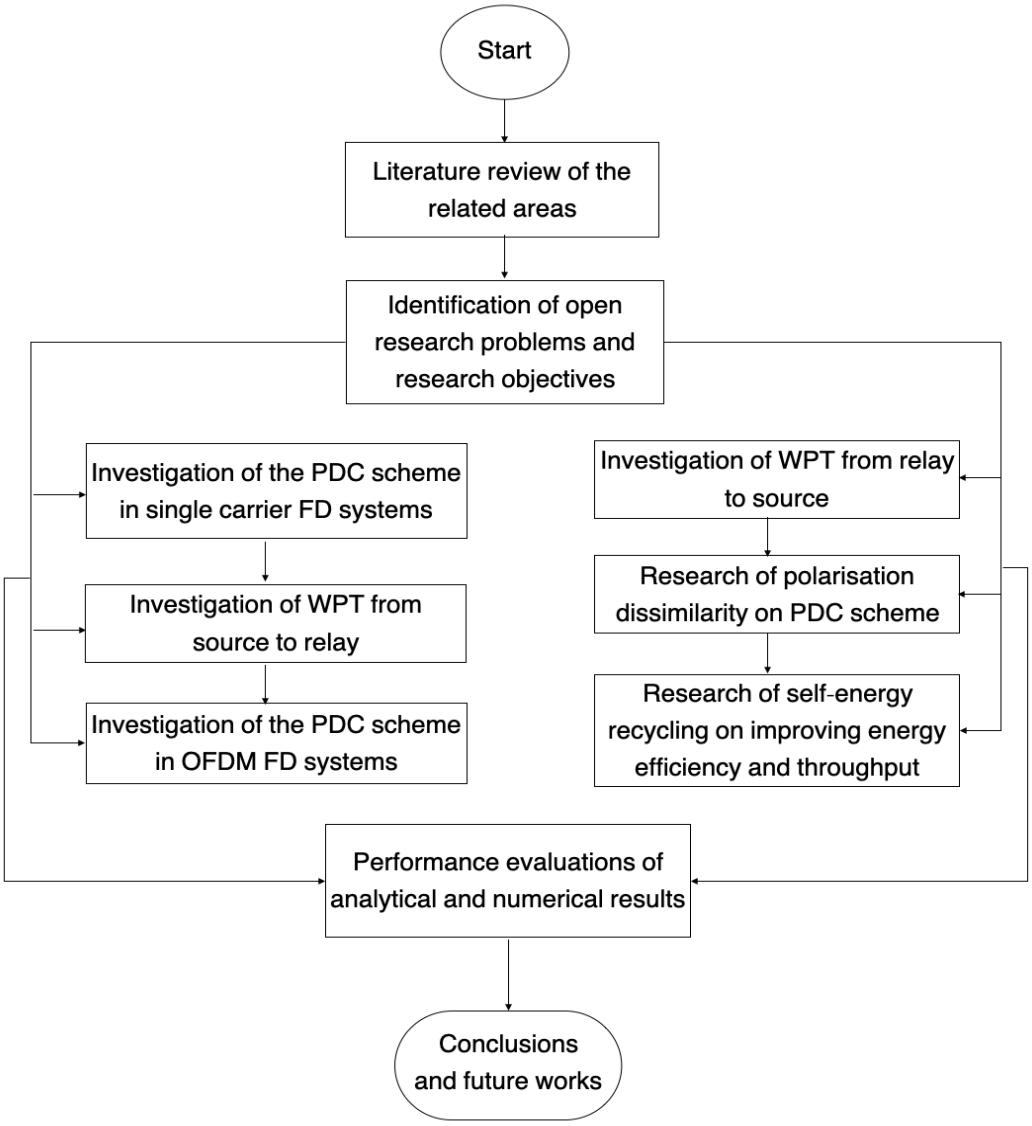

Figure 1.1: The flow chat of research approaches.

fading channels. It considers EH at the relay, followed by the EH at the source, and then the SER at the relay alongside the EH at the source. In all cases, the performance of the proposed system is compared with the HD or non-energy recycling counterpart. The performance evaluations of analytical and simulation results are detailed to elaborate our discussions.

1.3 Contributions of the Thesis

The main contributions of this thesis are summarized as follows.

1. Adaptation of the PDC scheme to deploy in both single-carrier and OFDM FD relaying systems with WPT from the source to the relay.

   The PDC scheme effectively eliminates the SI signal and suppresses a part of the noise in both single-carrier Rayleigh flat fading channels and OFDM multipath frequency selective fading channels. Simulation results of these two systems are provided and compared to the HD EH relaying system. The PDC scheme does not require knowledge of the instantaneous CSI of the SI channels. Therefore, the complexity and overhead of the FD system are reduced.

2. Derivation of the analytical expressions of the outage probability and the system throughput in two different methods in the OFDM FD EH relaying systems.

   The optimal time split between the EH and information exchange phases to maximize the system throughput is calculated numerically. At a high transmit SNR, we simplify the expressions of the outage probability and the system throughput to obtain the corresponding asymptotic lines. By comparing the FD and HD relaying architectures, the thesis demonstrates that FD relaying can boost significantly the system throughput in many cases.

3. Development of a two-hop FD relaying system with the WPT from the relay to the source.

   The mathematical expressions of the outage probability and throughput are presented. Besides, we research the influence of the dissimilarity between the polar-

ization states of the relay antennas on the cancellation effect of the PDC scheme. It reveals that when the dissimilarity factor is 1 (i.e., polarization states are orthogonal), the PDC scheme can suppress best interference and noise. However, even the dissimilarity factor is smaller, the FD relaying can still boost significantly the system throughput in various scenarios.

4. Proposal of a two-hop PDC-based FD-SER system with EH capabilities at both the source node and the relay node.

   The trade-off between the proposed system and the FD non-energy-recycling (NER) one (i.e., the system proposed in the point 3 mentioned above), using the same total consumption power, is examined. It is revealed that, with energy recycling, the consumed power in the system can be saved by up to 80% to achieve the same level of throughput in the non-recycling system for a small-to-medium distance range between the source and the destination. Alternatively, the proposed FD-SER system can boost the system throughput by 1.61 times, compared to the non-recycling counterpart using the same amount of total consumption power.

1.4 Outline of the Thesis

This thesis includes 8 chapters as outlined in the following.

In Chapter 1, the research background and objectives of this thesis are first discussed. Then, we elaborate on the research approaches, followed by the main contributions of the thesis, the outline of the thesis, and our publications.

In Chapter 2, the background information and the state of the art related to our researches are discussed, which include cooperative networks, wireless energy harvesting, FD communication, self-interference cancellations, and SER techniques.

In Chapter 3, the performance evaluation, i.e., throughput and BER, of a single-carrier FD relaying system with the radio frequency (RF) WPT from the source to the relay is discussed. Besides, the working principles and properties of the PDC scheme are explained in this chapter. We quantify the impact of the EH and PDC scheme on the throughput and

BER performance of the FD EH relaying system in comparison with the HD EH relaying system.

In Chapter 4, the performance of a PDC-based FD OFDM relaying system with the WPT from the source to the relay in multipath fading channels is investigated. The simulation results of throughput and BER of this system are then presented.

In Chapter 5, a two-hop PDC-based FD OFDM relaying network, where the relay operates based on a time-switching architecture to harvest energy from the RF signals, is considered. We provide a comprehensive analysis of the system performances in terms of the outage probability and throughput over multipath Rayleigh fading channels. The analytical expressions of the outage probability and throughput are derived in two different approaches. Besides, we also derive the asymptotic approximations to simplify the expressions of outage probability and throughput at a high transmit SNR.

In Chapter 6, we investigate a two-hop PDC-based FD communication system in which the source utilizes the RF EH for the transmission of information. Besides, the influence of the polarization dissimilarity factor of the antennas on the system throughput is investigated.

In Chapter 7, a PDC-based FD relaying network with an EH-enabled source and a SER-enabled relay is proposed. In-depth analyses and comparisons of the system throughput of the proposed system with that of the non-recycling system, presented in Chapter 6, are presented.

In Chapter 8, we present the summaries of this thesis and discuss possible future works.

1.5 Publications

This thesis is based on the following five papers, which have been published as three journal papers at the IEEE Access – a high standard journal in this discipline, and two conference papers.

Journal Papers

1. J. Li, L. C. Tran, and F. Safaei, "Wireless information and power transfer using full-duplex self-energy recycling relays," *IEEE Access*, vol. 9, pp. 158808–158819, Nov. 2021.

   – The contents of this publication are included in Chapter 7.

2. J. Li, L. C. Tran, and F. Safaei, "Throughput analysis of in-band full-duplex transmission networks with wireless energy harvesting enabled sources," *IEEE Access*, vol. 9, pp. 74989–75002, May 2021.

   – The contents of this publication are included in Chapter 3 and 6.

3. J. Li, L. C. Tran, and F. Safaei, "Outage probability and throughput analyses in full-duplex relaying systems with energy transfer," *IEEE Access*, vol. 8, pp. 150150–150161, Aug. 2020.

   – The contents of this publication are included in Chapter 3 and 5.

Conference Papers

1. J. Li, L. C. Tran, and F. Safaei, "Full-duplex OFDM relaying systems with energy harvesting in multipath fading channels," in *Proc. IEEE VTC2019- Fall*, Honolulu, HI, USA, Sep. 2019, pp. 1–5.

   – The contents of this publication are included in Chapter 4.

2. J. Li, L. C. Tran, and F. Safaei, "Performance evaluation of full-duplex energy harvesting relaying networks using PDC self-interference cancellation," in *Proc. IEEE ICSPCS*, Cairns, QLD, Australia, Dec. 2018, pp. 1–6.

   – The contents of this publication are included in Chapter 3.

Chapter 2

Literature Review

2.1 Cooperative Networks

Relay-assisted cooperative communication has been proposed in the literature to expand the transmission coverage [1]–[10]. So, a deep understanding of what cooperative communication is and how its models are constructed is significantly important. Cooperative communication is different from conventional point-to-point communication. Its transmissions from the source to the destination depend on the help of relays. As illustrated in Fig. 2.1, signals are transmitted from the base station (BS) to users through relays.

Since the core idea of relay-assisted cooperative networks is to expand the communication range from the source to the destination, most works in the literature, such as [11]–[13], have researched relaying systems without a direct link between the source and the destination. This assumption is applicable to the situations where the distance between the source and the destination is large so that the destination is not within the coverage area of the source or where the direct link is heavily shadowed by obstructions. In cooperative communication, the two most commonly used relaying protocols include the amplify-and-forward (AF) relaying protocol and the decode-and-forward (DF) relaying protocol. Their main difference is the signal processing manner of the relay nodes. In the AF protocol, the relay node amplifies the received signal from the source and then forwards to the destination [12], [14]–[18] while the DF protocol decodes the received signal at the relay before forwarding it to the destination [11], [16], [17], [19], [20].

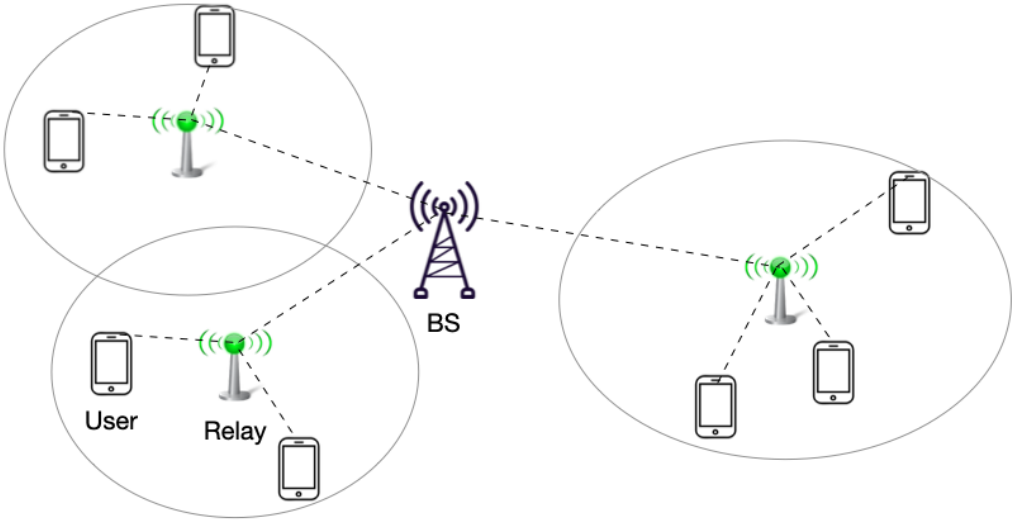

Figure 2.1: Illustration of a wireless cooperative network.

2.2 IBFD Communication

Currently, the HD for wireless communication is relatively mature while FD is still under development. In the HD transmission, data can be transmitted in both directions on one carrier, but not at the same time. Specifically, the HD relaying system consists of one-way transmission and bidirectional transmission. A single node in a one-way transmission system is either transmitting or receiving the data, but it can switch between the role of a transmitter and a receiver in a bidirectional mode. The authors in [21] research the HD communication where the source node broadcasts its information to both the relay and the destination. The relay node then uses an auxiliary channel to forward the same information to the destination. In this case, the end-node receives duplicated versions of transmitted packets. This specific system benefits significantly when the source-to-destination channel is very bad. The paper also provides symbol error rate analysis of both DF and AF protocols. The limitation of [21] is that the system ignores the path loss effect during signal transmission. In fact, it is usually the case that the transmit signal experiences an obvious path loss, especially for a long-distance transmission from the source to the destination. To overcome this problem, the path loss is considered in [14], [22], where the path loss is related to the transmission distance and the path loss exponent.

The HD relaying architecture is widely used in conventional wireless networks due to its simpler system design. However, HD transmission leads to a loss of spectrum efficiency because a transceiver cannot transmit and receive signals at the same time.

In contrast, IBFD communication allows simultaneous transmission and reception in the same frequency band, which possesses multiple advantages. The IBFD wireless communication systems can mainly be classified into end-to-end bi-directional systems and cooperative systems, which have the potential of double the spectral efficiency, compared to the HD system [23]. The results in [24] show that the channel capacity of the FD system is nearly doubled even with the phase noise of the oscillator. Besides, in relay systems, transmission delay in the end-to-end system can be reduced by the FD transmission [25]. In [16], the throughput performance and the optimal time splitting in the FD relaying system with wireless power transfer for single-carrier communication systems are studied. In [17], a partial relay selection scheme is proposed to implement FD transmission, where the best relay is selected based on the maximum SNR of the received information signal at the relay. However, these works neither consider multipath frequency-selective fading channels nor any specific SIC method. The work in [26] simulates the throughput and BER performances of an FD EH relaying system in comparison with those of an HD EH relaying system. It considers flat-fading channels with a single carrier system. The authors in [27] derive the analytical expressions of outage probability and throughput for a multi-carrier system and frequency selective fading channels. In [28], a joint antenna and relay selection technology in one-source, one-destination, and multiple-AF relay networks is proposed. The relays work in an FD mode, and each relay has two antennas where one for transmission and the other for reception. The optimal relay is jointly selected according to the instantaneous channel conditions. Besides, each activated relay can also choose certain transmit and receive antennas to optimize the performance of the system. Therefore, this proposed scheme has the merit of increasing the degree of freedom and providing better performances than the conventional relay selection scheme. However, it has a performance floor at a high SNR because of the existence of SI in the FD relaying system [28]. This means that although IBFD communication is an impor-

tant technique to improve system throughput by concurrent transmission and reception in the same band [29], [30], SIC schemes must be included to recover the desired signal. A comprehensive SIC solution includes three stages, which occur in the propagation domain, analog domain, and digital domain. The SIC schemes in each domain have been extensively researched in the literature.

2.3 Wireless Energy Harvesting

In the previous part, the cooperative communication is discussed. The conventional energy-constrained wireless networks, such as wireless sensor networks, have a limited lifetime. For the energy-limited sensors, recharging or replacing batteries is periodically performed to sustain network operations, which is costly, time-consuming, and sometimes infeasible due to some physical limitations, such as hazardous environments [31]. Wireless EH techniques provide a solution to realize the long-term operation of the sensors in this kind of scenarios. Some preliminary works [32]–[34] rely on natural energy sources, such as solar, wind, and thermoelectric effects to provide EH. However, these sources cannot be easily controlled and often intermittent. Recently, EH techniques using RF signals and electromagnetic (EM) induction to achieve energy transfer have attracted significant interest because the man-made RF signal and EM induction can steadily deliver energy to the destination to provide a reliable energy supply. In [35], the authors consider a system with a single transmit antenna and multiple receive antennas, where the energy is transferred to the destination through RF signals. The diversity combining technique is used to improve the EH performance. The works in [36]–[38] propose methods that use the EM induction mechanism to achieve EH, where the EM energy conversion is based on Faraday's law. However, wireless EH from an EM induction usually works in a short distance while RF signals can readily carry both energy and information at the same time to the receiver at distance. Besides, since the information signals are usually RF signals, adopting the RF EH to the conventional wireless networks is easily compatible with the hardware, which makes the system cost-effective [26], [27], [39]–[41]. Thus, the EH from RF signals is an advanced promising method to prolong the lifetime of wireless

communication systems.

2.3.1 EH Relaying Networks

In recent years, the combination of the EH technique with the relay cooperative communication technique is attractive to researchers [42]. In [14], the authors consider an HD system in which the relay transmits and receives information in different time slots over Rayleigh flat-fading channels. They derive the analytical expression of the outage probability and the ergodic capacity to determine the throughput performance and investigate the effect of various system parameters on the performance of wireless EH relaying systems. In [11], a relay selection protocol for EH systems with no direct link between the source and destination is proposed, where the highest energy signal is chosen by the relay for harvesting energy. The system performance in terms of outage probability is researched over Rayleigh fading channels. In [14], the expressions of the ergodic capacity and the outage probability are derived to determine the throughput performance of the HD relay system. In [15], the average throughput is analyzed for the EH cooperative system by considering both continuous-time and discrete-time EH protocols over Rician fading channels. In [18], the non-linear energy harvester at the relay is studied over Nakagami-m fading channels. The work in [19] considers the Nth best-relay selection scheme in EH systems, where the destination selects the relay based on the Nth-order channel gains. The authors evaluate the exact outage probabilities of the time-switching-based relaying (TSR) protocol and the power-splitting-based relaying (PSR) protocol. In [13], the authors investigate the achievable information rate in the MIMO OFDM networks with a wireless powered relay. However, it is worth noting that all these works are limited to the HD mechanism, i.e., the relay node cannot receive and transmit information simultaneously in the same frequency band.

The authors in [43] research the characteristics of HD and FD EH systems with the AF and DF relaying protocols. The system has one source node, one destination node, and one EH relay. It is assumed that there is no direct link between the source and the destination, which means all communication goes through the cooperative relay. The EH relay

node harvests energy from the source-transmitted signal and uses the harvested energy to forward the information to the destination node. The main attribution of [43] is the consideration of FD communication in log-normal fading channels. The log-normal fading statistically characterizes indoor propagation scenarios, shadowing effects in outdoor scenarios, and wide-band channel scenarios [44]. The quasi-static block-fading channel is also usually considered in relay networks [14]. The channel gains are constant within each block but change randomly from one block to another, which are assumed to be independent and identically distributed following the Rayleigh distribution. There are two well-known EH relaying protocols, namely TSR and PSR [14], [43]. The optimal value of the EH time in the TSR protocol and the optimal value of the power splitting ratio in the PSR protocol are investigated in [14] to study the influence of various system parameters. The TSR protocol for EH can be further divided into continuous-time EH and discrete-time EH. In the continuous-time EH, each block consists of an EH part and an information transmission (IT) part. The relay needs to harvest enough amount of energy within each block and uses it to complete the subsequent data transmission processes. In contrast, the discrete-time EH protocol allows each block to be used either for EH or IT. The protocol presets a threshold value. At the beginning of each block, the initial energy E(0) is compared with the threshold. If E(0) is less than the threshold, the relay will work in the EH mode within the whole block. If E(0) is bigger than the threshold at the beginning of the block, the relay starts IT. In summary, the ergodic capacity [43] for delay-tolerant systems, throughput for delay limited systems, energy efficiency, and BER are usually used to quantify the performance of EH systems.

2.3.2 WPT from Sources to Relays

Two commonly used EH cooperative networks include the relaying system with EH relay nodes [14], [16], [17], [27], [45], [46], [54]–[56] and the ones with EH source nodes [47]–[51]. Comparisons of some recent works in the literature are shown in Table 2.1. Chapter 6 of this thesis is also added in this table for comparison. The authors in [14], [16], [17], [27], [45], [46], [56] consider two-hop scenarios with EH relay nodes, of which [14], [45]

Table 2.1: Literature comparison of cooperative communication with EH, where ($\surd$) represents Yes and ($\times$) represents No.

	[14]	[45]	[17]	[16]	[27]	[46]	[47]	[48]	[49]	[50]	[51]	[52]	[53]	Chapter 6
No. of EH nodes	1	1	Multiple	1	1	1	1	2	1	1	1	Multiple	Multiple	1
EH relay	$\surd$	$\surd$	$\surd$	$\surd$	$\surd$	$\surd$	$\times$	$\times$	$\times$	$\times$	$\times$	$\times$	$\times$	$\times$
EH source	$\times$	$\times$	$\times$	$\times$	$\times$	$\times$	$\surd$	$\surd$	$\surd$	$\surd$	$\surd$	$\surd$	$\surd$	$\surd$
Antenna	Single-antenna at S and D; Two-antenna at R	Single-antenna at S and D; Multiple-antennas at R	Single-antenna at S and D; Two-antennas at Rs	Single-antenna at S and D; Two-antennas at R	Orthogonal dual-polarized antenna; Single at S and D and two at R	Single-antenna at S and D; Multiple-antennas at R	Single-antenna at S and D; Two-antennas at R	Single-antenna at S and D; Multiple-antennas at R	N/A	Single-antenna at S, R, and D	Single-antenna at S and D; Two-antennas at R	Single-antenna at S and D; Multiple-antennas at R	Single-antenna at S and D; Multiple-antennas at R	Dual-polarized antenna; Single at S and D and two at R
Transmission mode	HD	HD	IBFD; SWIPT	IBFD; WPT	IBFD; WPT	IBFD; WPT	HD	HD	HD	HD	Out-of-band FD; SWIPT	IBFD; WPT	IBFD; WPT	IBFD; WPT
Channel model	Rayleigh fading channels	Rayleigh fading channels	Rayleigh fading channels	Rayleigh fading channels	Rayleigh fading channels	Rayleigh fading channels	Rayleigh fading channels	Rayleigh fading channels	Constant channel power gains	Rician fading of S-R link; Rayleigh fading of R-D link	Real-valued AWGN channel	Cluster based channel model; One ring channel model	Small-scale fading channels	Rayleigh fading channels
Direct link	No	No	Yes	No	No	No	No	No	With and without	No	No	Yes	Yes	No
Relaying protocol	AF	AF	AF and DF	AF and DF	AF	DF	DF	AF	DF	N/A	DF	N/A	N/A	AF
OFDM	$\times$	$\times$	$\times$	$\times$	$\surd$	$\times$	$\times$	$\times$	$\times$	$\times$	$\times$	$\times$	$\times$	$\times$
SI Channel estimation	$\times$	$\times$	$\times$	$\times$	$\times$	$\surd$	$\times$	$\times$	$\times$	$\times$	$\times$	$\surd$	$\surd$	$\times$
SIC	$\times$	$\times$	$\times$	$\times$	$\surd$	$\surd$	$\times$	$\times$	$\times$	$\times$	$\times$	$\surd$	$\surd$	$\surd$
Antenna selection	$\times$	$\surd$	$\times$	$\times$	$\times$	$\times$	$\times$	$\times$	$\times$	$\surd$	$\times$	$\times$	$\times$	$\times$
Relay selection	$\times$	$\times$	$\surd$	$\times$	$\times$	$\times$	$\times$	$\surd$	$\times$	$\times$	$\times$	$\times$	$\times$	$\times$

deploy the HD mechanism while [16], [17], [27], [46], [56] deploy the FD mechanism. In [14], an HD "harvest-then-transmit" time switching-based relaying protocol is proposed. The throughput is determined by deriving the outage probability and the ergodic capacity for delay-limited and delay-tolerant transmission modes, respectively. In [45], a multiple-antenna relay system with a "harvest-then-transmit" strategy is considered. In the first phase, the relay receives signals from the source where some antennas are used to process information while the remaining antennas are used to harvest energy based on the power splitting protocol. In the second phase, the relay uses the harvested energy to forward signals to the destination. The presented joint power splitting and antenna selection technique outperforms the conventional relay-assisted transmission. However, the deployed HD mode in [14], [45] cannot achieve bi-directional transmission simultaneously in the same frequency band, thus having a low spectral efficiency.

With the advances in signal processing technologies, FD transmission has attracted the interest of researchers, which can transmit and receive information concurrently in the same frequency band. This FD mode is a solution to improve spectral efficiency and decrease transmission delay in the networks. In [17], a two-phase protocol is used to conduct FD transmission in the multi-relay system where the total transmission block time is divided into two subslots equally. In the first subslot, the source node transmits information to relays. Then a suitable relay is selected based on the best instantaneous signal-to-noise ratio (SNR) received from the source. In the second subslot, the chosen relay receives the energy signal from the source and, at the same time, forwards information signals to the destination. The authors in [16], [27] adopt the protocol where a fraction of time is used for harvesting energy and the remaining time is used for FD information transmission. The authors in [16] consider a single-carrier system while the authors in [27] consider a multi-carrier system and adopt the polarization-enabled digital cancellation scheme with orthogonal polarization states to cancel SI signals. However, the works in [14], [16], [17], [27], [45] consider that the source has its own power supply and does not need EH.

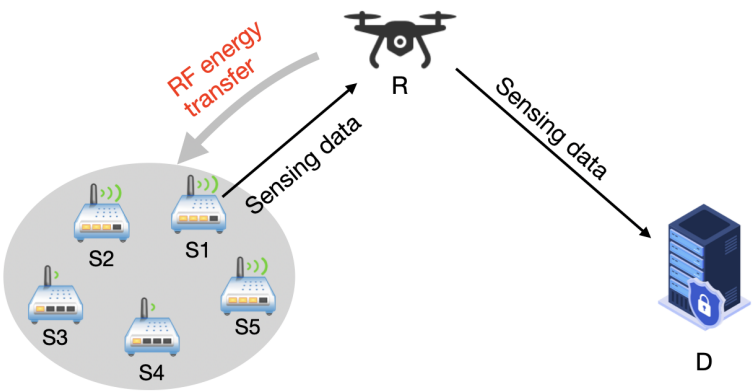

Figure 2.2: An unmanned aerial vehicle assisted sensor network with EH sources.

2.3.3 WPT from Relays to Sources

The two-hop relaying system where the energy-limited relay relies on the energy harvested from RF signals to transmit information to the destination usually has a short communication range. This is because of two main reasons. Firstly, the source-relay distance is limited due to the path loss from the source to the relay and the available transmitting power at the source. The RF energy emitted from the WPT transmitter is always attenuated severely when it propagates toward the relay due to the high path loss [57]. Secondly, the relay-destination distance is constrained by the path loss from the relay to the destination and the harvested energy at the relay [58]. This means that the inadequate energy at the relay restricts further the transmission distance. Thus, the system throughput decreases significantly for a long-distance transmission. The relay-assisted system with an EH-capable source and a relay powered by a fixed and perpetual power supply is less reliant on the distance [58]. Such a system is preferred in many practical scenarios, such as the ones shown in Figs. 2.2 and 2.3. In Fig. 2.2, an unmanned aerial vehicle (UAV) works as a relay that transfers RF energy to nearby sensors $S_1 - S_5$ and then relays the sensing data, e.g., position, temperature, or timing, from the sources to the destination. Fig. 2.3 shows the scenario that an energy-limited source is placed within a tunnel. The unsafe environment in the tunnel leads to the difficulty of replacing its battery. An EH source system can ensure its proper operations, and with the assistance of the relay, the source node can consume a small amount of energy to transmit information to a distant

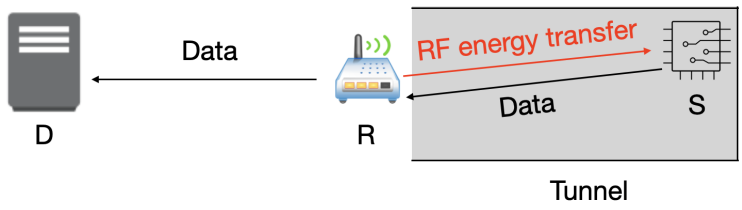

Figure 2.3: A relaying network that an EH source within a tunnel filled with toxic gas.

destination.

The two-hop relay-assisted networks with WPT from the relay to the source are studied in [47]–[51]. The authors in [47] consider a DF HD system where the two proposed schemes, namely, jointly optimal power-and-time fraction allocation and optimal power allocation with a fixed time fraction, are superior to fixed power and fixed time fraction allocations. A two-way relaying system with two EH sources and K relays is researched in [48]. The transmission nodes work in an HD time-division mode. A joint beam-forming and relay selection method is investigated to improve system throughput. The works in [49], [50] consider HD transmissions as well as simultaneous energy transfer and information transmission by utilizing the characteristics of RF signals. In the first time slot, the source transmits data to the relay. In the second phase, the relay forwards signals to both source and destination. The source harvests energy from the RF signal from the relay while the destination receives the desired information from the relay-transmitted signal. A communication system consists of an EH source and an out-of-band full-duplex relay node is investigated in [51]. The channel capacity is derived in two scenarios that the EH source can store energy using a battery and the EH source does not have a storage capacity. The above works consider HD and out-of-band FD transmission. As a result, these schemes have a limited throughput or a low spectral efficiency.

Conversely, the system proposed in Chapter 6 of this thesis considers EH-enabled source and IBFD transmission with the PDC scheme, thus it possesses a higher spectral efficiency and a higher system throughput.

2.4 Self-Interference Cancellations

2.4.1 Overview

IBFD is a technology in which simultaneous transmission and reception of information are achieved in the same frequency band. The definition and advantages of FD communication are mentioned in Section 2.2. However, because a local transmitter is way closer to the local receiver than the far-end transmitters, the SI signal usually thousands of times stronger than the signal of interest received from the far end. In [59], the results show that the power of SI is 80 dB stronger than the desired signal and 95 dB stronger than the noise floor. The desired signal is contaminated, which leads to unsuccessful decoding of the received signals. Therefore, SIC methods are required to enable the FD communication. By now many techniques to suppress SI signals have been researched. Generally, SIC is divided into three types, which are passive cancellation, analog cancellation, and digital cancellation, respectively. Passive cancellation is to isolate the transmitted signal from the received signal by, for example, exploiting a circulator, an isolation technology, or directional antennas. The analog cancellation aims to design a RF circuit with a corresponding control algorithm to cancel SI in the analog domain. Digital cancellation involves designing an interference cancellation module in the base-band. In general, the SIC algorithms aim to mimic the linear distortion and the non-linear distortion that the transmitted signal has gone through. The algorithms then reconstruct the SI signal. The impact of the SI signal will be canceled by subtracting the estimated SI from the received signal. Usually, these three cancellation techniques are combined in order to minimize SI in FD systems. The three SIC types will be mentioned in more details as below.

2.4.2 Passive Cancellations

Passive cancellation techniques cancel SI before it reaches the RF chain circuits of the receive node [60], [61]. It mainly utilizes pass loss to achieve cancellation [60]. As demonstrated in [62], the passive SIC is researched which includes directional isolation, absorptive shielding, and cross-polarization. Although [62] shows that over 70 dB of passive cancellation can be obtained in a certain environment, the passive method alone

is still insufficient to cancel all the SI completely. According to Duarte and Sabharwal in [63], the amount of SI linearly ascends with the transmitting power.

Numerous research papers focus on improving hardware designs to suppress SI in the IBFD systems. The paper [64] proposes a transceiver prototype that relies on the electrical balance duplexer to suppress SI. The electrical duplexer is automatically tuned by a digital base-band algorithm that can track antenna impedance variations. Different factors, such as antenna movements and surrounding conditions, affect the antenna impedance. The results show that the electrical balance duplexer can suppress SI by 20 dB without any tuning algorithm over a bandwidth of 20 MHz. If the electrical balance duplexer combines with the proposed tuning algorithm, the SIC performance is significantly improved. The average SIC suppression achieves up to 50 dB among different scenarios [64]. Similarly, Zhuang et al. in [65] design a novel duplexer to implement SIC. This method improves the traditional parallel directional coupler to prevent power leakage from the transmit circuit to the receive circuit. The coupler consists of four ports. Port 1 and Port 4 are on the left opposing to Port 2 and Port 3, respectively. Port 1 is connected to the transmit antenna and Port 2 is connected to the receive antenna. Port 4 produces an impedance mismatching effect by adding an open-circuit line in this port to reflect the coupling signal from Port 1 to Port 3. Ideally, the leak signal and the reflected signal cancel each other to achieve the desired cancellation. Evidently, the key point affecting the cancellation performance is the reflection coefficient. Therefore, the optimal reflection coefficient is calculated in Port 4. The SI suppression capacity of the proposed technique is significant with more than 36 dB suppression for both 4MHz and 8MHz bandwidth [65].

2.4.3 Analog Cancellations

The analog cancellation techniques suppress SI in the analog circuit to prevent SI enters the analog-to-digital converter (ADC) [60], [66]. There are two types of analog cancellations. The first type works by attenuating and delaying the digital base-band signal, up-converting it to the analog domain, and then injecting it to the input of the low noise amplifier (LNA) to cancel the SI [63], [67]. The block diagram is shown in Fig. 2.4. It is

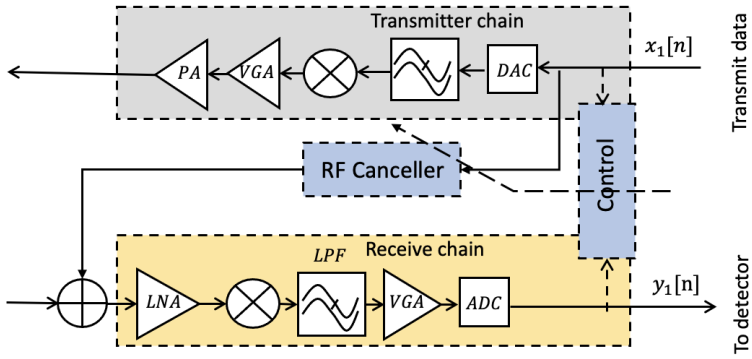

Figure 2.4: Block diagram of the first type analog cancellation.

complex in hardware but has the advantage of taking the non-linearity of the transmitter chain into account to achieve maximum SIC.

The second type replicas the RF transmit signal then applies attenuation and phase to it before injecting it to the LNA [66], [68]–[71], as shown in Fig. 2.5. The control unit in this figure is in the digital domain but it can also be in the analog domain. An adaptive RF SIC method tuned by a digital variable-step steepest descent algorithm is presented in [69]. The results show that this SIC can provide a maximum of 33 dB cancellation for a 20 MHz bandwidth. Besides, a digital-controlled RF SIC method and a complete demonstrator board have been proposed in [72]. This paper focuses on an FD system with frequency-selective fading channels. This developed canceller is able to adaptively track time-varying SI signals in a wide band. The results show that over 40 dB RF cancellation is obtained when the transmission bandwidth of the FD system is below 80 MHz. In [73], a novel multi-tap RF canceller is proposed for a wideband cancellation. This cancellation has self-adaptive properties to automatically track SI-channel changes caused by, for examples, reflections from the antenna and surrounding objects. This paper reports the bandwidth up to 100 MHz in circulator and dual-antenna scenarios. For the circulator case, 18 dB suppression is achieved while for the dual-antenna one, 15 dB suppression is reported. In [30], an analog least mean square (ALMS) loop is employed to suppress SI in IBFD OFDM systems. The SIC performance relies on the windowing function used in the system. The ALMS loop is simple and adaptive for SI mitigation which does not require

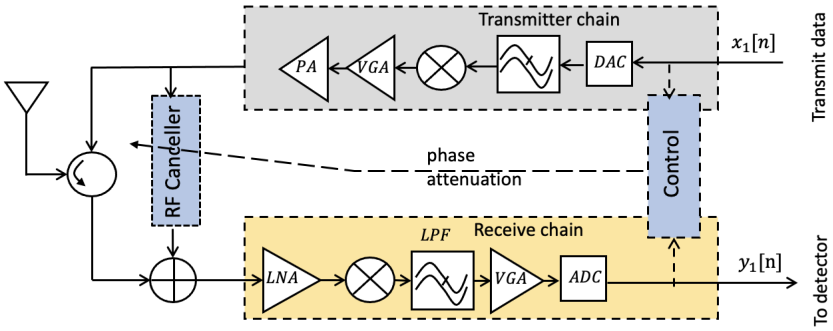

Figure 2.5: Block diagram of analog cancellation case 2.

the CSI of the SI channel. However, it may face an in-phase/quadrature (I/Q) imbalance problem. The authors in [74] investigate the impact of I/Q imbalance on the cancellation performance of the ALMS loop. In [75], a promising ALMS adaptive filter is proposed to be implemented by an analog domain for an IBFD MIMO system. The ALMS loops have a clear advantage that they can prevent a receiver from being saturated caused by SI before signals proceed to the ADC.

2.4.4 Digital Cancellations

Digital cancellation techniques are usually used in the last stage, which handle any residual SI after the ADC [60], [76]. The block diagram is shown in Fig. 2.6. Digital cancellation mainly handles two types of residual SI, which is channel estimation error [66], [69] as well as transceiver impairment [77].

The authors in [78] propose a digital cancellation method and research three different estimators, which are least squares (LS), normalized least mean squares (NLMS), and minimum mean square error (MMSE), to estimate the SI signal. The defined SI channel here contains the transmitter chain, electrical balance circuit, and receiver chain. In this way, multiple elements are considered in the SI channel estimation process, so the estimated SI is approaching reality. The results show that, for the quadrature phase-shift keying modulation, LS, NLMS, and MMSE estimations all estimators perform well because the BER performances are all close to the interference-free case. However, for the

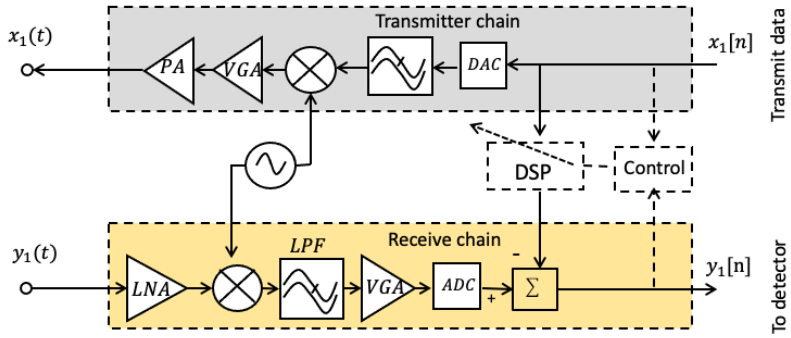

Figure 2.6: Block diagram of digital cancellation.

16 quadrature amplitude modulation, LS and NLMS have relatively a high BER while the performance of MMSE closes to the interference-free case. The paper [79] proposes a single channel digital cancellation method. The main challenge is to create a cancellation signal which is a resembled duplicate of the SI signal by adaptively adjusting the filter's parameters. The adaptive filter adopts the least mean square (LMS) algorithm to track the amplitude and phase variations of the SI signal. In this paper, the digital SIC technique has a great convergence rate and can cancel about 20 dB interference alone.

The transceiver impairments include the power amplifier (PA) non-linearity, I/Q imbalance, oscillator phase noise, and the resolution of the ADC. The paper [77] proposes an adaptive nonlinear digital SI canceller to suppress the PA non-linearity. Besides, [77] employs an orthogonalization procedure before utilizing an LMS-based parameter learning algorithm to track the time-varying SI channel and to suppress the PA non-linearity. In [80], for a relatively low transmit power ranged from 0 dBm to 10 dBm, the proposed adaptive real-time digital canceller achieves 25 dB to 35 dB suppression. For the bandwidth of 20 MHz, the proposed nonlinear digital cancellation with orthogonalization provides 46 dB SI reduction, compared to 22 dB for the linear digital cancellation method. In [81], the parallel Hammerstein model is extended to modeling the nonlinear SI channel, including the nonlinear PA, the linear multipath channels, and the RF SI canceller. The results show that the proposed digital cancellation technique allows the FD system to use a higher transmit power, i.e., up to 20 dBm, or a lower-quality PA. The digital SIC developed in [82] focuses on overcoming the problem of transmitter

nonlinearity caused by a power amplifier, but it is different from the previous nonlinear SIC methods. The proposed pre-calibration method employs a pre-calibrator before the digital-to-analog converter (DAC) to linearize the transmitter. This method has the advantages of low computational complexity than the nonlinear method and provides 43 dB cancellation performance in fast fading channels. However, the pre-calibration method is unstable because there are unwanted peaks. The reason is that the system generates an inaccurate pre-calibrator in certain frames. In [83], four canceller structures, including linear-digital canceller, widely linear-digital canceller, nonlinear digital canceller, and augmented nonlinear digital canceller, are proposed. These solutions are corresponding to different approximation models. The maximum suppression is provided by the augmented nonlinear digital canceller with 30 dB suppression alone. Oscillator phase noises are researched in [24], [84]. The method in [84] considers the inter-carrier interference (ICI) caused by phase noises and uses the MMSE algorithm to jointly estimate phase noises of the transmitter and the receiver. The results show that the proposed digital canceller provides 9 dB more suppression than the scheme that ignores ICI.

In [85], a PDC scheme is proposed to distinguish the desired signal from the SI signal. This method differs from most existing cancellation approaches [77] in reconstructing the SI signal. This scheme distinguishes and cancels effectively the unexpected SI signal from the desired information signal. The PDC scheme is associated with antenna polarization, and includes two steps, namely, oblique projection and scalarization. The objective of the oblique projection is to cancel the residual SI. The scalarization aims to transform the vector signal to the scalar form. The PDC is powerful, which has the advantages of suppressing both SI and additive white Gaussian noise (AWGN). In addition, the channel estimation of the SI channel is not required in the PDC scheme, and the polarization states can be unchanged among different blocks. This means that the relay only needs to synchronize its polarization state with the source and destination once. For these reasons, the PDC scheme will be researched deeply in this thesis.

2.4.5 Combination of Cancellations

The total SIC achieved by combining the cancellation techniques in the analog domain and digital domain have been investigated in the literature. In [86], a single antenna system with both analog and digital cancellations is researched. For the analog approach, a significant SI suppression of 75 dB is observed in the 10 MHz bandwidth. For the digital approach, the LMS algorithm is used. The performances show that, with the digital canceller, BER is decreased while the system throughput is increased. In [66], a compressed-sensing-based SI channel estimation technique is proposed in the analog domain and a subspace-based algorithm is developed in the digital domain to further cancel the residual SI. In the first stage, the compressed-sensing-based technique reduces the power of the SI signal to the same level as the desired signal. In the second stage, the subspace-based algorithm takes the IQ imbalance and PA non-linearity into account and estimates both the coefficients of the residual SI channel and the desired channel in order to improve cancellation performance. The suppression level of 40 dB is observed in the OFDM systems. In [63], the cancellation performances of passive, digital, and analog SIC mechanisms are investigated. A maximum of 80 dB suppression is achieved when those three methods are combined and the local transmitter and receiver are separated by a 40 cm distance. However, the limitation of this research is that a narrow bandwidth of only 625 kHz is considered. In paper [87], a single antenna cancellation method is proposed to cancel the antenna reflection and circulator leakage. The network consists of two quadrature hybrids, two circulators, and a single circularly polarized patch antenna. The signal at the transmitter is split into two portions by the first quadrature hybrids before reaching the antenna. Then, the two-port antenna reflects two signals which have 180-degree phase differences at the receiver. The balanced network combines the reflected signal at the Rx output port to cancel the antenna reflection and circulator leakage. The results show that this technique achieves 40 dB isolation alone and 59 dB cancellation when combining with the analog cancellation technique. A novel analog cancellation circuit and digital cancellation method are researched in [88] which provide totally 110dB SIC. However, this solution is limited to WiFi 802.11ac single-antenna circulator systems.

The combination of FD and MIMO relaying in simultaneous wireless information and power transfer systems is promising as spectral efficiency is improved. However, the associated interference control is challenging [56]. The work in [46] assumes an imperfect analog/digital interference cancellation scheme is applied at the relay. The residual loop-back interference channels are without a line-of-sight component between transmit antennas and receive antennas [46]. The spatial cancellation technique is deployed to suppress the residual interference. However, the instantaneous CSI of the SI channel is required in such a SI cancellation method. A new framework of interference mitigation is considered in [52], [53]. The residual SI is suppressed by using the information of direction-of-arrival (DOA) and direction-of-departure (DOD) of the SI channel instead of the instantaneous CSI. The long-term estimation of DOA/DOD is feasible as the DOA/DOD changes more slowly than the instantaneous CSI. However, since the DOA/DOD is required, the system complexity and overhead are significant.

2.5 Self-Energy Recycling Techniques

Energy harvesting technologies have become increasingly attractive as an appealing solution to provide long-lasting power for energy-constrained wireless sensor networks. Different from absorbing energy from the intermittent and unpredictable natural resources, such as solar, wind, and vibration, harvesting energy from the RF signal radiated by ambient transmitters has received tremendous attentions. The RF signal can convey both information and energy at the same time, which facilitates the development of simultaneous wireless information and power transfer (SWIPT). Besides, ambient RF is widely available from base stations, WIFI hot spots, and mobile phones in the current information era. The RF approach is cost-effective for communication networks as peripheral equipment needed to utilize external energy sources can be avoided.

Relaying and FD techniques have gained considerable attraction from researchers for their ability to improve system throughput. Besides, the demand for low-labor-cost and long-lifetime wireless communication systems has been increasing in recent years. Thus, the FD relaying system with wireless power transfer has also attracted the attention of

Table 2.2: The literature comparison of wireless power transfer-aided SER relaying systems, where ($\surd$) represents Yes, ($\times$) represents No, ($-$) represents SIC Schemes are Not Applicable, and ($\diagdown$) represents No Specific Scheme is Mentioned.

	No. of nodes	Assumption of direct link from S to D	Energy harvesting at S	Energy harvesting at R	Self-energy Recycling at R	Antennas	Protocol	Simultaneous transmission and reception of information at R	Active SIC scheme
[89]	4	$\surd$	$\times$	$\surd$	$\surd$	Single at S and D; Two at R	Decode-and-Forward;	$\times$	$-$
[90]	3	$\times$	$\times$	$\surd$	$\surd$	Multiple-Input Single-Output	Amplify-and-Forward;	$\times$	$-$
[91]	3	$\times$	$\times$	$\surd$	$\surd$	Multiple at S and R; Single at D	Amplify-and-Forward;	$\times$	$-$
[92]	3	$\times$	$\times$	$\surd$	$\surd$	Single at S and D; Two at R	Amplify-and-Forward;	$\times$	$-$
[93]	3	$\times$	$\times$	$\surd$	$\surd$	Multiple at S and R; Single at D	Amplify-and-Forward;	$\times$	$-$
[94]	4	$\times$	$\times$	$\surd$	$\surd$	Multiple at S and R; Single at D	Amplify-and-Forward;	$\times$	$-$
[95]	3	$\surd$	$\times$	$\surd$	$\surd$	Single at S and D; Two at R	Amplify-and-Forward; Decode-and-Forward; Quantize-Map-Forward;	$\times$	$-$
[96]	3	$\times$	$\times$	$\surd$	$\surd$	Multiple at S, R, and D	Amplify-and-Forward;	$\times$	$-$
[97]	3	$\times$	$\times$	$\surd$	$\surd$	Single at S and D; Two at R	Decode-and-Forward;	$\times$	$-$
[98]	3	$\times$	$\times$	$\surd$	$\surd$	Multiple at S and R; Single at D	Decode-and-Forward	$\surd$	$\diagdown$
[99]	3	$\times$	$\times$	$\surd$	$\surd$	Single at S and D; Two at R	Decode-and-Forward;	$\surd$	$\diagdown$
[100]	3	$\times$	$\times$	$\surd$	$\surd$	Multiple at R; Single at S and D	Decode-and-Forward	$\surd$	$\diagdown$
[101]	3	$\times$	$\times$	$\surd$	$\surd$	Multiple at S and R; Single at D	Amplify-and-Forward	$\surd$	$\diagdown$
Chapter 7	3	$\times$	$\surd$	$\surd$	$\surd$	Dual-polarized antennas; Single at S and D; Two at R	Amplify-and-Forward	$\surd$	$\surd$

many scholars. However, the main challenge for the FD transmission is to deal with the SI signal. SI signals can be suppressed by SIC methods. As mentioned in Section 2.4, the three main types of SIC methods are passive cancellations, digital cancellations, and analog cancellations, which can be applied jointly to maximize the SI suppression [102]. The FD EH relaying systems are studied in [26], [27], [40], [103] to increase system spectral efficiency, where SIC methods are applied to suppress SI signals. Alternatively, SI signals can also be utilized in a self-energy recycling (SER) process [89]–[101] to improve the energy efficiency.

The literature comparison of wireless power transfer-aided SER relaying systems is illustrated in Table 2.2, where Chapter 7 of this thesis is also added for comparison. More specifically, in [89], a buffer-aided HD wireless-powered SER relay system with two antennas at the relay and one antenna at the source and destination is considered. A fixed-antenna assignment and an adaptive-antenna assignment are proposed to improve the system throughput. The authors in [90]–[97] consider two-phase SWIPT systems with SER at the relay node. With T representing the total block duration, the first phase of the duration $T/2$ is used by the source for sending information to the relay. The second phase of the remaining time $T/2$ is used by the relay for receiving energy signals from the source, and concurrently, transmitting information to the destination. Particularly, a portion of its own transmit signal can be harvested and reused by the relay via the loopback channel. The SI signal at the relay is in fact beneficial since the relay not only harvests energy from the source, but also recycles energy from the self-interfering link. In all these time-switching-based SWIPT relaying systems [90]–[97], the information signal is transmitted and received in two different phases, so that the SIC is not required to eliminate SI. However, this also means that the relay cannot receive information from the source and transmit information to the destination at the same time, thus limiting the system throughput.

In [98], [99], the SER-based decode-and-forward FD relaying networks are studied with an efficient power allocation strategy. The relay in these systems works in an FD mode and receives information from the source and its own transmitter. A portion of the

received signal is used for the EH process while the remaining portion of the received signal is used for the decoding and forwarding information to the destination. However, the disadvantage of the methods proposed in [98], [99] is that the practical EH circuits cannot forward the received information and simultaneously extract power from the same received signal [104]. In [100], the authors consider an FD relaying system with multiple transmit and receive antennas at the relay. The proposed antenna allocation scheme can allot the antennas at both transmit and receive ends for either SER or information relaying. The spectral efficiency and energy efficiency are improved at the cost of a complicated antenna allocation technique. In [101], the authors study a power-splitting based amplify-and-forward FD system, where the signal transmission and reception and SER are performed in one phase. However, there are no specific SIC schemes mentioned in [98]–[101].

Chapter 7 of this thesis will propose a SER-based system to improve the energy efficiency and overcome the aforementioned shortcomings.

2.6 Open Issues and Research Objectives

In this chapter, we first provide an overview and up-to-date literature review of cooperative networks, IBFD communication, and wireless EH techniques. Especially, SI cancellations, including passive cancellations, analog cancellations, and digital cancellations, are reviewed as they are the keys to facilitating the IBFD transmission. The state-of-art of SER techniques is also reviewed which is proposed to improve energy efficiency. The literature review reveals that the open research question is how to construct an IBFD EH relaying network that is cost-effective and has high throughput and energy efficiencies, as well as long-distance coverage. The project mainly focuses on the SIC technique of IBFD communication and improving the throughput of the system. The IBFD system has a serious SI problem, which makes it impossible to receive signals from the transmitter. So the first objective of this thesis is implementing IBFD communication based on signal processing technology. The second objective of this thesis is combining IBFD and WPT technologies, designing protocols, and optimizing parameters to allocate the time

for signal transfer and energy transfer to optimize the throughput of the system. Thus, this thesis proposes novel IBFD relaying systems, utilizing the emerging PDC, antenna polarization, EH, and SER techniques with necessary adaptations. The proposed IBFD EH relaying system will be mentioned in detail in the following chapters.

Chapter 3

Performance Evaluation of Single-Carrier PDC-Based Full-Duplex Networks with EH-Enabled Relay

3.1 Introduction

In a system where there is no direct link between the source node and the destination node, the assistance of other nodes is needed to forward information to the destination. Thus, relaying networks and their characteristics are important to investigate. Meanwhile, EH techniques, which allow nodes to harvest energy from RF electromagnetic radiation, have attracted a significant interest, since the lifetime of wireless sensor nodes can be prolonged. For example, the work in [14], [22] investigates relaying systems with wireless EH. The relay node converts the energy from the source into its own energy to forward the signal to the destination, but the relay is limited to the HD mechanism. In [16], an IBFD relaying network is investigated, which allows simultaneous transmission and reception of information in the same frequency band. The network provides higher spectrum efficiency compared to time division duplex and frequency division duplex. In such an IBFD relaying system, the signal received at the relay from the distant transmitter is referred to as the desired signal, while the transmitted signal from the local relaying transmitter is the SI signal. Because transmission and reception in an IBFD system occur at the same time and in the same frequency band, the SI signal is mixed with the desired signal, leading to a signal corruption at the receiver of the relay. Thus, it is crucial that the SI signal is

suppressed in the relay node before the desired signal is amplified and forwarded to the destination. Referring to Chapter 2, some pioneering work about suppressing SI signals has been researched. Most of the existing cancellation methods depend on reconstructing the SI signal and then subtracting it from the received signal to extract the desired signal. In contrast, the PDC scheme proposed by Liu et al. in [85] distinguishes the SI signal from the desired signal in the propagation domain and cancels the SI using an oblique projection in the digital domain. However, this proposal does not consider the EH mechanism and is not applied to relaying systems. To the best of our knowledge, no works, especially in the antenna polarization domain, have considered the performance of SIC methods in the IBFD relaying system with EH. Given that both IBFD communications and EH are important emerging technologies for 5G systems and beyond, the performance evaluation of IBFD EH relaying networks is of considerable importance. This is the motivation of our researches. For simplicity, in the following chapters of this thesis, we use FD to represent IBFD.

In this chapter, we consider a two-hop FD relaying system, where the relaying node harvests the RF energy from the source node, then uses this energy to amplify and forward the signal to the destination. We assume there is no direct link between the source node and the destination node. Thus, the relay is used to assist the transmission from the source to the destination. We also assume that the time switching method [16] is used at the relay to harvest the RF energy and the PDC scheme is used to cancel SI at the relay. The main contributions of the chapter are summarized as follows.

- We investigate the throughput of an FD relaying system assisted by RF EH and the PDC scheme. We consider the system throughput in relation with the fraction of time α used to harvest energy for a range of transmit SNR and modulation methods. We show that the maximum throughput appears at a lower range of α values for a higher transmit SNR, while this optimal α is invariant for different modulation methods. This observation means that to achieve a high throughput, a joint combination of a high transmit SNR value and a low α value is expected.

- The BER performances under the impacts of RF EH and the PDC scheme are ex-

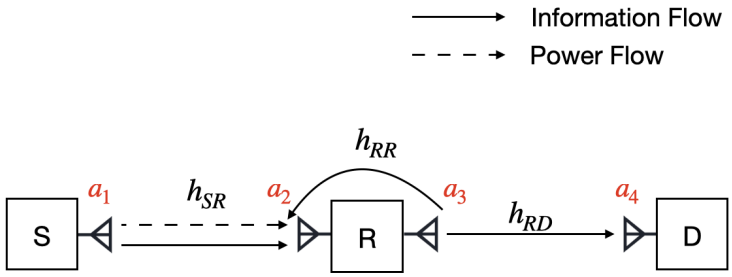

Figure 3.1: Single carrier FD-EH relaying system.

amined. It is revealed that for the same transmit SNR, the BER performance of the system only improves slightly when α increases. Combined with the above observation, this result means that the EH scheme can be optimized to improve significantly the system throughput without sacrificing much the BER performance.

- The impacts of the EH and PDC schemes on the BER performance are qualified in comparison with the HD EH relaying system. Our results show that the PDC scheme can effectively cancel the SI in the FD system. In particular, if the relay transmission power (per symbol) is the same in both FD and HD systems, the BER performance curve of the former is within 2 dB inferior compared to that of the latter. Thus, applying the PDC cancellation scheme to achieve a high throughput and reasonable BER for our FD EH relaying system is feasible.

The content of this chapter has been published in our paper [26] and partly in our paper [27], [105].

The rest of chapter is organized as follows. In Section 3.2, the system model is presented. In Section 3.3, the theory of the PDC scheme is discussed in detail, and in Section 3.4, the signal model is described. The simulation results and performance analysis are presented in Section 3.5. Section 3.6 concludes this chapter.

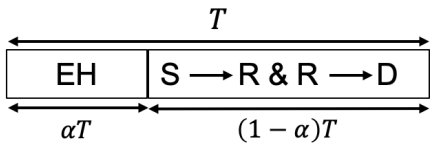

Figure 3.2: Time-switching EH architecture in an FD system.

3.2 System Model

In this chapter, the two-hop FD relaying system with EH at the relay node is considered. We assume that there is no direct link between the source node and the destination node. Thus, an intermediate relay is used to assist the transmission from the source to the destination as shown in Fig. 3.1. The system has a single source node, a relay node, and a destination node. Denote a_1 to a_4 as orthogonally dual-polarized antennas, in which the antennas a_1 and a_3 are used for transmission, while a_2 and a_4 are used for reception. The flat-fading channel gains from the source to the relay and from the relay to the destination are denoted as h_{SR} and h_{RD}, and the distances between them are presented as d_1 and d_2 respectively. As the system is an FD one, the relay is able to receive signals from the source while transmitting signals to the destination at the same time in the same frequency band. Thus the local transmit antenna a_3 causes the SI signals, which will be mixed with the desired signal at the receive antenna a_2. Denote h_{RR} as the propagation coefficient of the SI channel which is assumed to follow a Rayleigh distribution. The PDC scheme [85] is applied at the relay to cancel SI signals.

In addition, the relay node is equipped with the TSR protocol [16] for EH and information processing. The FD TSR protocol is depicted in Fig. 3.2. The whole signal block lasting T (seconds) is divided into an EH section and an information transmitting section. We define α, where $0 < \alpha < 1$, as the fraction of time in which the relay harvests the energy from its received signals. Thus, αT time is used for the EH and the remaining block time $(1-\alpha)T$ is used to transmit the desired signal in an FD transmission mode. The intermediate relay harvests energy from the RF signal transmitted from the source within the duration αT. Then, the relay uses the harvested energy as a source of transmitting

power to amplify and forward the source information to the destination within the duration $(1-\alpha)T$. Besides, the PDC scheme is activated during this period to cancel the SI signal. After SIC, the resulting signal is amplified by the relay before being forwarded to the destination. Finally, the received signal at the destination is detected by the maximum ratio combining (MRC) method.

3.3 PDC Scheme

In this section, we introduce the theory of using the PDC scheme at the relay to eliminate the loop-back SI. The PDC scheme [85], [106] in our system requires the orthogonal dual-polarized antennas at the three nodes as well as the adoption of the oblique projection at the relay node.

We first introduce the Jones vector $\mathbf{J} = [\mathrm{J}_H \quad \mathrm{J}_V]^{\mathrm{T}} = [\cos(\varepsilon) \quad \sin(\varepsilon)\exp(j\delta)]^{\mathrm{T}}$ to express the signal polarization, where $(.)^{\mathrm{T}}$ represents the transpose of a vector, J_H represents the horizontal component, J_V represents the vertical component of the transmitted signal, $\varepsilon \in [0, \pi/2]$ represents the polarization angle, and $\delta \in [0, 2\pi]$ represents the phase difference between the vertical and horizontal components. The polarization states of the desired information signal and the SI signal are denoted as $\mathbf{S}$ and $\mathbf{I}$ respectively.

$$\begin{aligned} \mathbf{S} &= \left[\cos(\varepsilon_s) \quad \sin(\varepsilon_s)\exp(j\delta_s)\right]^{\mathrm{T}} \\ \mathbf{I} &= \left[\cos(\varepsilon_i) \quad \sin(\varepsilon_i)\exp(j\delta_i)\right]^{\mathrm{T}}, \end{aligned} \tag{3.1}$$

where $\varepsilon_i, \varepsilon_s \in [0, \pi/2]$ are polarized angles of the dual-polarized antennas, $\delta_i, \delta_s \in [0, 2\pi]$ are phase differences between the vertical and horizontal polarized components of the dual-polarized antennas. $\mathbf{S}$ and $\mathbf{I}$ are unit vectors, i.e., $\mathbf{S}^{\mathrm{H}}\mathbf{S} = \mathbf{I}^{\mathrm{H}}\mathbf{I} = 1$ and $\mathbf{S} \neq \mathbf{I}$, where $(.)^{\mathrm{H}}$ is the complex conjugate. In the source-to-relay (S-R) link, the polarization state $\mathbf{S}$ is used, while, in the relay-to-destination (R-D) link, the polarization state $\mathbf{I}$ is used. It is worth noting that the re-transmitted signals from the relay to destination and the SI signal at the relay have the same polarization state $\mathbf{I}$.

To explain the oblique projections, we first introduce the orthogonal projections. An orthogonal projection has a null space that is orthogonal to its range [106]. For an orthog-

onal projection $\mathbf{P}_{\mathrm{S}}$ whose range is $\langle \mathbf{S} \rangle$ and null space is $\langle \mathbf{I} \rangle = \langle \mathbf{S} \rangle^{\perp}$, we have

$$\begin{aligned} \mathbf{P}_{\mathrm{S}}\mathbf{S} &= \mathbf{S}, \\ \mathbf{P}_{\mathrm{S}}\mathbf{I} &= \mathbf{0}, \end{aligned} \tag{3.2}$$

where $\mathbf{0}$ is a zero vector, i.e., $\mathbf{0} = \begin{bmatrix} 0 & 0 \end{bmatrix}^{\mathrm{T}}$.

The well-known formulas to build orthogonal projections with the range $\langle \mathbf{S} \rangle$ and $\langle \mathbf{I} \rangle$, respectively, are given by

$$\begin{aligned} \mathbf{P}_{\mathrm{S}} &= \mathbf{S}(\mathbf{S}^{\mathrm{H}}\mathbf{S})^{-1}\mathbf{S}^{\mathrm{H}}, \\ \mathbf{P}_{\mathrm{I}} &= \mathbf{I}(\mathbf{I}^{\mathrm{H}}\mathbf{I})^{-1}\mathbf{I}^{\mathrm{H}}, \end{aligned} \tag{3.3}$$

where $(.)^{\mathrm{H}}$ is the Hermitian transposition of a complex vector or matrix, and $(.)^{-1}$ is the matrix inversion. $\mathbf{P}_{\mathrm{S}}$ is called the projector onto $\langle \mathbf{S} \rangle$. The orthogonal projection with the range $\langle \mathbf{S} \rangle^{\perp}$ is

$$\begin{aligned} \mathbf{P}_{\mathrm{S}}^{\perp} &= \mathbf{E} - \mathbf{P}_{\mathrm{S}} \\ &= \mathbf{E} - \mathbf{S}\mathbf{S}^{\mathrm{H}}, \end{aligned} \tag{3.4}$$

where

$$\mathbf{E} = \begin{bmatrix} 1 & 0 \\ 0 & 1 \end{bmatrix}. \tag{3.5}$$

Then, we introduce the vector $\mathbf{V}$ as the received signal at the relay, which includes both desired information signal received from the source node and its SI signal. In order to preserve the information signal and cancel the SI signal at the same time, the oblique projection is applied. As shown in Fig. 3.3, the orthogonal projection in the space $\langle \mathbf{A}, \mathbf{S}, \mathbf{S}^{\perp} \rangle$ is denoted as $\mathbf{P}$ with subscripts, which includes two components, $\mathbf{P}_{\mathrm{SI}}$ and $\mathbf{P}_{\mathrm{A}}$ projections. The oblique projection is denoted as $\mathbf{E}$ with the subscripts indicating the respective ranges.

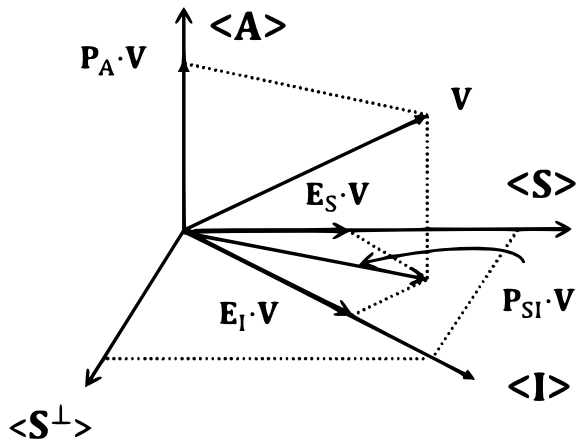

Figure 3.3: Three-way resolution of Euclidean space.

Based on (3.3), the orthogonal projection onto the linear subspace $\langle \mathbf{S}\,\mathbf{I} \rangle$ is given by [106]

$$\mathbf{P}_{\mathrm{SI}} = \begin{bmatrix} \mathbf{S} & \mathbf{I} \end{bmatrix} \begin{bmatrix} \mathbf{S}^{\mathrm{H}}\mathbf{S} & \mathbf{S}^{\mathrm{H}}\mathbf{I} \\ \mathbf{I}^{\mathrm{H}}\mathbf{S} & \mathbf{I}^{\mathrm{H}}\mathbf{I} \end{bmatrix}^{-1} \begin{bmatrix} \mathbf{S}^{\mathrm{H}} \\ \mathbf{I}^{\mathrm{H}} \end{bmatrix}, \tag{3.6}$$

where the sub-spaces $\langle \mathbf{S} \rangle$ and $\langle \mathbf{I} \rangle$ are non-overlapping or disjoint. This orthogonal projection can be decomposed as

$$\mathbf{P}_{\mathrm{SI}} = \mathbf{E}_{\mathrm{S}} + \mathbf{E}_{\mathrm{I}}, \tag{3.7}$$

where $\mathbf{E}_{\mathrm{S}}$ and $\mathbf{E}_{\mathrm{I}}$ are two oblique projections with the respective ranges $\langle \mathbf{S} \rangle$ and $\langle \mathbf{I} \rangle$ and the respective null spaces $\langle \mathbf{I} \rangle$ and $\langle \mathbf{S} \rangle$, which are given by

$$\begin{aligned} \mathbf{E}_{\mathrm{S}} &= \begin{bmatrix} \mathbf{S} & \mathbf{0} \end{bmatrix} \begin{bmatrix} \mathbf{S}^{\mathrm{H}}\mathbf{S} & \mathbf{S}^{\mathrm{H}}\mathbf{I} \\ \mathbf{I}^{\mathrm{H}}\mathbf{S} & \mathbf{I}^{\mathrm{H}}\mathbf{I} \end{bmatrix}^{-1} \begin{bmatrix} \mathbf{S}^{\mathrm{H}} \\ \mathbf{I}^{\mathrm{H}} \end{bmatrix}, \\ \mathbf{E}_{\mathrm{I}} &= \begin{bmatrix} \mathbf{0} & \mathbf{I} \end{bmatrix} \begin{bmatrix} \mathbf{S}^{\mathrm{H}}\mathbf{S} & \mathbf{S}^{\mathrm{H}}\mathbf{I} \\ \mathbf{I}^{\mathrm{H}}\mathbf{S} & \mathbf{I}^{\mathrm{H}}\mathbf{I} \end{bmatrix}^{-1} \begin{bmatrix} \mathbf{S}^{\mathrm{H}} \\ \mathbf{I}^{\mathrm{H}} \end{bmatrix}. \end{aligned} \tag{3.8}$$

We choose $\mathbf{Q}_{\mathrm{SI}} = \mathbf{E}_{\mathrm{S}}$ to be the oblique projection operator of the PDC scheme as we aim to maintain the desired signal with the polarization state $\mathbf{S}$ while canceling the SI signal with the polarization state $\mathbf{I}$ [85]. From (3.8), the oblique projection with the range $\langle \mathbf{S} \rangle$

can be simplified to

$$\mathbf{Q}_{\mathrm{SI}} = \mathbf{S}\left[\mathbf{S}^{\mathrm{H}}\mathbf{P}_{\mathrm{I}}^{\perp}\mathbf{S}\right]^{-1}\mathbf{S}^{\mathrm{H}}\mathbf{P}_{\mathrm{I}}^{\perp}, \tag{3.9}$$

where $\mathbf{P}_{\mathrm{I}}^{\perp} = \mathbf{E} - \mathbf{P}_{\mathrm{I}} = (\mathbf{E} - \mathbf{I}\mathbf{I}^{\mathrm{H}})$, which is the orthogonal projection with the range $\langle \mathbf{I} \rangle^{\perp}$, i.e., $\mathbf{P}_{\mathrm{I}}^{\perp}\mathbf{I} = \mathbf{0}$. The operator $\mathbf{Q}_{\mathrm{SI}}$ is used at the relay as a digital signal processing module to cancel SI.

It can be easily shown that

$$\mathbf{Q}_{\mathrm{SI}}\mathbf{S} = \mathbf{S}\left[\mathbf{S}^{\mathrm{H}}\mathbf{P}_{\mathrm{I}}^{\perp}\mathbf{S}\right]^{-1}\mathbf{S}^{\mathrm{H}}\mathbf{P}_{\mathrm{I}}^{\perp}\mathbf{S} = \mathbf{S}, \tag{3.10}$$

$$\mathbf{Q}_{\mathrm{SI}}\mathbf{I} = \mathbf{S}\left[\mathbf{S}^{\mathrm{H}}\mathbf{P}_{\mathrm{I}}^{\perp}\mathbf{S}\right]^{-1}\mathbf{S}^{\mathrm{H}}\mathbf{P}_{\mathrm{I}}^{\perp}\mathbf{I} = \mathbf{0}. \tag{3.11}$$

In (3.11), we use the fact that $\mathbf{P}_{\mathrm{I}}^{\perp}\mathbf{I} = \mathbf{0}$ as mentioned before. Eqs. (3.10) and (3.11) indicate the oblique projection $\mathbf{Q}_{\mathrm{SI}}$ has the range $\langle \mathbf{S} \rangle$ and null space $\langle \mathbf{I} \rangle$. The property $\mathbf{Q}_{\mathrm{SI}}[\mathbf{S} \quad \mathbf{I}] = [\mathbf{S} \quad \mathbf{0}]$ is the key to canceling SI in the PDC scheme. Although the incoming signal y_{in} of the PDC scheme consists of the desired signal and the SI signal, the product of the matrix $\mathbf{S}^{\mathrm{H}}\mathbf{Q}_{\mathrm{SI}}$ and y_{in} can effectively preserve the desired signal and cancel the SI signal at the same time. The detailed analyses will be presented in Section 3.4. The PDC scheme at the relay node may consume some power. In this work, we do not consider processing power consumption of the PDC cancellation technique, which is an interesting future direction worth more research [46].

3.4 Signal Model

3.4.1 Energy Harvesting

In Phase I of the FD TSR protocol, the RF signal x_e is sent from the source to the EH receiver at the relay node. During this EH phase, the received energy signal at the relay can be expressed as

$$y_e[i] = \sqrt{\frac{P_s}{d_1^m}} h_{SR} x_e[i] + n_r[i], \tag{3.12}$$

where h_{SR} is the channel coefficient of the $S-R$ channel and d_1 is the distance between the source and relay. P_s is the constant transmitted power of the source node, x_e is the energy symbol transmitted from the source at the time instant i with the expectation value $E\{|x_e[i]|^2\} = 1$, and $n_r[i]$ is the AWGN at the relay with the variance of N_0. We assume that the harvested energy due to the noise is small and thus ignored [46], [56]. Hence, the harvested energy at the relay during the time αT is

$$E_r = \eta \alpha T \left(\frac{P_s |h_{SR}|^2}{d_1^m} \right), \tag{3.13}$$

where $0 < \eta < 1$ is the energy conversion efficiency. We assume all the harvested energy E_r at the relay is used in Phase II for relaying information signals to the destination. The transmission power of the relay is

$$P_r = \frac{E_r}{(1-\alpha)T} = \frac{\alpha \eta P_s |h_{SR}|^2}{(1-\alpha) d_1^m}. \tag{3.14}$$

3.4.2 Information Transmission

Denote m as the path loss exponent, P_s as the source transmit power, and P_i as the interference power at the receive antenna of the relay. The channel coefficients are presented in Fig. 3.1. Then, in a conventional non-polarized FD system, the received temporal signal $y_r[i]$ at the relay is

$$y_r[i] = \left(\frac{1}{\sqrt{d_1^m}} \right) \sqrt{P_s} h_{SR} x_s[i] + n_r[i]. \tag{3.15}$$

However, in our proposed system, since the orthogonally dual-polarized antennas are used to transmit and receive the polarized signals, the relay receives the polarized signals, each of which has a horizontally polarized component (H) and a vertically polarized component (V). Thus, the polarized received signal at the relay node, namely the input signal of the PDC scheme, can be written as

$$y_r[i] = \sqrt{\frac{P_s}{d_1^m}} h_{SR} \mathbf{S} x_s[i] + \sqrt{P_i} h_{RR} \mathbf{I} x_r[i] + \mathbf{N}_r[i], \tag{3.16}$$

where $x_s[i]$ is the information signal transmitted by the source and $x_r[i]$ is the loopback interference due to the FD transmission at the relay with $E\{|x_s[i]|^2\} = 1$ and $E\{|x_r[i]|^2\} = 1$. h_{SR} is the channel coefficient of the S$-$R channel and h_{RR} is the loopback interference channel gain. P_i is the power of the loopback interference signal, which is assumed to be less than the transmitting power of the relay P_r, due to some passive SIC technologies used at the relay, such as absorptive shielding [62], the difference in polarization of the transmit and receive antennas at the relay, and the path loss between the transmit antenna and the receive antenna of the relay. In the later simulation, for illustration and without loss of generality, we assume P_i is 25 dB smaller than P_r. $\mathbf{N}_r[i]$ is the AWGN at the relay node, which can be represented as

$$\mathbf{N}_r[i] = \begin{bmatrix} \mathrm{n}_H[i] \\ \mathrm{n}_V[i] \end{bmatrix}, \tag{3.17}$$

where $\mathrm{n}_H[i]$ represents the horizontal polarized component and $\mathrm{n}_V[i]$ represents the vertical polarized component. $\mathrm{n}_H[i]$ and $\mathrm{n}_V[i]$ obey the Gaussian distribution with a zero mean and a variance of $\frac{N_0}{2}$. From (3.16), the relay not only receives the information signal $x_s[i]$ from the source but also receives the SI signal from its own transmitter. The signal $y_r[i]$ is then processed by the PDC scheme. The output signal y_{out} of the PDC scheme is

$$\begin{aligned} y_{out}[i] &= \mathbf{S}^{\mathrm{H}}\mathbf{Q}_{\mathrm{SI}}\, y_r[i] \\ &= \sqrt{\frac{P_s}{d_1^m}} h_{SR} x_s[i] + \mathbf{S}^{\mathrm{H}}\mathbf{Q}_{\mathrm{SI}}\mathbf{N}_r[i], \end{aligned} \tag{3.18}$$

where $\mathbf{S}^{\mathrm{H}}\mathbf{Q}_{\mathrm{SI}}\mathbf{N}_r[I]$ is the noise of the output of the PDC scheme. This noise term can be considered as the side-effect of the PDC scheme. The signal y_{out} in (3.18) is then amplified and forwarded by the relay. Denote the variance of $\mathbf{S}^{\mathrm{H}}\mathbf{Q}_{\mathrm{SI}}\mathbf{N}_r[i]$ as δ_p^2. The transmitted signal at the relay $x_r[i]$ is given by

$$x_r[i] = \sqrt{\frac{P_r}{\frac{|h_{SR}|^2 P_s}{d_1^m} + \delta_p^2}}\, y_{out}[i-\tau], \tag{3.19}$$

where τ is the time delay caused by the relay processing. The received signal at the destination is

$$\begin{aligned} y_d[i] &= \frac{1}{\sqrt{d_2^m}} h_{RD} x_r[i] + n_d[i] \\ &= \sqrt{\frac{\eta \alpha P_s \varepsilon}{(1-\alpha) d_1^m d_2^m}} h_{SR} h_{RD} x_s[i] + \sqrt{\frac{\eta \alpha \varepsilon}{(1-\alpha) d_2^m}} h_{RD} \mathbf{S}^{\mathrm{H}} \mathbf{Q}_{\mathrm{SI}} \mathbf{N}_r[i] + n_d[i], \end{aligned} \tag{3.20}$$

where $n_d[i]$ is the AWGN at the destination with the variance of N_0, and $\varepsilon = \frac{|h_{SR}|^2 P_s}{|h_{SR}|^2 P_s + d_1^m \delta_p^2}$. The signal $y_d[i]$ is then processed by the maximum ratio combining (MRC) detection method. Denote $(.)^*$ as the conjugate of a single number, the resulting signal $y_{de}[i]$ used for demodulation is

$$\begin{aligned} y_{de}[i] &= h_{SR}^* h_{RD}^* y_d[i] \\ &= h_{SR}^* h_{RD}^* \left(\sqrt{\frac{\eta \alpha P_s \varepsilon}{(1-\alpha) d_1^m d_2^m}} h_{SR} h_{RD} x_s[i] + \sqrt{\frac{\eta \alpha \varepsilon}{(1-\alpha) d_2^m}} h_{RD} \mathbf{S}^{\mathrm{H}} \mathbf{Q}_{\mathrm{SI}} \mathbf{N}_r[i] + n_d[i] \right). \end{aligned} \tag{3.21}$$

3.5 Simulation Results

In this section, simulation results are presented to reveal the throughput and BER performances of both HD EH relaying system and FD EH relaying system. In the first part, we investigate the impact of transmit SNR ,i.e., transmit SNR= $\frac{P_s}{N_0}$, and modulation schemes on the system throughput when the value of α is varied. In the second part, we investigate the impact of α and modulation schemes on the BER with the change of transmit SNR from 0 dB to 40 dB. P_s and P_r represent the transmission power of the source and the relay, respectively. The source transmission rate is set as $R_{c1} = 2$ bits/sec/Hz for quadrature phase-shift keying (QPSK) modulation and $R_{c2} = 4$ bits/sec/Hz for 16 phase-shift keying (16-PSK) modulation, hence, the total numbers of transmitted symbols in both QPSK and 16-PSK cases are the same. We set the corresponding outage SNR threshold to achieve the desired transmission rates R_1 and R_2 as $\gamma_{th1} = 2^{R_{c1}} - 1 = 3$ and $\gamma_{th2} = 2^{R_{c2}} - 1 = 7$, respectively. The path loss exponent is $m = 4$, the source-relay distance d_1 and relay-destination distance d_2 are 1 meter, and the EH efficiency $\eta = 1$. Besides, we assume that

the signal channels and the SI channels satisfy Rayleigh flat fading.

3.5.1 Throughput Performances

The system outage probability can be calculated as

$$p_{out} = P(\gamma < \gamma_{th}), \tag{3.22}$$

where γ is the instantaneous SNR per symbol of the received signal at the destination and γ_{th} is the SNR threshold. Specifically, the threshold of QPSK modulation is γ_{th1} while that of 16-PSK modulation is γ_{th2}. The system throughput R can be calculated as

$$R = (1 - p_{out})R_c(1 - \alpha), \tag{3.23}$$

where R_c is the transmission rate. Recall that the transmission rate of QPSK modulation is R_{c1} while that of the 16-PSK modulation is R_{c2}. The simulation results of the throughput are shown in Figs. 3.4 and 3.5.

Fig 3.4 illustrates the throughput of both HD and FD relaying systems for different values of α. In both systems, the relay node is powered by the EH technique and the modulation scheme is 16-PSK. From Fig 3.4, we have three observations. Firstly, a continuous increase of α is not necessary to improve the system throughput. For the four different scenarios in Fig 3.4, the throughput curves are concave, i.e., the throughput reaches its maximum value at a certain α. This is because the system throughput R is a function of both p_{out} and $(1 - \alpha)$ as shown in (3.23). Any increase in α results in a larger transmission power P_r of the relay, i.e., a smaller outage probability p_{out}, but also a shorter time duration $(1 - \alpha)T$ used for transmission of information. For a small value of α, the throughput depends more on p_{out}, while it depends more on $(1 - \alpha)$ when α becomes larger. Secondly, for different values of the transmit SNR, the throughput of the FD system in all cases is around 1.6 times of the HD case. The reason is that although FD carries a doubled amount of symbols compared to HD during the duration $(1 - \alpha)T$, the total harvested energy during the αT time for relay transmission is the same. This means the relay transmission powers per symbol P_r of FD is half of HD, which decreases

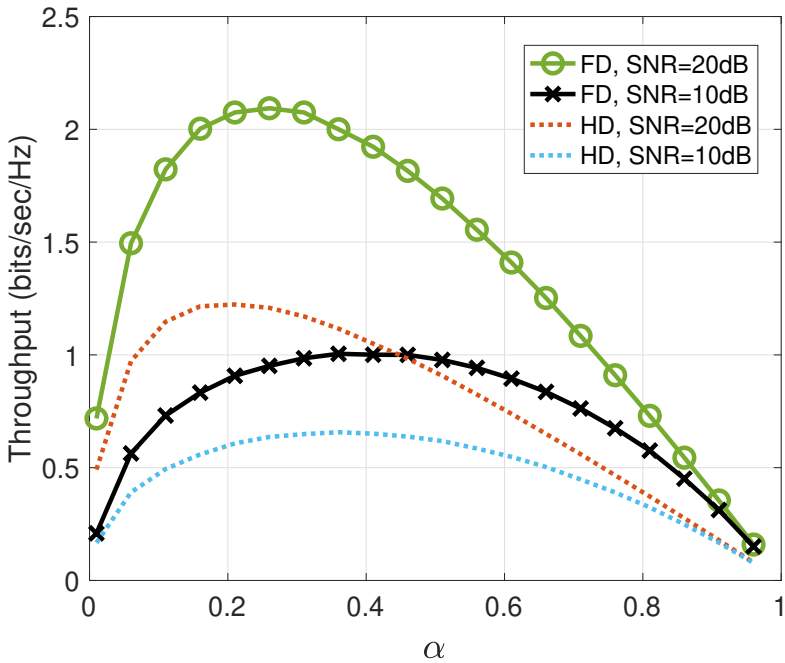

Figure 3.4: Throughput comparison between HD EH relaying system and FD EH relaying system using 16-PSK modulation.

the throughput by 0.4 times. Thirdly, when the transmit SNR is larger, the maximum throughput appears at a lower α value. For example, at SNR $= 20$ dB, the throughput in FD is peaked at around $\alpha = 0.18$, while for SNR $= 10$ dB, it is maximum at $\alpha = 0.33$. The reason is that, for the same transmission rate R_c, the throughput is a function of both p_{out} and α. The maximum throughput appears at the intersection of the two curves representing $1 - p_{out}$ and $R_c(1-\alpha)$. When the transmit SNR increases, the function $R_c(1-\alpha)$ is unchanged while $1 - p_{out}$ increases. This results in the intersection point of the two curves to be shifted to the left-hand side. Thus, the maximum throughput appears at a lower α value.

Fig 3.5 compares the throughputs of the FD and HD systems for QPSK and 16-PSK modulations at SNR $= 20$ dB, which shows that the 16-PSK modulation significantly improves the throughput, compared to the QPSK modulation. The optimal α value for achieving the maximum throughput is invariant for these two modulation methods. The modulation method also has influences on the BER performance as detailed in the following section.

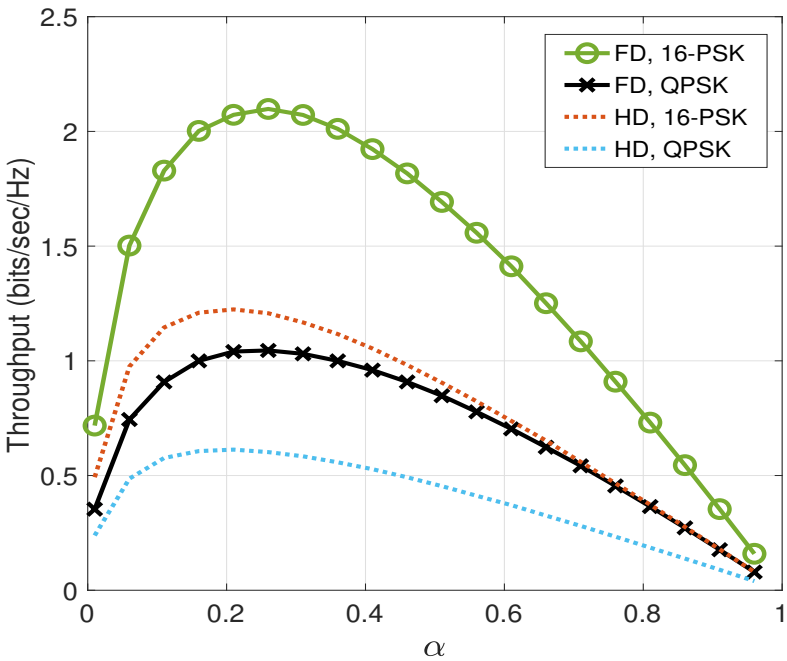

Figure 3.5: Throughput comparison between QPSK and 16-PSK modulations with the transmit SNR = 20 dB.

3.5.2 Bit Error Rate

In this section, we examine the influence of modulation schemes and α on BER of the FD-EH relaying system. Besides, we quantify the SIC performance of the PDC scheme in the FD system and compare it with the HD system.

Fig. 3.6 compares the BER for QPSK and 16-PSK modulation schemes. The result shows that the BER of QPSK is superior to 16-PSK and the difference between them is about 7.9 dB in FD systems and 8.6 dB in HD systems when the transmit SNR is 40 dB. This is because, in our EH system, the relay transmission power per symbol is the same in the two modulation schemes, thus power per bit of QPSK is double that of 16-PSK while the Euclidean distance between the two nearest constellation points is much larger, compared to 16-PSK. Fig. 3.6 also compares the BER of an HD EH relaying system and that of an FD EH relaying one with $\alpha = 0.2$. As mentioned in Section 3.5.1, $\alpha = 0.2$ can provide a large throughput but a low harvested energy. Within the duration αT, the total harvested energy of HD and FD systems are equal, but in the information transmission period, the number of the transmitted information bits is doubled for the FD scenario, compared to the HD one. This means that the transmission power per bit at the relay of

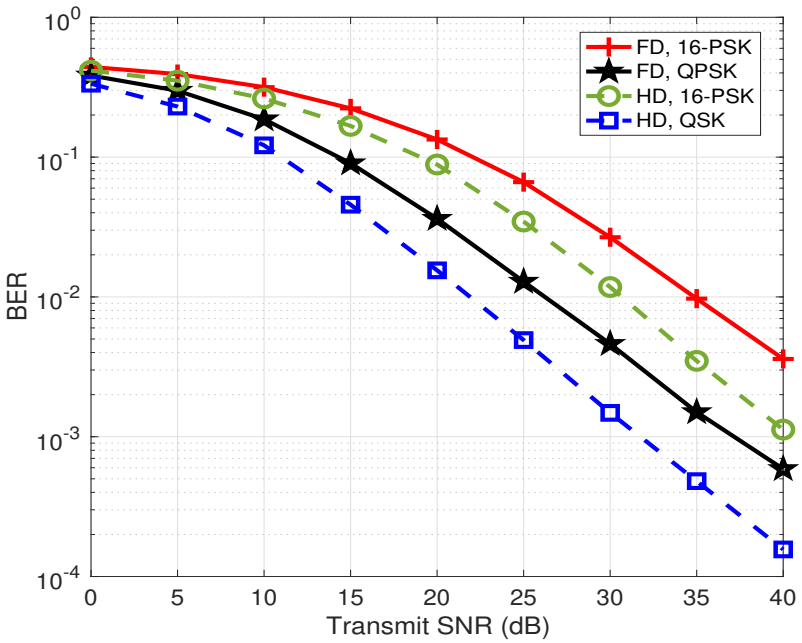

Figure 3.6: HD EH relaying system vs. FD EH relaying system with PDC for $\alpha = 0.2$.

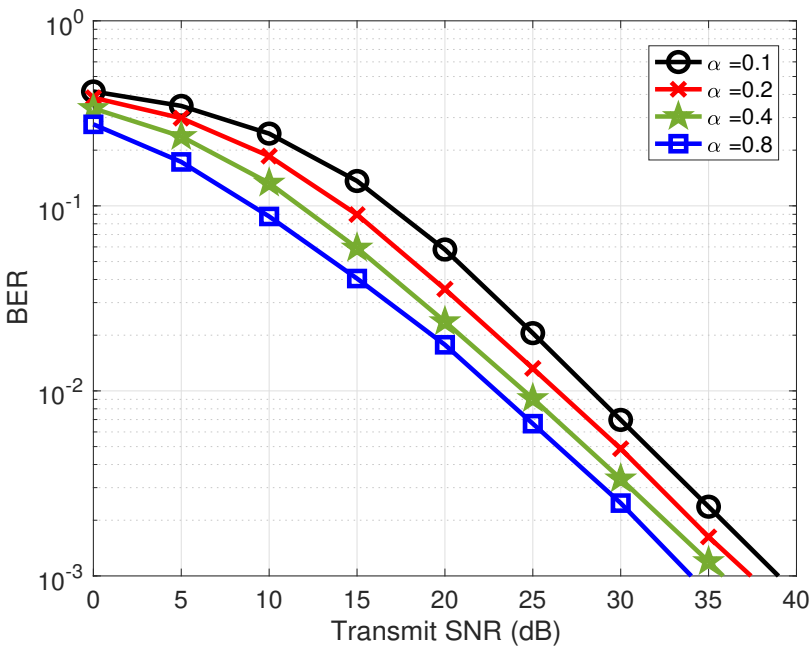

Figure 3.7: Influence of α on BER of FD EH relaying system using QPSK.

the FD system is half that in the HD one. The PDC system achieves a BER around -32 dB for QPSK and -24 dB for 16-PSK at SNR = 40 dB. The HD system achieves a BER around -38 dB for QPSK and -29 dB for 16-PSK at SNR = 40 dB. Thus, although the BER performance curve of the FD system is 5 dB inferior to that of the HD one in the 16-PSK modulation schemes, 3 dB of its inferiority is accounted for the less transmission power per bit at the relay. Equivalently, the BER curve of the FD system is only 2 dB inferior to that of the HD one if the two powers are equal. Without the PDC scheme, the desired signal cannot be detected as it is seriously corrupted by the SI signal. However, the side effect of the PDC scheme is the resulting noise as discussed in (3.18) in Section 3.4.

Fig. 3.7 examines the impact of the time fraction α on BER of the FD-EH relaying system using the QPSK modulation. The value of α decides the total harvested energy. At a high SNR value, e.g., SNR = 40 dB, BER can reach 10^{-3} even with α being as small as 0.1. When α is getting larger, especially when $\alpha > 0.5$, BER continues to be improved, but the additional BER improvement becomes smaller.

We recall from Figs. 3.4 and 3.5 that, the system throughput is high when α is in the lower half of its range; a higher value of SNR leads to a higher system throughput for all values of α, and when SNR increases, the maximum throughput appears at a lower α value. From Figs. 3.6 and 3.7, when SNR increases, the BER decreases. These observations suggest that if we want to achieve a relatively high throughput along with a low BER in an FD-EH relaying system, a joint combination of a high transmit SNR value and a low α value is expected.

3.6 Chapter Summary

In this chapter, we propose an FD relaying system assisted by the RF EH technique and the PDC scheme. In particular, the relay node harvests power from the wireless RF signal transmitted from the source node and uses this power to amplify and forward signals to the destination. Meanwhile, the PDC scheme is used at the relay node to cancel the SI signal in order to facilitate the concurrent in-band transmission and reception. The throughput and bit error performances of our system are then investigated. The simulation results

show that the EH mechanism has an influence on the system throughput and BER. An FD EH relaying system using the PDC can almost double the system throughput, compared to an HD EH relaying one. However, this high throughput in the FD system is achieved at the cost of an inferior BER performance due to the characteristics of our EH system that the FD system uses the same harvested energy as in the HD one to transmit a doubled amount of information. A relatively good performance from both throughput and BER performance perspectives can be achieved in the FD system by jointly optimizing SNR and α. For example, for the case of a medium or high transmit SNR, the value of α should be in its lower range.

This chapter considers a single-carrier FD-EH relaying system in flat fading channels with the deployment of the PDC scheme. The next chapter will consider adapting the PDC scheme to a multi-carrier OFDM FD-EH relaying system in frequency selective fading channels.

Chapter 4

Performance Evaluation of Full-Duplex OFDM Relaying Systems with Energy Harvesting in Multipath Fading Channels

4.1 Introduction

Orthogonal frequency division multiplexing (OFDM) is a spectrum-efficient technology that has been widely used in practice and is one of the candidates for 5G systems and beyond. On the other hand, EH is capable of prolonging the lifetime of energy-constrained devices. RF EH has become an important concept in 5G. An EH device fulfills its role by collecting energy from the ambient or received RF signals to replenish its energy. EH can be applied in HD single carrier relaying systems [14], HD MIMO-OFDM relaying systems [13], and orthogonal frequency division multiple access (OFDMA) downlink networks [107].

In this chapter, the performance of FD OFDM relaying systems with EH and SI cancellation using the PDC scheme is analyzed. Specifically, we use the time switching-based relaying protocol to implement EH. The harvested energy is used by the relay to forward the transmitted information from the source. To cancel the SI, the PDC scheme mentioned previously in Chapter 3 is deployed at the relay. To the best of our knowledge, our work is the pioneering work to analyze the performance of FD OFDM EH relaying networks

with the PDC cancellation method in multipath fading channels and compare it with the performance of the HD OFDM EH relaying system.

For brevity, unless otherwise stated, we refer to the *full-duplex OFDM energy harvesting relaying system* as the FD system and the *half-duplex OFDM energy harvesting relaying system* as the HD system in this chapter. The main contributions of the chapter include

- The throughput and BER performance of the FD OFDM system are investigated. It is shown that the system throughput is maximized when the time splitting factor for EH is in its lower range, typically less than 0.3. However, a small factor increases the BER. Thus, there exists a trade-off between the throughput and the BER when selecting the time splitting factor.

- We reveal that the PDC scheme effectively cancels the SI in the FD system in multipath fading channels. For the case of 16 discrete Fourier transform points, the SNR of the FD PDC system needs to increase by no more than 1 dB to achieve the same BER as the ideal full-duplex (IFD) system (without SI) and no more than to match the BER of the HD counterpart. It is worth noting that the HD counterpart only has half system throughput of the FD system. Therefore, the FD system can double the throughput and has the same BER as the HD system with a modest SNR increase.

- The maximum throughput of the FD system almost doubles that of HD system at medium-to-high SNR ranges.

The content of this chapter has been published in [40].

The rest of this chapter is organized as follows. Section 4.2 introduces the system model of our FD EH relaying system. Section 4.3 presents mathematical formulas of the signal processing. Section 4.4 provides simulation results and discussions on optimization. Finally, Section 4.5 summarizes the chapter.

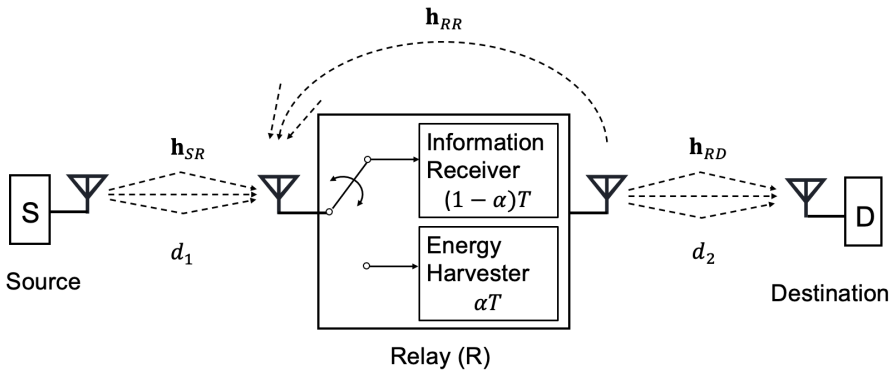

Figure 4.1: System model with multipath propagation.

4.2 System Description

We consider a dual-hop AF relaying system with FD transmission and wireless power transfer, as shown in Fig. 4.1, in which the source (S) communicates with the destination (D) with the help of the relay (R) as the direct link does not exist. The source and destination are equipped with one orthogonal dual-polarized antenna while the relay is equipped with two orthogonal dual-polarized antennas [85], i.e., one for transmission and one for the reception during the information transmission phase [40], [108]. The source node has a fixed energy supply while the relay only has a limited power supply and relies on EH from the source transmitting signals [14]. The EH model at the relay is assumed as a linear RF model [12], [14], which is applicable to the scenario when the input RF power is high [109], [110]. Besides, we adopt the OFDM technique that divides the total system bandwidth B into N sub-bands, which effectively produce N frequency-flat fading channels. At the relay, we adopt the PDC scheme to remove the SI signals in our FD system.

Let d_1 and d_2 be the distances from S to R and from R to D respectively. We use the model $\lambda_1 = d_1^{-m}$ and $\lambda_2 = d_2^{-m}$ to take into account path loss, where m denotes the path loss exponent. The channel coefficient vector of S$-$R is $\mathbf{h}_{SR} = [h_{SR,1}, \cdots, h_{SR,L}]$, R$-$D is $\mathbf{h}_{RD} = [h_{RD,1}, \cdots, h_{RD,L}]$, and the loop-back self-interference channel of the relay is $\mathbf{h}_{RR} = [h_{RR,1}, \cdots, h_{RR,L}]$, where L is the number of multipath channels.

To enable FD communication in our system, we adopt the FD TSR protocol in [16], [26], hence the whole communication process includes two phases as shown in Fig. 4.2.

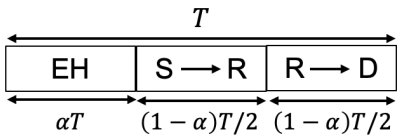

Figure 4.2: Time-switching EH architecture in a HD system.

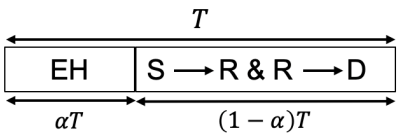

Figure 4.3: Time-switching EH architecture in a FD system.

We define T (seconds) as the whole block time, and $0 < \alpha < 1$ as the time splitting factor, then the first duration αT is used for the relay to harvest energy. The remaining block time $(1-\alpha)T$ is used for information transmission. In particular, during this phase, the transmissions between the source and relay as well as the transmission between the relay and destination occur at the same time and in the same frequency band to increase spectral efficiency. For comparison, we also consider the HD EH relaying system with the TSR protocol as shown in Fig. 4.3, where the whole process is divided into three phases. The αT duration is used for EH, the first $(1-\alpha)T/2$ time is used for information transmission from the source to the relay, and the remaining $(1-\alpha)T/2$ time is used for information transmission from the relay to the destination.

4.3 Signal Modeling

In this chapter, the lower case letter denotes the time domain scalar signal while the capital letter denotes the frequency domain scalar signal. The bold letter represents a vector or matrix in the corresponding domain. The notation ifft denotes the inverse fast Fourier transform (IFFT) and fft denotes the fast Fourier transform (FFT).

Define $\mathbf{x}$ and $\mathbf{z}$ as the macro OFDM symbols transmitted by the source and the relay with the length of N. After adding a cyclic prefix (CP) with the length of N_{CP}, $\mathbf{x}_{cp}$ is

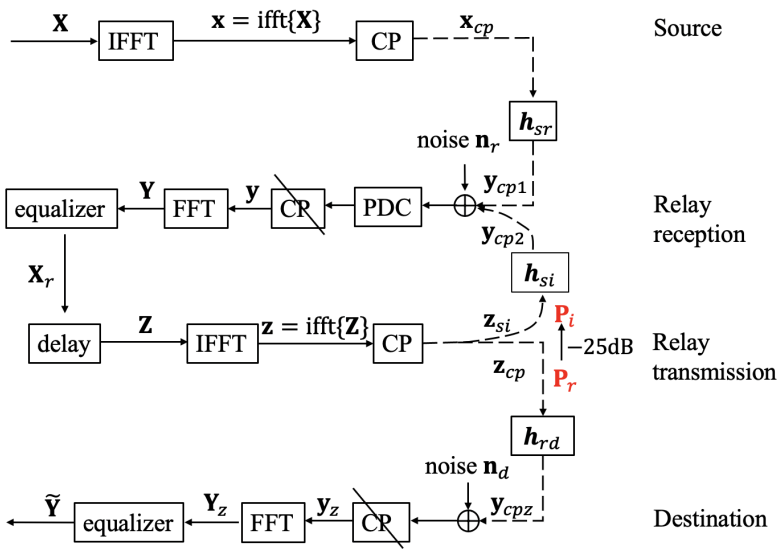

Figure 4.4: Signal diagram of a relaying, FD OFDM system with PDC scheme.

transmitted to the relay through the channel $\mathbf{h}_{SR}$ and simultaneously $\mathbf{z}_{cp}$ is transmitted to the destination through the channel $\mathbf{h}_{RD}$, where $\mathbf{x}_{cp}$ and $\mathbf{z}_{cp}$ are of the length $N_{\text{SYM}} = N + N_{\text{CP}}$. Since the relay works in the FD mode, there exists the looped-back signal denoted as $\mathbf{z}_{si}$, being propagated to its local receiver. As shown in Fig. 4.4, the relay receives the desired signal $\mathbf{y}_{cp1}$ and SI signal $\mathbf{y}_{cp2}$ from its own transmitter. Define P_s as the source transmit power, and P_r as the relay transmit power harvested within the duration αT. The power of the SI signal is P_i which is assumed to be 25 dB less than P_r, i.e., $\mathrm{P}_i = \mathrm{P}_r - 25$ dB, because of the passive cancellation technique at the relay [62], such as absorptive shielding, circulators and directional isolation, and the path loss due to the distance between the transmit and receive antennas of the relay.

Referring to Section 3.3 (cf. Eq. (3.16)), the input time-domain signal $\mathbf{y}_{in,i}$ of the PDC scheme at the relay after adding noise is

$$\mathbf{y}_{in,i} = \sqrt{\mathrm{P}_s}\,\mathbf{S}\,\mathrm{y}_{cp1,i} + \sqrt{\mathrm{P}_i}\,\mathbf{I}\,\mathrm{y}_{cp2,i} + \mathbf{n}_{r,i}, \tag{4.1}$$

where $\mathbf{n}_{r,i} = [\mathrm{n}_H \quad \mathrm{n}_V]^{\mathrm{T}}$ for $i = 1, 2, \cdots, N_{\text{SYM}} + L - 1$ is the polarized noise, $(.)^{\mathrm{T}}$ represents transpose, $\mathrm{y}_{cp1,i} \in \mathbf{y}_{cp1}$ and $\mathrm{y}_{cp2,i} \in \mathbf{y}_{cp2}$ are the $i-$th time samples of $\mathbf{y}_{cp1}$ and $\mathbf{y}_{cp2}$,

respectively. The expressions of $\mathbf{y}_{cp1}$ and $\mathbf{y}_{cp2}$ are

$$\begin{aligned}\mathbf{y}_{cp1} &= d_1^{-\frac{m}{2}}(\mathbf{x}_{cp} * \mathbf{h}_{SR}),\\ \mathbf{y}_{cp2} &= \mathbf{z}_{si} * \mathbf{h}_{RR},\end{aligned} \tag{4.2}$$

where * denotes the linear convolution between two vectors and m denotes the path loss exponent. Note that the path loss of the signal $\mathbf{y}_{cp2}$ has been considered in P_i as mentioned above.

The signal $\mathbf{y}_{in,i}$ is then processed by the PDC scheme to cancel the received SI signal $\mathrm{y}_{cp2,i}$. The output signal $\mathrm{y}_{out,i}$ of the PDC scheme is

$$\begin{aligned}\mathrm{y}_{out,i} &= \mathbf{S}^{\mathrm{H}}(\mathbf{Q}_{\mathrm{SI}}\,\mathbf{y}_{in,i})\\ &= \sqrt{\mathrm{P}_s}\,\mathbf{S}^{\mathrm{H}}(\mathbf{Q}_{\mathrm{SI}}\,\mathbf{S})\,\mathrm{y}_{cp1,i} + \sqrt{\mathrm{P}_i}\,\mathbf{S}^{\mathrm{H}}(\mathbf{Q}_{\mathrm{SI}}\,\mathbf{I})\,\mathrm{y}_{cp2,i} + \mathbf{S}^{\mathrm{H}}\,\mathbf{Q}_{\mathrm{SI}}\,\mathbf{n}_{r,i}\\ &= \sqrt{\mathrm{P}_s}\,\mathrm{y}_{cp1,i} + \mathscr{N}_{r,i},\end{aligned} \tag{4.3}$$

where $\mathscr{N}_{r,i} = \mathbf{S}^{\mathrm{H}}\,\mathbf{Q}_{\mathrm{SI}}\,\mathbf{n}_{r,i}$ is the scalar time-domain noise signal at the output of the PDC scheme. The overall output signal in a vector form for transmitting one OFDM symbol is $\mathbf{y}_{out}$. We have

$$\mathbf{y}_{out} = \sqrt{\mathrm{P}_s}\,\mathbf{y}_{cp1} + \boldsymbol{\mathcal{N}}_r = (\mathrm{P}_s/d_1^m)^{\frac{1}{2}}(\mathbf{x}_{cp} * \mathbf{h}_{SR}) + \boldsymbol{\mathcal{N}}_r, \tag{4.4}$$

where $\mathbf{y}_{out} = \{y_{out,i}\}_{i=1}^{N_{SYM}+L-1}$, $\mathbf{y}_{cp1} = \{y_{cp1,i}\}_{i=1}^{N_{SYM}+L-1}$, and $\boldsymbol{\mathcal{N}}_r = \{\mathscr{N}_{r,i}\}_{i=1}^{N_{SYM}+L-1} = \mathbf{S}^{\mathrm{H}}\,\mathbf{Q}_{\mathrm{SI}}\,\mathbf{n}_r$. The output signal $\mathbf{y}_{out}$ after removing CP is denoted as $\mathbf{y}$

$$\begin{aligned}\mathbf{y} &= (\mathrm{P}_s/d_1^m)^{\frac{1}{2}}(\mathbf{x} \oplus \mathbf{h}_{SR}) + \boldsymbol{\mathcal{N}}_r\\ &= \sqrt{\mathrm{P}_a}\,\{\mathrm{ifft}[\mathrm{fft}(\mathbf{x})\,.*\,\mathrm{fft}(\mathbf{h}_{SR})]\} + \boldsymbol{\mathcal{N}}_r\\ &= \sqrt{\mathrm{P}_a}\,\{\mathrm{ifft}[\mathrm{fft}(\mathrm{ifft}(\mathbf{X}))\,.*\,\mathrm{fft}(\mathbf{h}_{SR})]\} + \boldsymbol{\mathcal{N}}_r\\ &= \sqrt{\mathrm{P}_a}\,\{\mathrm{ifft}(\mathbf{X}\,.*\,\mathrm{fft}(\mathbf{h}_{SR}))\} + \boldsymbol{\mathcal{N}}_r,\end{aligned} \tag{4.5}$$

where $\mathrm{P}_a = \frac{\mathrm{P}_s}{d_1^m}$, $\oplus$ denotes the cyclic convolution and .* denotes the element-wise multi-

plication. After applying FFT to $\mathbf{y}$, the received signal is

$$\mathbf{Y} = \sqrt{\mathrm{P}_a}(\mathbf{X}.*\mathbf{H}_{SR}) + \mathrm{fft}(\mathcal{N}_r), \tag{4.6}$$

where $\mathbf{H}_{SR} = \mathrm{fft}(\mathbf{h}_{SR})$. Denote P_r as the average harvested power per symbol at the relay [26], and $./$ as the element-wise division between vectors. The relay transmitted signal $\mathbf{Z}$ is

$$\begin{aligned}\mathbf{Z} &= (\mathrm{P}_r/\mathrm{P}_a)^{\frac{1}{2}}(\mathbf{Y}./\mathbf{H}_{SR}) \\ &= \sqrt{\mathrm{P}_r}\mathbf{X} + [(\mathrm{P}_r/\mathrm{P}_a)^{\frac{1}{2}}\mathrm{fft}(\mathcal{N}_r)]./\mathbf{H}_{SR},\end{aligned} \tag{4.7}$$

which will be converted to the time domain, denoted as $\mathbf{z}$ in Fig. 4.4, and added with the CP. The transmitted signal from the relay in the time domain is denoted as $\mathbf{z}_{cp}$. The received signal $\mathbf{y}_{cpz}$ at the destination is

$$\mathbf{y}_{cpz} = d_2^{-\frac{m}{2}}(\mathbf{z}_{cp} * \mathbf{h}_{RD}) + \mathbf{n}_d. \tag{4.8}$$

After removing CP, the received signal at the destination is

$$\begin{aligned}\mathbf{y}_z &= d_2^{-\frac{m}{2}}(\mathbf{z} \oplus \mathbf{h}_{RD}) + \mathbf{n}_d \\ &= d_2^{-\frac{m}{2}}[\mathrm{ifft}(\mathrm{fft}(\mathbf{z}).*\mathrm{fft}(\mathbf{h}_{RD}))] + \mathbf{n}_d \\ &= d_2^{-\frac{m}{2}}[\mathrm{ifft}(\mathbf{Z}.*\mathrm{fft}(\mathbf{h}_{RD}))] + \mathbf{n}_d,\end{aligned} \tag{4.9}$$

where $\mathbf{n}_d$ is the noise at the destination with zero mean and variance σ^2. The received signal at the destination after FFT is

$$\begin{aligned}\mathbf{Y}_z &= \mathrm{fft}(\mathbf{y}_z) \\ &= d_2^{-\frac{m}{2}}(\mathbf{Z}.*\mathbf{H}_{RD}) + \mathrm{fft}(\mathbf{n}_d) \\ &= \sqrt{\mathrm{P}_b}\left[\mathbf{X} + \frac{\mathrm{fft}(\mathcal{N}_r)}{\sqrt{\mathrm{P}_a}}./\mathbf{H}_{SR}\right].*\mathbf{H}_{RD} + \mathrm{fft}(\mathbf{n}_d),\end{aligned} \tag{4.10}$$

where $\mathbf{H}_{RD} = \mathrm{fft}(\mathbf{h}_{RD})$ and $\mathrm{P}_b = \frac{\mathrm{P}_r}{d_2^m}$. The signal $\mathbf{Y}_z$ is then processed by the equalizer,

resulting the output signal $\widetilde{\mathbf{Y}}$

$$\begin{aligned}\widetilde{\mathbf{Y}} &= \mathbf{Y}_z ./(\sqrt{\mathrm{P}_b}\mathbf{H}_{RD}) \\ &= \mathbf{X} + \frac{\mathrm{fft}(\mathcal{N}_r)}{\sqrt{\mathrm{P}_a}} ./\mathbf{H}_{SR} + \frac{\mathrm{fft}(\mathbf{n}_d)}{\sqrt{\mathrm{P}_b}} ./\mathbf{H}_{RD}. \end{aligned} \tag{4.11}$$

where $\mathbf{X}$ is the signal vector transmitted from the source node presented in the frequency domain.

4.4 Simulation Results

In this section, the throughput and BER performances of the proposed FD OFDM system with an EH relay associated with the PDC scheme are analyzed. The throughput R is defined as

$$R = \mathrm{R}_c(1-\mathrm{P}_{out})(1-\alpha) \text{ bits/sec/Hz}, \tag{4.12}$$

where $\mathrm{R}_c \triangleq \log_2(1+\gamma_{\mathrm{th}})$ is the source transmission rate normalized by the system bandwidth, P_{out} is the system outage probability, defined as the probability that the received SNR is less than the threshold, i.e., $\mathrm{P}_{out} = \mathrm{p}(\gamma < \gamma_{\mathrm{th}})$, γ is the received instantaneous SNR per symbol at the destination and the threshold $\gamma_{\mathrm{th}} = 2^{\mathrm{R}_c} - 1$.

For illustration, we set the total bandwidth of the OFDM system as $B = 20$ MHz [111], distances as $d_1 = d_2 = 1$ m (except Fig. 4.5), the energy harvesting efficiency as $\eta = 1$ [14], the path loss exponent as $m = 4$, the source transmission rate as $\mathrm{R}_c = 1$ bits/sec/Hz, the CP length as $N_{\mathrm{CP}} = 4$, and the modulation scheme as binary phase-shift keying (BPSK). We define the transmit SNR as the ratio of transmitted power per OFDM symbol to the noise power. The study range of transmit SNR in this chapter is up to 50 dB [16], [17]. The noise power is $N_0 = -100$ dBm at the temperature 290°K. The performance analysis is divided into two subsections. Subsection 4.4.1 investigates the influences of the discrete FFT size N, the number of multipaths L, and SNR on the throughput. In Subsection 4.4.2, we evaluate the impact of α on the throughput for these scenarios within the range $0 < \alpha < 1$ and examines the BER when N, α and L vary.

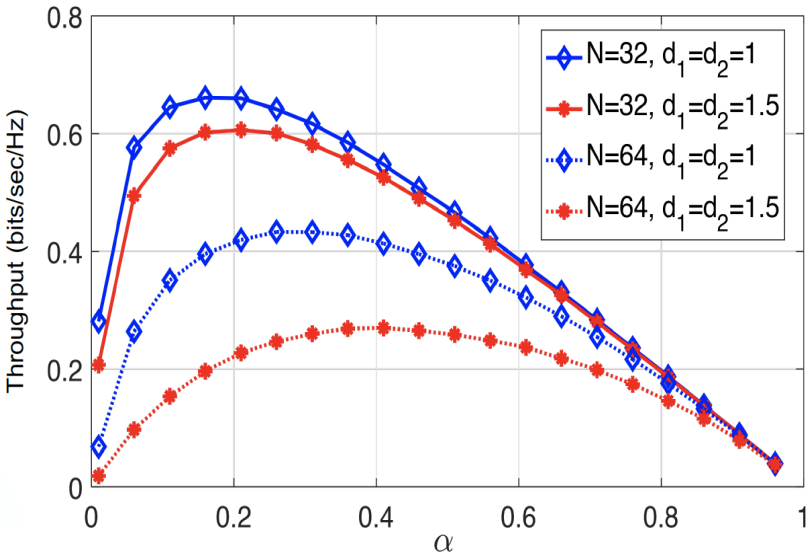

Figure 4.5: Throughput performances for different numbers of OFDM sub-bands in the FD PDC system with SNR = 50 dB and $L = 3$.

4.4.1 Throughput Performances

Fig. 4.5 examines the throughput performances in the FD system when varying the FFT size N and distances d_1 and d_2 while keeping the transmit SNR = 50 dB and $L = 3$ for a fair comparison. We assume each sub-band is a flat fading channel. Simulation results show that a higher throughput can be achieved by using a smaller N. This is because a large N narrows the sub-bands since we keep the total bandwidth of the OFDM system unchanged, which results in the increase of the inter-carrier interference (ICI) [112]. Thus, the throughput decreases when N increases. The results also show that increasing the distance significantly decreases the system throughput. This is because, in our EH relaying system, the distance affects both energy transfer and information transmission due to the path loss.

Fig. 4.6 compares the throughput performances between the FD system (solid lines) and the HD system (dashed lines) for different transmit SNR values. The system parameters are $N = 16$ and $L = 3$. Fig. 4.6 shows that, with 4 dB increase in SNR, the FD system possesses the maximum throughput of about 2.1 times higher than the HD system (e.g., $R = 0.55$ at SNR = 34 dB in the FD system vs. $R = 0.26$ at SNR = 30 dB for the HD counterpart). As pointed out later in Fig. 4.9, with this 4 dB higher SNR,

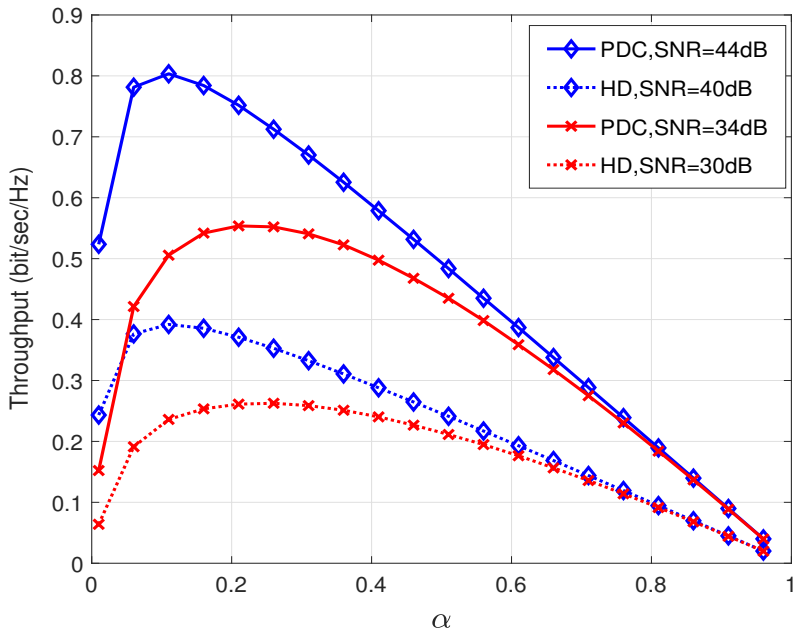

Figure 4.6: Throughput comparisons between HD system and FD PDC system for different SNR with $N = 16$ and $L = 3$.

the two systems have the same BER performances. In addition, as shown in Fig. 4.6, the maximum throughput of the HD system can only increase by 1.5 times when SNR increases by 10 dB. These two observations clearly show that our FD system significantly improves throughput compared to the HD system with only a modest SNR increase. Fig. 4.6 also shows that, a higher SNR leads to an increase of throughput for all values of α due to the fact that a high transmission power results in a lower P_{out}. Finally, when SNR increases, the optimal value of α decrease (e.g., $\alpha = 0.2$ for SNR $= 34$ dB and $\alpha = 0.1$ for SNR $= 44$ dB). The reason is that a high transmission power decreases the harvesting time required for collecting the same amount of power P_r at the relay, thus lowering the optimal time fraction α.

Fig. 4.7 illustrates the influence of the number of multipaths L on the throughput of the FD system, when $N = 16$ and SNR $= 30$ dB. It indicates a larger L results in a smaller peak throughput because the inter-symbol interference (ISI) caused by the multipath propagation increases. However, when L increases, the signal diversity also increases, which counteracts the above effect to some degree. Hence the throughput deterioration rate becomes smaller.

Fig. 4.8 compares the maximum throughput of the FD and HD systems when $N = 16$

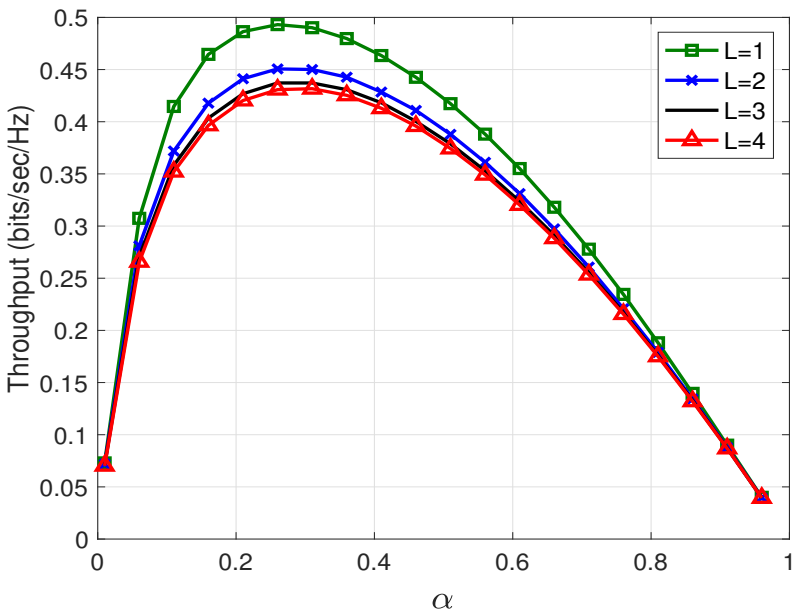

Figure 4.7: The influence of L on the system throughput in the FD system with SNR $=$ 30 dB and $N = 16$.

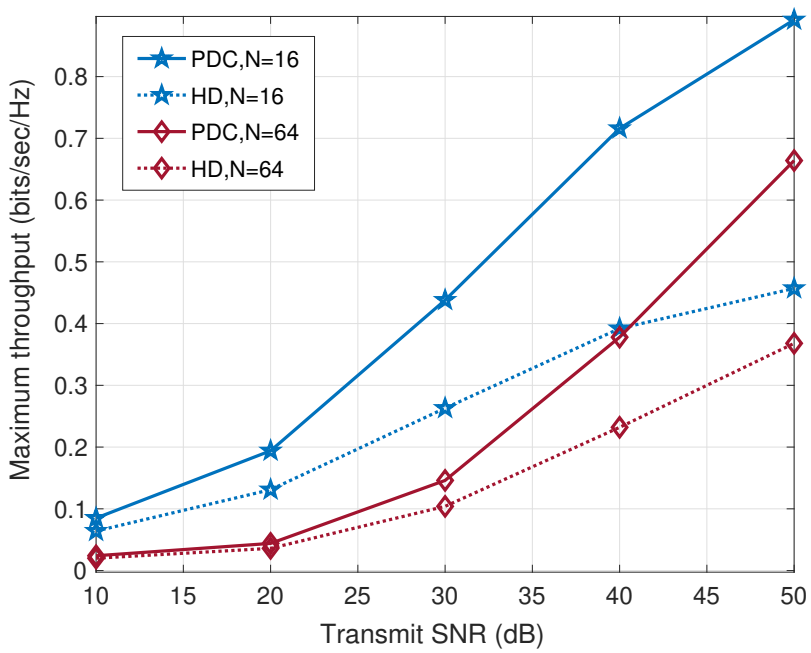

Figure 4.8: The maximum throughput comparison between HD systems and FD PDC systems with $L = 3$.

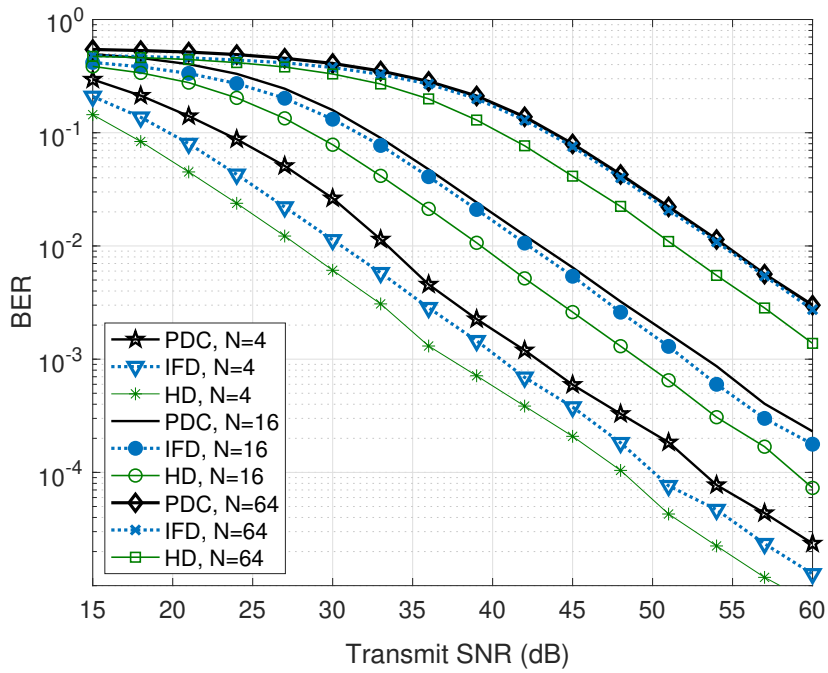

Figure 4.9: The BER performance comparison among HD, IFD and FD PDC systems for different numbers of OFDM sub-bands with $L = 3$ and $\alpha = 0.2$.

and $N = 64$. Clearly, when SNR increases, the advantage of the FD system in terms of throughput is more significant. At the high transmit SNRs, e.g., SNR $= 50$ dB, the throughput of FD systems is almost twice the HD case when $N = 16$ and 1.8 times higher when $N = 64$.

4.4.2 Bit Error Rate

Fig. 4.9 compares the BER of the HD system, the IFD system without SI, and the FD system with SI canceled by the PDC scheme when varying N. We assume $L = 3$ and $\alpha = 0.2$. For a given SNR value, the HD system performs better than the IFD system and the PDC system. To match the BER performance of the HD system in case $N = 16$, for instance, the increases of 1 dB and 4 dB in SNR are needed for the IFD system and the PDC system, respectively. Recall from Fig. 4.6 that, with this extra 4 dB in SNR, the throughput in the PDC system increases about 2.1 times over that of the HD system. This observation proves that the PDC relaying system improves the system throughput significantly at the cost of a modest SNR increase. Fig. 4.9 also shows that a smaller N results in a lower BER due to the less ICI. Recall from Fig. 4.5 that, the system throughput

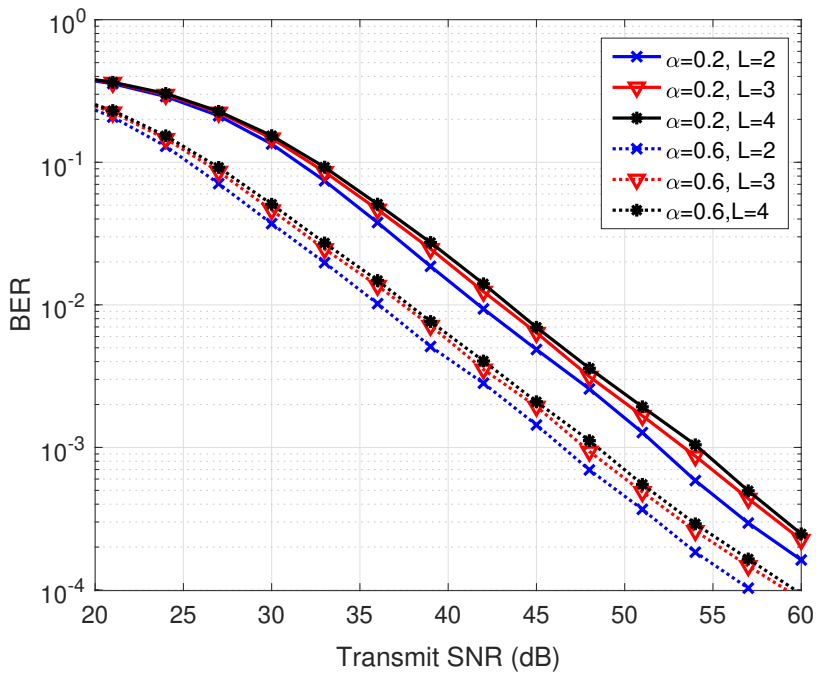

Figure 4.10: The influence of α and L on BER in FD PDC system with $N = 16$.

increases for smaller values of N. Thus the FFT size N should be chosen to be small enough, provided that each sub-band still experiences a flat fading channel, to achieve a higher throughput and a better BER performance.

Fig. 4.10 presents the impact of L and α on the BER performance of the FD system for $N = 16$. From Figs. 4.7 and 4.10, clearly, both the system throughput and BER become worse when the channels are more dispersive. Further, from Figs. 4.6 and 4.10, a higher α results in a better BER performance, but at the same time, reduces the maximum throughput. Thus there is a trade-off between throughput and BER when selecting α.

4.5 Chapter Summary

This chapter provides comprehensive throughput and BER analyses of an FD OFDM EH relaying system, where SI is eliminated by the PDC scheme, in multipath fading channels. The numerical results for the whole OFDM band are discussed in detail. The FD system substantially improves the system throughput, while maintaining the same BER by a modest increase in SNR compared to the HD counterpart. For selecting the optimal value of α, there is a trade-off between the system throughput and BER performance.

In addition, for a given α, the number of sub-bands should be chosen small enough, provided that each sub-band still experiences a flat fading channel, to achieve both high system throughput and a good BER performance. It is also revealed that the optimal time splitting factor should be less than 0.3 to maximize the FD system throughput.

In the next chapter, the analytical and numerical results of a sub-band for an FD OFDM EH relaying system will be researched.

Chapter 5

Outage Probability and Throughput Analyses in Full-Duplex OFDM Relaying Systems with Energy Harvesting

5.1 Introduction

The main aim of this chapter is to focus on a two-hop scenario where the direct link from the source to destination is not available due to obstructions or distance. An intermediary relay is deployed, which is powered by the wireless RF signal in the first phase and implements simultaneous transmission and reception at the same frequency band in the second phase. This system model can be potentially applied in various energy-constrained scenarios. For example, in wireless sensor networks, a node with a fixed power supply wants to send information to a sensor. The direct link between them is not available. So, the node needs an intermediary sensor to assist its information transmission. To prolong the lifetime of the intermediary sensor, the EH sensor is used instead of a battery-limited sensor. Another example is that a source station wants to transmit data to a destination station that is far away from the source. A relay node with a fixed energy supply is unavailable due to the rugged environment. In this scenario, deploying an EH relay is a more convenient solution to help information transmission from the source to the destination. As for the SIC, we consider the combination of antenna polarization and oblique

projection, i.e., the polarization-enabled digital self-interference cancellation scheme, to eliminate the SI at the relay. In order to demonstrate the outage probability and throughput of our proposed system, the performance of the HD EH relaying system in [14] is used as a benchmark. In this chapter, we consider a two-hop FD, amplify-and-forward, OFDM relaying network, where the relay operates based on a time-switching architecture to harvest energy from RF signals. We use a PDC scheme to cancel the self-interference signal at the relay in order to achieve FD communications. The chapter provides a comprehensive analysis of the system performances in terms of outage probability and throughput over multipath Rayleigh fading channels. Furthermore, the optimal time split between the duration of energy harvesting and signal transmission to maximize the system throughput is numerically calculated. We also derive the asymptotic lines for the expressions of outage probability and throughput at high transmit SNR. Our analysis and simulation results show that the proposed FD relaying system by utilizing a proper time split fraction can boost the system throughput significantly over an appreciable range of transmitting SNR values compared to HD relaying systems.

The main contributions of the chapter include:

- We present analytical expressions of the outage probability and the system throughput for a OFDM sub-band. Specifically, the expressions of the outage probability are derived using two methods. Our findings show that, the method that considers the product distribution of the source-relay channel and relay-destination channel is more accurate at low SNRs, and both methods are accurate at high SNRs.

- The optimal time split between the EH and information exchange phases is calculated numerically to maximize the system throughput. The outage probability decreases with the increase of the EH duration.

- A PDC scheme is used at the relay to cancel the SI signal. The results show that with this cancellation technique, the throughput of our FD relaying system can be nearly doubled compared to that of the HD relaying system.

- By comparing the FD and HD relaying architectures, the chapter demonstrates that

FD relaying can boost the system throughput with a proper time split and transmit SNR. Although HD relaying outperforms the FD relaying in terms of outage probability, the performance gap gradually diminishes when the time split factor is large.

- At a high transmit SNR, we simplify the expressions for the outage probability and the system throughput to obtain the corresponding asymptotic lines.

The content of this chapter has been published in [27].

The rest of this chapter is organized as follows. Section 5.2 introduces the system model of our FD EH relaying system and the theory of using oblique projection to cancel the SI signals at the relay. Section 5.3 models EH and information transmission processes and illustrates the analytical expressions of the outage probability, throughput, and optimal time splitting. Section 5.4 illustrates numerical results to validate the theoretical analyses and provides comparisons with a existing solution in the literature to demonstrate system performances. Section 5.5 concludes this chapter.

5.2 System and Signal Model

The system model in this chapter is same as Chapter 4. The two-hop AF FD relaying system with wireless power transfer is shown in Fig. 4.1, where no direct link between the source node and the destination node is considered. The OFDM system has M sub-bands and the FD TSR protocol is shown in Fig. 4.2. For comparison, we also consider the HD EH relaying system with the TSR protocol as shown in Fig. 4.3.

5.2.1 Relay-Assisted Transmission

In this chapter, we assume the channel coefficients $|h_{SR,l}|^2$ and $|h_{RD,l}|^2$ are independent and identically distributed (i.i.d.) exponential random variables. We have the following theorem.

Theorem 1: If $\mathbf{h}_{SR} = [h_{SR,1}, h_{SR,2}, \cdots, h_{SR,L}]$ where $h_{SR,l} \sim \mathscr{CN}(0,\Omega)$ (i.e. $|h_{SR,l}| \sim$ Rayleigh$(\Omega), l = 1, \cdots, L$), and $\mathbf{H}_{SR} = [H_{SR,1}, \cdots, H_{SR,M}] = \text{fft}(\mathbf{h}_{SR})$, where M is the num-

ber of sub-bands in the OFDM system, then $H_{SR,m}$, where $m = 1, \cdots, M$, are also Rayleigh random variables $|H_{SR,m}| \sim \text{Rayleigh}(L\Omega/M)$ if $M \geqslant L$ [71].

Proof: A Rayleigh random variable $h_{SR,l} \sim \mathscr{CN}(0,\Omega)$ with $\mathbb{E}\{|h_{SR,l}|^2\} = 1$ can be considered as a Nakagami-m random variable, i.e., $h_{SR,l} \sim$ Nakagami-m$(1,\Omega)$. It is known that $|H_{SR,m}|$ follows Nakagami-m(k',Ω'), where $k' = L/(L-1+1) = 1$ and $\Omega' = (1/M)\sum_{l=1}^{L-1}\Omega = L\Omega/M$ [72]. Thus, $|H_{SR,m}| \sim \text{Rayleigh}(L\Omega/M)$ [71].

From *Theorem* 1, it is clear that $X = |H_{SR,m}|^2$ and $Y = |H_{RD,m}|^2$ are exponentially distributed random variables. We set the mean values of X and Y as λ_s and λ_d respectively. The probability density function (PDF) $f_X(x)$ of X, the cumulative distribution function (CDF) $F_Y(y)$ of Y and the cumulative distribution function $F_Z(z)$ of $Z = XY$ can be expressed as [11], [16]

$$f_X(x) = f_{|H_{SR,m}|^2}(x) = \frac{1}{\lambda_s} e^{-\frac{x}{\lambda_s}}, \tag{5.1}$$

$$F_Y(y) = \Pr(Y < y) = 1 - e^{-\frac{y}{\lambda_d}}, \tag{5.2}$$

$$F_Z(z) = 1 - 2\sqrt{\frac{z}{\lambda_s\lambda_d}} K_1\left(2\sqrt{\frac{z}{\lambda_s\lambda_d}}\right), \tag{5.3}$$

where $K_1(\cdot)$ is the first-order modified Bessel function of the second kind [21]. In this chapter, we consider the normalised channels for fair comparisons, thus $\lambda_s = 1$ and $\lambda_d = 1$.

Let us begin with the EH phase. Define $\mathbf{X}_e = [\mathrm{X}_{e,1}, \cdots, \mathrm{X}_{e,M}]$ as the original transmitted vector in the frequency domain which contains modulated energy symbols and $\mathbf{e} = [e_1, \cdots, e_M]$ as the transmitted symbol vector used to deliver energy from the source to the relay before cyclic prefix (CP) is added. The received base-band energy signal after CP removal at the relay is expressed as

$$\begin{aligned} \mathbf{y}_e &= \sqrt{\mathrm{P}_a}(\mathbf{e} \oplus \mathbf{h}_{SR}) + \mathbf{n}_e \\ &= \sqrt{\mathrm{P}_a}\left[\text{ifft}(\text{fft}(\mathbf{e}) .* \text{fft}(\mathbf{h}_{SR}))\right] + \mathbf{n}_e, \end{aligned} \tag{5.4}$$

where $\mathrm{P}_a = \frac{\mathrm{P}_s}{d_1^m}$ and P_s represents the transmission power at the source, $\oplus$ represents cyclic

convolution, $.*$ represents element-wise multiplication, $\mathbf{n}_e$ represents the AWGN at the relay with the variance of N_0, fft represents fast Fourier transform and ifft represents inverse fast Fourier transform. Then, the received signal in the frequency domain is

$$\mathbf{Y}_e = \text{fft}(\mathbf{y}_e) = \sqrt{\text{P}_a}(\mathbf{X}_e.*\mathbf{H}_{SR}) + \mathbf{N}_e, \tag{5.5}$$

where $\mathbf{X}_e = \text{fft}(\mathbf{e})$, $\mathbf{H}_{SR} = \text{fft}(\mathbf{h}_{SR})$ and $\mathbf{N}_e = \text{fft}(\mathbf{n}_e)$. Using (5.5), the harvested energy $E_{h,m}$ for the m-th sub-carrier at the relay during αT time is given by [61]

$$E_{h,m} = \frac{\eta P_s |H_{SR,m}|^2}{d_1^m} \alpha T, \tag{5.6}$$

where $m = 1, \cdots, M$ and $0 < \eta < 1$ is the energy conversion efficiency. The relay transmitting power for the m-th sub-carrier is

$$P_{r,m} = \frac{E_{h,m}}{(1-\alpha)T} = \frac{\eta \alpha P_s X}{(1-\alpha) d_1^m}. \tag{5.7}$$

Now, we consider the FD information transmission phase. Denote $\mathbf{x} = [x_1, \cdots, x_M]$ as the transmitted information signal at the source before adding CP with the assumption of $\mathbb{E}\{|x_m|^2\} = 1$. Denote $\mathbf{z} = [z_1, \cdots, z_M]$ as the SI signal, which is the delayed version of $\mathbf{x}$ caused by the processing time of the relay. In the system with multipath transmissions, the desired received signal from the source transmitter and received SI signal from the local transmitter at the relay are denoted by $\mathbf{y}_{cp1}$ and $\mathbf{y}_{cp2}$ respectively. As a result, the overall received signal at the relay in the conventional system, i.e., without polarization, is given by

$$\mathbf{y}_r = \mathbf{y}_{cp1} + \mathbf{y}_{cp2} + \mathbf{n}_r, \tag{5.8}$$

where $\mathbf{n}_r$ is the AWGN at the relay with the variance of N_0.

As opposed to the conventional system, our system uses the dual-polarized antennas for transmission and reception. In particular, $\mathbf{x}_{cp}$ is polarized by the PS of the information signal $\mathbf{S}$, and $\mathbf{z}_{cp}$ is polarized by the PS of the SI signal $\mathbf{I}$. Thus, the desired received signal and SI signal have both horizontal and vertical components. The overall received signal

at the relay in our system is represented as

$$\begin{aligned}\mathbf{y}_r &= \mathbf{S}\mathbf{y}_{cp1} + \mathbf{I}\mathbf{y}_{cp2} + \mathbf{n}_r \\ &= \begin{bmatrix}\mathbf{y}_{1H}\\ \mathbf{y}_{1V}\end{bmatrix} + \begin{bmatrix}\mathbf{y}_{2H}\\ \mathbf{y}_{2V}\end{bmatrix} + \begin{bmatrix}\mathbf{n}_H\\ \mathbf{n}_V\end{bmatrix},\end{aligned} \tag{5.9}$$

where $\mathbf{y}_{1H}$, $\mathbf{y}_{2H}$ and $\mathbf{n}_H$ represent the horizontal components and $\mathbf{y}_{1V}$, $\mathbf{y}_{2V}$ and $\mathbf{n}_V$ represent the vertical components. After applying FFT to $\mathbf{y}_r$, the received OFDM symbol at the relay in the frequency domain is

$$\begin{aligned}\mathbf{Y}_{in} &= \mathrm{fft}(\mathbf{y}_r) \\ &= \begin{bmatrix}\mathrm{S}_1\sqrt{\mathrm{P}_a}\mathbf{X}.*\mathbf{H}_{SR}\\ \mathrm{S}_2\sqrt{\mathrm{P}_a}\mathbf{X}.*\mathbf{H}_{SR}\end{bmatrix} + \begin{bmatrix}\mathrm{I}_1\left(\sqrt{\mathbf{P}_i}.*\mathbf{Z}\right).*\mathbf{H}_{RR}\\ \mathrm{I}_2\left(\sqrt{\mathbf{P}_i}.*\mathbf{Z}\right).*\mathbf{H}_{RR}\end{bmatrix} + \mathbf{N}_r \\ &= \mathbf{S}(\sqrt{\mathrm{P}_a}\mathbf{X}.*\mathbf{H}_{SR}) + \mathbf{I}(\sqrt{\mathbf{P}_i}.*\mathbf{Z}.*\mathbf{H}_{RR}) + \mathbf{N}_r,\end{aligned} \tag{5.10}$$

where $\mathbf{X} = \mathrm{fft}(\mathbf{x})$, $\mathbf{H}_{SR} = \mathrm{fft}(\mathbf{h}_{SR})$, $\mathbf{Z} = \mathrm{fft}(\mathbf{z})$, $\mathbf{H}_{RR} = \mathrm{fft}(\mathbf{h}_{RR})$ and $\mathbf{N}_r = \begin{bmatrix}\mathrm{fft}(\mathbf{n}_H)\\ \mathrm{fft}(\mathbf{n}_V)\end{bmatrix}$. $\mathbf{P}_i$ is the power of the SI signal at the relay. $\mathbf{P}_i$ is assumed to be smaller than the transmitted power (by the relay) by 25 dB, where $\mathbf{P}_i = [P_{i,1}, \cdots, P_{i,M}]$, due to the difference in polarization schemes as well as some passive SI cancellation techniques, such as absorptive shielding, circulator and directional isolation [70]. Then, $\mathbf{Y}_{in}$ is processed by the PDC scheme, which includes two main operations. Firstly, we use the oblique projection operator $\mathbf{Q}_{\mathrm{SI}}$ to maintain the desired signal and cancel the SI signal of $\mathbf{Y}_{in}$, i.e., $\mathbf{Q}_{\mathrm{SI}}[\mathbf{S} \quad \mathbf{I}] = [\mathbf{S} \quad \mathbf{0}]$. Secondly, we use $\mathbf{S}^{\mathrm{H}}$ to de-polarize the desired signal, i.e., $\mathbf{S}^{\mathrm{H}}\mathbf{S} = 1$. Thus, the output signal $\mathbf{Y}_{out}$ of the PDC scheme is given by

$$\begin{aligned}\mathbf{Y}_{out} &= \mathbf{S}^{\mathrm{H}}\mathbf{Q}_{\mathrm{SI}}\mathbf{Y}_{in} \\ &= \mathbf{S}^{\mathrm{H}}\mathbf{Q}_{\mathrm{SI}}\mathbf{S}(\sqrt{\mathrm{P}_a}\mathbf{X}.*\mathbf{H}_{SR}) \\ &+ \mathbf{S}^{\mathrm{H}}\mathbf{Q}_{\mathrm{SI}}\mathbf{I}(\sqrt{\mathbf{P}_i}.*\mathbf{Z}.*\mathbf{H}_{RR}) + \mathbf{S}^{\mathrm{H}}\mathbf{Q}_{\mathrm{SI}}\mathbf{N}_r \\ &= \sqrt{\mathrm{P}_a}(\mathbf{X}.*\mathbf{H}_{SR}) + \mathcal{N}_r,\end{aligned} \tag{5.11}$$

where $\mathcal{N}_r = \mathbf{S}^{\mathrm{H}}\mathbf{Q}_{\mathrm{SI}}\mathbf{N}_r$ is the additional noise component caused by the PDC scheme, which has a variance of $\frac{MN_0}{2}$. After applying equalization to the signal $\mathbf{Y}_{out}$, we obtain $\mathbf{Y}_r$

$$\mathbf{Y}_r = \sqrt{\mathrm{P}_a}\mathbf{X} + \mathcal{N}_r./\mathbf{H}_{SR}. \tag{5.12}$$

With the AF protocol, the power of the input signal for the m-th sub-carrier will be amplified at the relay by a factor $\xi_m^{\frac{1}{2}}$ which is given by

$$\xi_m = \frac{P_{r,m}}{\frac{P_s}{d_1^m} + \frac{N_0}{2}\frac{1}{X}}, \tag{5.13}$$

where the denominator $\frac{P_s}{d_1^m} + \frac{N_0}{2X}$ is the power constraint factor, i.e., the power of the received signal per sub-carrier at the relay using (5.12). Substitute (5.7) into (5.13), we obtain

$$\xi_m = \frac{2\alpha\eta P_s X^2}{(1-\alpha)(2P_s X + N_0 d_1^m)}. \tag{5.14}$$

Thus, the polarized received OFDM symbol at the destination after FFT is

$$\mathbf{Y}_p = \sqrt{d_2^{-m}}\mathbf{I}\big(\boldsymbol{\xi}^{\frac{1}{2}}.*\mathbf{Y}_r.*\mathbf{H}_{RD}\big) + \mathbf{N}_d, \tag{5.15}$$

where $\boldsymbol{\xi} = [\xi_1, \cdots, \xi_M]$, $\mathbf{H}_{RD} = \mathrm{fft}(\mathbf{h}_{RD})$ and $\mathbf{N}_d = \begin{bmatrix} \mathrm{fft}(\mathbf{n}_{dH}) \\ \mathrm{fft}(\mathbf{n}_{dV}) \end{bmatrix}$ is the AWGN at the destination with variance of N_0, where $\mathbf{n}_{dH}$ represents the horizontal component and $\mathbf{n}_{dV}$ represents the vertical component. The signal $\mathbf{Y}_p$ then is de-polarized by $\mathbf{I}^{\mathrm{H}}$. The received OFDM symbol at the destination after de-polarization and equalization is

$$\begin{aligned}
\mathbf{Y}_d &= \Big[\sqrt{d_2^{-m}}\mathbf{I}^{\mathrm{H}}\mathbf{I}\big(\boldsymbol{\xi}^{\frac{1}{2}}.*\mathbf{Y}_r.*\mathbf{H}_{RD}\big) + \mathbf{N}_d\Big]./\mathbf{H}_{RD} \\
&= \sqrt{d_2^{-m}}\Big[\boldsymbol{\xi}^{\frac{1}{2}}.*\big(\sqrt{\mathrm{P}_a}\mathbf{X} + \mathcal{N}_r./\mathbf{H}_{SR}\big)\Big] + \mathbf{N}_d./\mathbf{H}_{RD} \\
&= \underbrace{\sqrt{\frac{P_s\boldsymbol{\xi}}{d_1^m d_2^m}}.*\mathbf{X}}_{\text{signal}} + \underbrace{\sqrt{\frac{\boldsymbol{\xi}}{d_2^m}}.*\mathcal{N}_r./\mathbf{H}_{SR} + \mathbf{N}_d./\mathbf{H}_{RD}}_{\text{noise}},
\end{aligned} \tag{5.16}$$

In theory, as illustrated in (3.10), (3.11), and (5.11), the oblique projection operator of the PDC scheme is able to completely cancel the SI signal. However, as a side effect,

the cancellation scheme changes the power of the noise at the relay as shown in (5.11), which will impact the outage probability and throughput. As a result, the impact of the cancellation scheme is considered in the new noise term, indicated as $\sqrt{\frac{\boldsymbol{\xi}}{d_2^m}}.*\boldsymbol{\mathcal{N}}_r./\mathbf{H}_{SR}$ in (5.16). Thus, the instantaneous SNR of m-th sub-carrier at the destination is considered, which is denoted as $\gamma_D = \frac{\text{signal power}}{\text{noise power}}$. The expression of γ_D is represented below in (5.17), where $X = |H_{SR,m}|^2$ and $Y = |H_{RD,m}|^2$.

5.2.2 Outage Probability

In our system, the outage probability P_{out} is defined as the instantaneous system SNR γ_D in a sub-carrier being smaller than a threshold SNR γ_{th}, where $\gamma_{th} = 2^{R_{th}} - 1$ and R_{th} is the threshold transmission rate in $bits/sec/Hz$. Using (5.17), the outage probability of m-th sub-carrier at the destination is given by

$$\begin{aligned} P_{out} &= \Pr\{\gamma_D < \gamma_{th}\} \\ &= \Pr\left\{\frac{b_1 X^2 Y}{b_2 X + c_1 + c_2 XY} < 1\right\}, \end{aligned} \tag{5.18}$$

where

$$\begin{aligned} b_1 &= 2\alpha\eta P_s^2, \\ b_2 &= \gamma_{th} 2 P_s N_0 d_1^m d_2^m (1-\alpha), \\ c_1 &= \gamma_{th} N_0^2 (d_1^m)^2 d_2^m (1-\alpha), \\ c_2 &= \gamma_{th} \alpha\eta N_0 d_1^m P_s. \end{aligned} \tag{5.19}$$

The outage probability of our FD EH relaying system is calculated by two methods, which are then compared with that in the HD EH relaying system proposed in [14]. The corresponding time-switching architectures are shown in Fig. 4.3. The aim of deriving two different methods to compute the outage probability is to show a trade-off between ac-

---

$$\gamma_D = \frac{\frac{P_s \xi_m}{d_1^m d_2^m}}{\frac{\xi_m N_0}{2 d_2^m X} + \frac{N_0}{Y}} = \frac{2\alpha\eta P_s^2 X^2 Y}{2 P_s N_0 d_1^m d_2^m (1-\alpha) X + N_0^2 (d_1^m)^2 d_2^m (1-\alpha) + \alpha\eta N_0 d_1^m P_s X Y}. \tag{5.17}$$

curacy, especially at low SNRs, and the computational complexity of the two methods. Theoretically, Method 1 considers the distributions of the exponential random variables X and Y independently. This method is simpler than Method 2, i.e., Method 1 only involves a Bessel function, while Method 2 involves the integral of a Bessel function. However, Method 2 considers the product distribution of the independent random variables X and Y, which we believe is a better model for relaying systems as the outage probability of the source-relay link affects the outage probability of the relay-destination link in practice. The detailed expressions and analyses are elaborated as follows.

Method 1

This method directly employs the PDF of the exponential random variable X in (5.1) and the CDF of the exponential random variable Y in (5.2). The outage probability derived by Method 1 is

$$\begin{aligned} P_{out1} &= \Pr\left\{\frac{b_1X^2Y}{b_2X+c_1+c_2XY} < 1\right\} \\ &= \Pr\left\{\left(b_1X^2-c_2X\right)Y < b_2X+c_1\right\} \\ &= \begin{cases} \Pr\left\{Y < \frac{b_2X+c_1}{b_1X^2-c_2X}\right\}, & X > \frac{c_2}{b_1} \\ 1, & X \leqslant \frac{c_2}{b_1} \end{cases}. \end{aligned} \tag{5.20}$$

The third equality in (5.20) follows from the fact that if $X \leqslant \frac{c_2}{b_1}$, then $b_1X^2 - c_2X$ will be a negative number, and the probability of Y being greater than a negative number is always 1. Substituting (5.1) and (5.2) into (5.20), we have

$$\begin{aligned} P_{out1} &= \int_{\frac{c_2}{b_1}}^{\infty} \Pr\left(Y < \frac{c_1+b_2x}{b_1x^2-c_2x}\right) f_X(x)dx + \int_0^{\frac{c_2}{b_1}} f_X(x)dx \\ &= \int_{\frac{c_2}{b_1}}^{\infty} \left[1 - e^{-\frac{b_2x+c_1}{\lambda_d(b_1x^2-c_2x)}}\right] f_X(x)dx + \int_0^{\frac{c_2}{b_1}} f_X(x)dx \\ &= 1 - \frac{1}{\lambda_s}\int_{\frac{c_2}{b_1}}^{\infty} e^{-\left(\frac{b_2x+c_1}{\lambda_d(b_1x^2-c_2x)}+\frac{x}{\lambda_s}\right)} dx. \end{aligned} \tag{5.21}$$

Equation (5.21) involves the integral of an exponential function in terms of the computational complexity. To obtain the closed-form analytical result of the outage probability,

we simplify (5.21) at high transmit SNRs. The factor $c_1 = \gamma_{th} N_0^2 (d_1^m)^2 d_2^m (1-\alpha) \approx 0$ at a high SNR because the noise variance terms N_0^2 is negligible. Using $\int_0^\infty e^{-\frac{\beta}{4x}-\gamma x} dx = \sqrt{\frac{\beta}{\gamma}} K_1(\sqrt{\beta\gamma})$ [21, §3.324.1], we obtain the approximated outage of Method 1 at high transmit SNRs as below

$$\tilde{P}_{out1} \approx 1 - \frac{1}{\lambda_s} \int_{\frac{c_2}{b_1}}^{\infty} e^{-\left(\frac{b_2}{\lambda_d (b_1 x - c_2)} + \frac{x}{\lambda_s}\right)} dx. \tag{5.22}$$

We define a new variable $z \triangleq b_1 x - c_2$.

$$\begin{aligned}
\tilde{P}_{out1} &\approx 1 - \frac{1}{\lambda_s} \int_0^{\infty} e^{-\left(\frac{b_2}{z\lambda_d} + \frac{z+c2}{b_1 \lambda_s}\right)} dz \\
&= 1 - \frac{e^{-\frac{c_2}{b_1 \lambda_s}}}{b_1 \lambda_s} \int_0^{\infty} e^{-\left(\frac{b_2}{z\lambda_d} + \frac{z}{b_1 \lambda_s}\right)} dz \\
&= 1 - e^{-\frac{c_2}{b_1 \lambda_s}} u K_1(u),
\end{aligned} \tag{5.23}$$

where $u = \sqrt{\frac{4b_2}{b_1 \lambda_s \lambda_d}}$ and $K_1(\cdot)$ is the first-order modified Bessel function of the second kind [21]. Thus, we obtain the closed-form expression of the approximated outage probability of Method 1. In (5.23), the expression involves the Bessel function. Although (5.23) is relatively simple to compute numerically by common mathematical software packages such as MATLAB and MAPLE, it can be simplified further in high transmit SNRs using the series expansion of $uK_1(u)$ at $u = 0$ to approximate the Bessel function by a polynomial. The derived asymptotic line of the outage probability of Method 1 against the transmit SNR values can be represented as

$$\begin{aligned}
P_\infty &= 1 - e^{-\frac{c_2}{b_1 \lambda_s}} \left(\lim_{\text{SNR}\to\infty} u K_1(u) \right) \\
&= 1 - e^{-\frac{c_2}{b_1 \lambda_s}} \Big(1 + \frac{1}{4} u^2 (2\log(u) + 2\gamma - 1 - \log(4)) \\
&+ \frac{1}{64} u^4 (4\log(u) + 4\gamma - 5 - 4\log(2)) + O(u^6) \Big),
\end{aligned} \tag{5.24}$$

where γ is the Euler-Mascheroni constant[73] and O is the Big-O notation[76].

Method 2

This method considers the product distribution of the independent random variables X and Y in (5.3). Using the definition of outage probability in (5.18), we have

$$P_{out} = \Pr\{\gamma_D < \gamma_{th}\}. \tag{5.25}$$

Substituting the instantaneous SNR in (5.17), the outage probability is

$$\begin{aligned} P_{out} &= \Pr\left\{\frac{b_1 X^2 Y}{b_2 X + c1 + c2XY} < 1\right\} \\ &= \Pr\left\{\left(b_1 X - c_2\right) XY < b_2 X + c_1\right\}, \end{aligned} \tag{5.26}$$

where $X = |H_{sr,m}|^2$ and $Y = |H_{rd,m}|^2$. Utilizing the expression in (5.1) and (5.3), the system outage probability can be derived by Method 2

$$\begin{aligned} P_{out2} &= \begin{cases} \Pr\left\{XY < \frac{c_1 + b_2 X}{b_1 X - c_2}\right\}, & X > \frac{c_2}{b_1} \\ 1, & X \leqslant \frac{c_2}{b_1} \end{cases} \\ &= \int_{\frac{c_2}{b_1}}^{\infty} \Pr\left(Z < \frac{c_1 + b_2 x}{b_1 x - c_2}\right) f_X(x) dx + \int_0^{\frac{c_2}{b_1}} f_X(x) dx. \end{aligned} \tag{5.27}$$

Using conditional probability, (5.27) can be rewritten as

$$\begin{aligned} P_{out2} &= \int_{\frac{c_2}{b_1}}^{\infty} F_Z\left(\frac{c_1 + b_2 x}{b_1 x - c_2}\right) f_X(x) dx + \int_0^{\frac{c_2}{b_1}} f_X(x) dx \\ &= \int_{\frac{c_2}{b_1}}^{\infty} \left[1 - v K_1(v)\right] f_X(x) dx + \int_0^{\frac{c_2}{b_1}} f_X(x) dx \\ &= 1 - \frac{1}{\lambda_s} \int_{\frac{c_2}{b_1}}^{\infty} e^{-\frac{x}{\lambda_s}} \left[v K_1(v)\right] dx, \end{aligned} \tag{5.28}$$

where $v = 2\sqrt{\frac{c_1 + b_2 x}{\lambda_s \lambda_d (b_1 x - c_2)}}$. The derivation of (5.28) is illustrated in Appendix A. The expression of the outage probability involves the integral of a product of an exponential function and a Bessel function. Finding a closed-form solution of the outage probability in this case is thus very challenging.

5.2.3 Throughput and Optimization

In the FD EH system with the AF protocol, the instantaneous throughput of m-th subcarrier at the destination is defined as

$$R_{AF}(\alpha) = (1 - P_{out}^{AF})(1-\alpha)R_{th}. \tag{5.29}$$

Using (5.23), if SNR $\to \infty$, $uK_1(u) \to 1$ we have the upper bound of the throughput

$$R_{up}(\alpha) = e^{-\frac{c_2}{b_1\lambda_s}}(1-\alpha)R_{th}. \tag{5.30}$$

The optimal α could be obtained by solving the equation $\frac{dR_{AF}(\alpha)}{d\alpha} = 0$. The first derivative D_{AF} of the throughput is given in (5.31), where $\sigma_1 = \sqrt{\frac{N_0 d_1^m d_2^m \gamma_{th}(1-\alpha)}{\lambda_s \lambda_d P_s \alpha \eta}}$. Thus, optimal α could be obtained by solving the following optimization problem

$$\begin{aligned} &\sigma_1 K_0(2\sigma_1) = \alpha K_1(2\sigma_1) \\ &\text{subject to } 0 < \alpha < 1. \end{aligned} \tag{5.32}$$

However, because the Bessel function is involved in the analytical expression, finding a closed-form solution of α is difficult. Therefore, the optimal α will be numerically evaluated using the Matlab build-in function "solve" based on the given system parameters, including, source power P_s, energy harvesting efficiency η, source to relay distance d_1, relay to destination distance d_2, path loss exponent m, noise variance N_0, threshold SNR γ_{th}, mean value λ_s of the variable X and mean value λ_d of the variable Y.

5.3 Numerical Results

In this section, we present simulation results to validate our previous analytical expression and investigate the influence of key system parameters, including the optimal time split-

---

$$D_{AF} = \frac{dR_{AF}(\alpha)}{d\alpha} = \frac{2N_0 R_{th} d_1^m d_2^m \gamma_{th} e^{-\frac{N_0 d_1^m \gamma_{th}}{2\lambda_s P_s}}(1-\alpha)(\sigma_1 K_0(2\sigma_1) - \alpha K_1(2\sigma_1))}{\lambda_s \lambda_d P_s \alpha^2 \eta \sigma_1}. \tag{5.31}$$

ting factor α in the TSR protocol and the SNR in the transmitter, on the outage probability and throughput of the system. The optimal α is numerically obtained, which results in the maximum system throughput. The channels are Rayleigh fading channels which contain random values drawn from the standard normal distribution. The 1024-point FFT is used in the OFDM system. N_s OFDM symbols are transmitted in total. The instantaneous SNR of a sub-carrier at the destination is calculated and compared with the threshold SNR γ_{th}. The outage probability in the simulation is calculated as the number of times when the instantaneous SNR of a sub-carrier is smaller than the threshold SNR γ_{th} divided by the total numbers of transmitting symbols N_s. Unless otherwise stated, we set the targeted source transmission rate as $R_{th} = 3$ bits/sec/Hz [11], [14], hence the outage SNR threshold is $\gamma_{th} = 2^{R_{th}} - 1 = 7$. The EH efficiency is set to $\eta = 0.9$. The path loss exponent is set to $m = 3$, which typically represents a path loss exponent in a wireless sensor network environment [113]. The mean values λ_s and λ_d are assumed to be one. We consider a small sensor network, where the direct link between the source and the destination is not available, for example, due to the obstructions. Therefore, a relay is deployed to assist their communications. For illustration, the S-R and the R-D distances are set to $d_1 = d_2 = 1.2$ m, except in Fig. 5.7 where distances vary up to 4 meters. It is worth noting that the analyses, mentioned in this chapter, is valid for any distance values.

Figs. 5.1 and 5.2 show the outage probability with respect to the transmit SNR. The derived analytical expressions of Method 1 and its approximation (defined in figure as "A.M1" and "A.$\tilde{M}$1") are shown in (5.20) and (5.23) respectively. The analytical expression of Method 2 in (5.28) is shown in Figs. 5.1 and 5.2 as "A.M2". The simulation result of the FD system defined in figures as "S. L=50" and the analytical result of the HD system defined as "A. HD".

Fig. 5.1 shows that the closed-form approximation result of Method 1 is reasonably accurate for calculating the system outage probability as it is very close to the exact analytical results. Besides, Fig. 5.1 also shows that analytically the outage probability of Method 2 is slightly higher than the Method 1 when the transmit SNR is smaller than 30 dB, especially in the large α ($\alpha = 0.6$) case. The similarity of these two methods

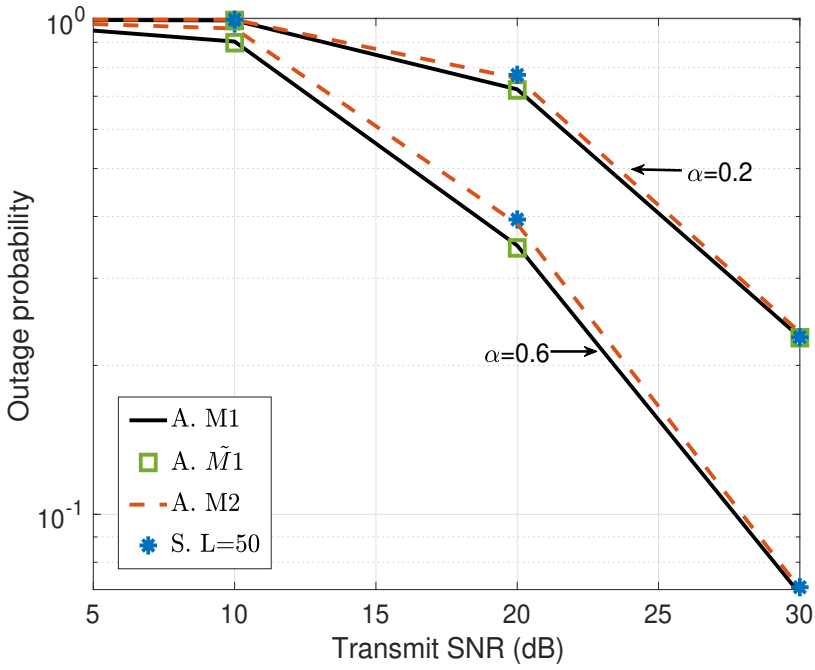

Figure 5.1: Outage probability vs. transmit SNR. Three analytical results compared with simulation in an FD system.

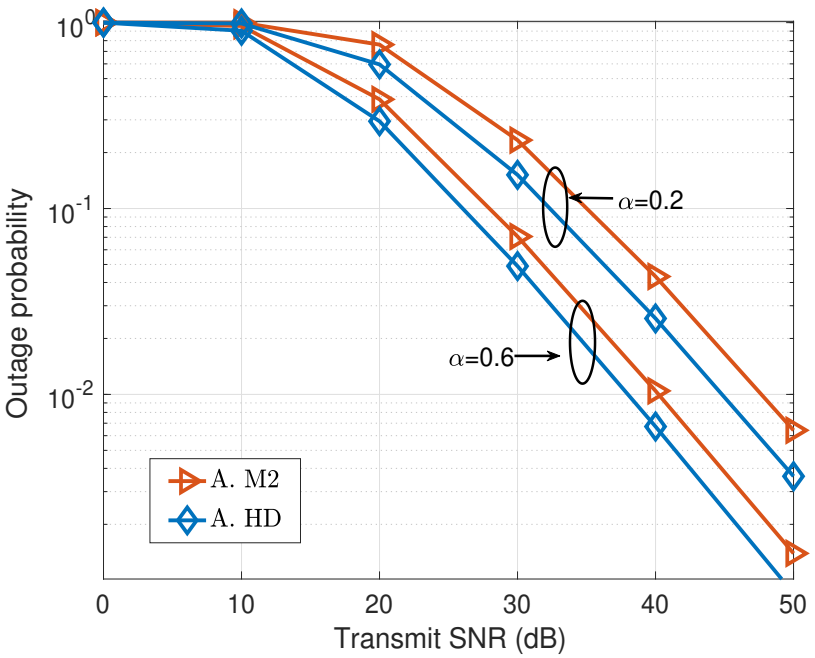

Figure 5.2: Outage probability vs. transmit SNR. The analytical result of Method 2 compared with analytical result in an HD system.

is that the variables X and Y are considered to be independent since there are Rayleigh fading channels in our system. However, the difference is that the Method 1 considers the PDF and CDF of the variables separately, i.e., $\Pr\{Y < \frac{c_1+b_2X}{b_1X^2-c_2X}\}$, while Method 2 constructs the product of two independent random variables to model the relaying system, i.e., $\Pr\{XY < \frac{c_1+b_2X}{b_1X-c_2}\}$. By comparing the analytical results with the simulation results, we find that Method 2 is more accurate than Method 1, i.e., the simulation result is much closer to Method 2, in the lower range of SNRs, while computationally more complex. Both methods have similar accuracy at high SNRs. This means that in the relaying system, the theoretical expression of outage probability is more accurate if we consider the product distribution of X and Y, rather than the PDF and CDF of X and Y respectively.

Fig. 5.2 compares the outage probabilities in our FD EH relaying system and the HD EH relaying system in [14]. As shown in Figs. 4.2 and 4.3, if FD systems spend the same amount of time on EH as in HD systems, theoretically double the amount of information can be transmitted in the former systems. This means the energy used to re-transmit each information symbol will be half than that in the HD counterpart. Thus, in Fig. 5.2, for a fair comparison, the transmitted power per OFDM symbol in FD systems at the relay is intentionally set to half of that in the HD systems. Fig. 5.2 shows that in 40 dB SNR, the outage probabilities of FD are 0.043 and 0.010 while those of HD are 0.026 and 0.007 respectively. The performance difference of the FD system and the HD system becomes smaller with an increase of α.

Fig. 5.3 plots the outage probability of analytical results and simulation results in the FD system for different values of α with the transmit SNR = 30 dB. The HD system is also plotted as the reference. The results show that with the increase of the number of multipath L, the system outage probability also increases. Besides, the simulation results match very well our theoretical results. In addition, the outage probability of the FD system is about 1.5 times higher than the HD system. Similar to Fig. 5.2, the reason for the HD communication being better than the FD communication in terms of the outage probability is that the HD consumes the same amount of harvested energy at the relay to transmit half the amount of information to the destination, compared with the FD. Note

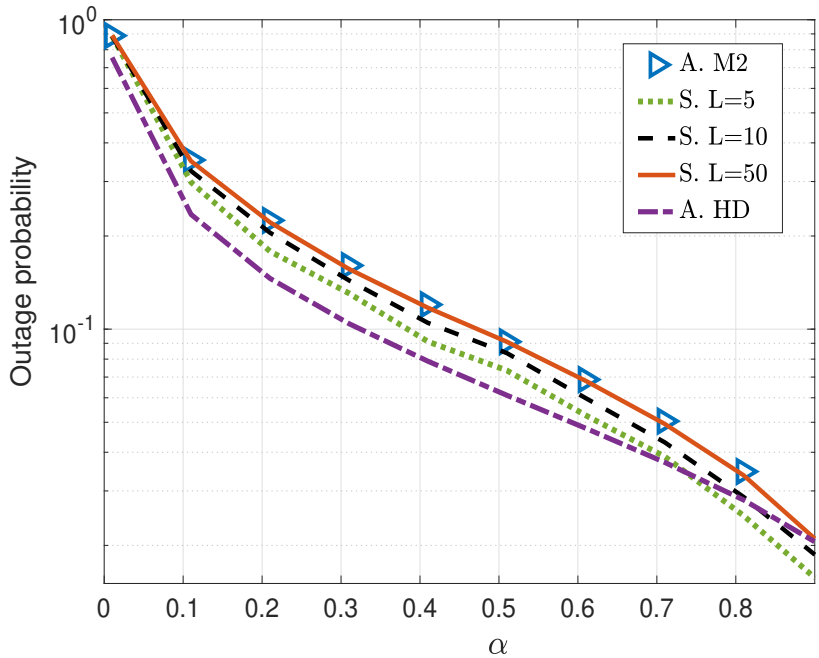

Figure 5.3: Outage probability vs. α for transmit SNR = 30 dB.

that although the HD system has a better outage probability, its spectral efficiency and throughput are significantly lower than those in the FD system as detailed below.

Fig. 5.4 illustrates the throughput comparison between the HD scenario and the FD scenario with the transmit SNR = 30 dB. Fig. 5.4 shows that for both FD and HD systems, throughput increase as α increases from 0 to the optimal α (0.2 for FD case and 0.16 for HD case) but later decreases from its optimal value. This is because if α is less than its optimal value, less energy is harvested, which results in a larger outage probability (cf. in (5.29)). On the other hand, more time is wasted on EH and less time is available for information transmission when α is greater than the optimal value. Thus, smaller values of throughput are observed when α is away from the optimal α value. In addition, when both the FD system and HD system choose their optimal α, the throughput of the former is 1.85 times than that of the latter even though the same amount of time is spent on EH. This figure also shows that the analytical result agrees with the simulation results, which verifies the analytical expression presented in (5.29).

Fig. 5.5 plots the first derivative of the FD system throughput (cf. in (5.31)) within the range $0 < \alpha < 1$. As shown in the figure, when $D_{AF} = 0$, we obtain the optimal α values, which are 0.41, 0.19, and 0.08 for transmit SNR values of 20 dB, 30 dB, and

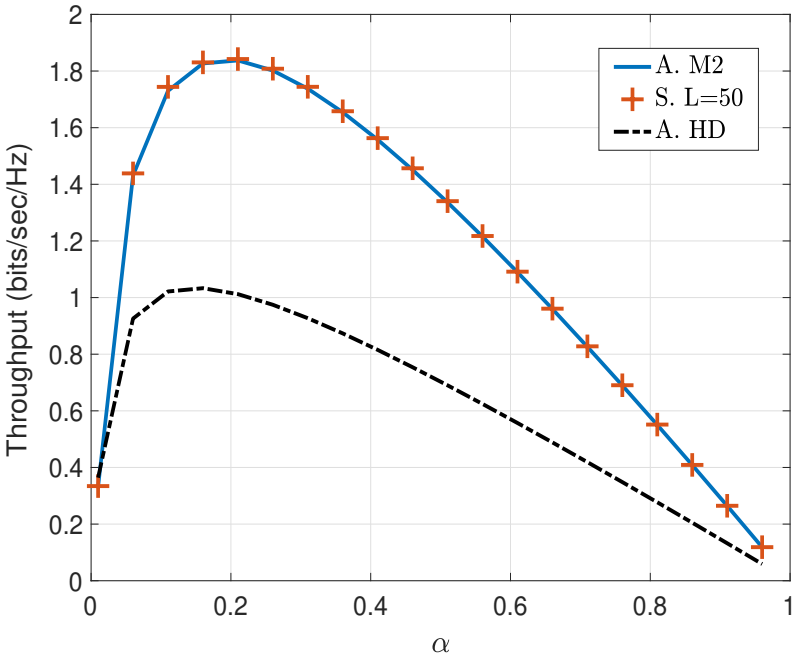

Figure 5.4: Throughput vs. α for transmit SNR = 30 dB.

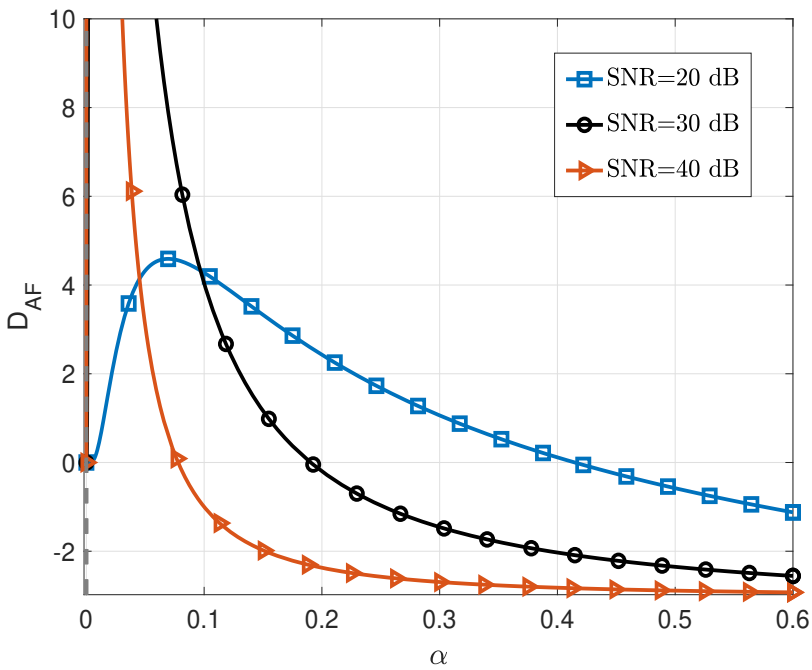

Figure 5.5: The first derivative of the throughput vs. α for the transmit SNR of 20, 30 and 40 dB.

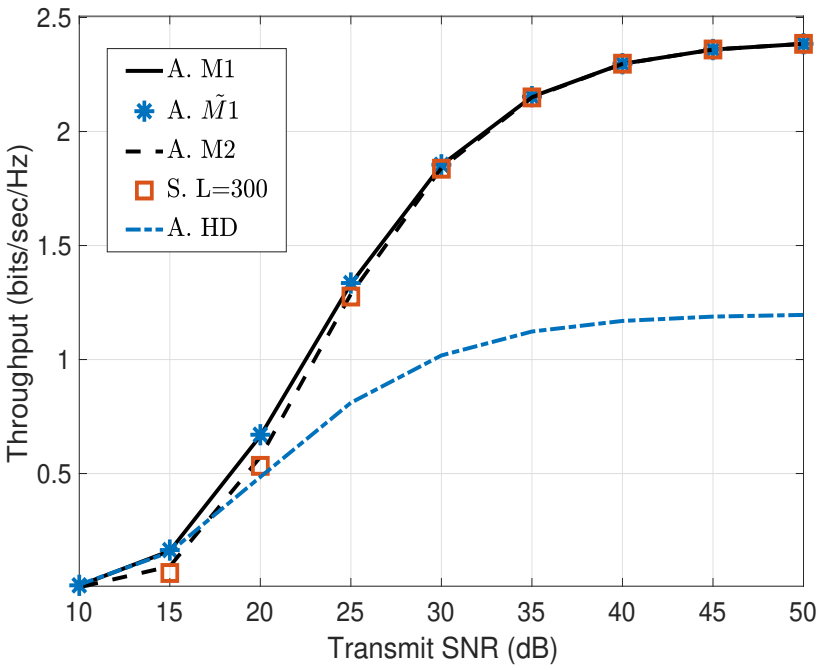

Figure 5.6: Throughput vs. transmit SNR for $\alpha = 0.2$.

40 dB respectively. This result shows that the optimal value decreases with the increase of the transmit SNR. Besides, the optimal value we obtained from the first derivative for the transmit SNR $= 30$dB is consistent with the optimal α obtained in Fig. 5.4. Thus, it is clear that the optimal α can be numerically calculated by giving system parameters as shown in (5.32).

Fig. 5.6 illustrates the throughput performances of three analytical results for the FD system with the analytical throughput of the HD system serving as a benchmark. The derived analytical expressions of Method 1 in (5.20) and its approximation in (5.23) are denoted in this figure as "A.$M1$" and "A.$\tilde{M}1$" respectively. The expression of Method 2 in (5.28) is defined as "A.$M2$". This figure also shows the simulated throughput of our FD system for $L = 300$. Referring to Figs. 5.1 and 5.6, Method 2 is seen to be a more accurate approach than Method 1 for both the outage probability and throughput when transmit SNR is less than 30 dB. When above 30 dB, all the theoretical results match the simulation results closely, so either approach would be accurate at high SNRs. From (5.7), it is clear that the relay transmitting power, i.e., the SI signal power, increases with the increase of transmit SNR. However, the superiority of the FD system over the HD counterpart is more significant when transmit SNR increases. In particular, the throughput

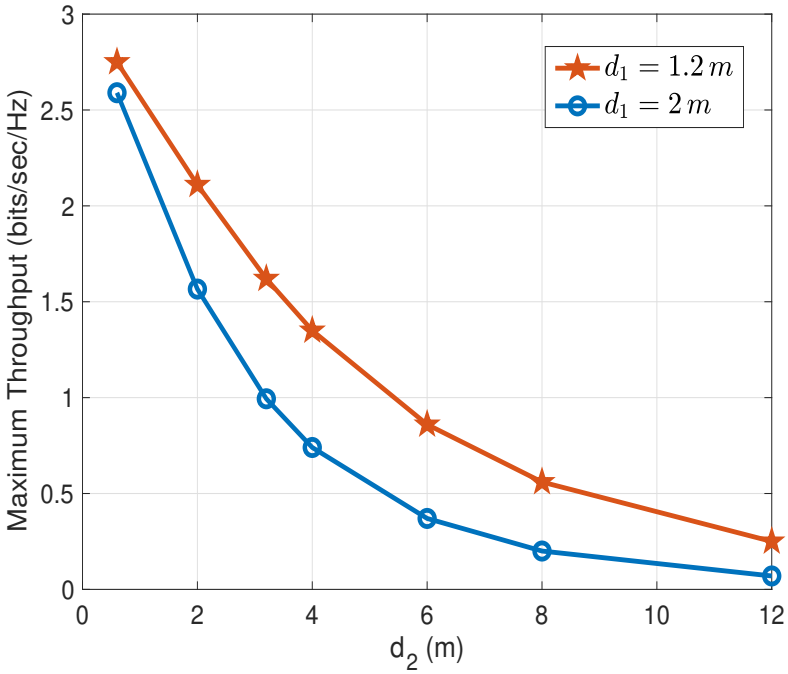

Figure 5.7: Maximum throughput vs. d_1 and d_2 for transmit SNR=40 dB.

gains of the FD system over the HD are 1.2, 1.85, and 1.95 at SNR values of 20, 30, and 50 dB, respectively. This result shows that, in FD systems, the PDC scheme can effectively cancel the loopback SI even when the power of the SI signal is high, which ensures the high system throughput. Besides, increasing the transmit SNR can improve more significantly the system throughput than in HD systems. Thus, it is important to research the throughput performance of FD systems in a high SNR regime.

Fig. 5.7 plots the system performances of the maximum throughput when considering different distances where d_1 is the S-R distance and d_2 is the R-D distance. The maximum throughput is obtained when the optimal α is calculated by using (5.32). Fig. 5.7 shows that when d_1 is fixed the maximum throughput exponentially decreases with the increase of d_2 due to the impact of the path loss between the relay and destination. Besides, the difference between the two lines increases from 0.16 bits/sec/Hz when d_2 equals to 0.6 m to a maximum value of 0.61 bits/sec/Hz when d_2 equals to 4 m. Then, the gap narrows to 0.18 bits/sec/Hz when d_2 equals to 12 m. The reason is that the increase of distance d_1 increases the path loss from the source to the relay and decreases the harvested energy at the relay. Thus, the decrease of the maximum throughput is more significant for $d_1 = 2$ m than that of $d_1 = 1.2$ m when d_2 is relatively small, i.e., d_2 is less than 4 m. However, with

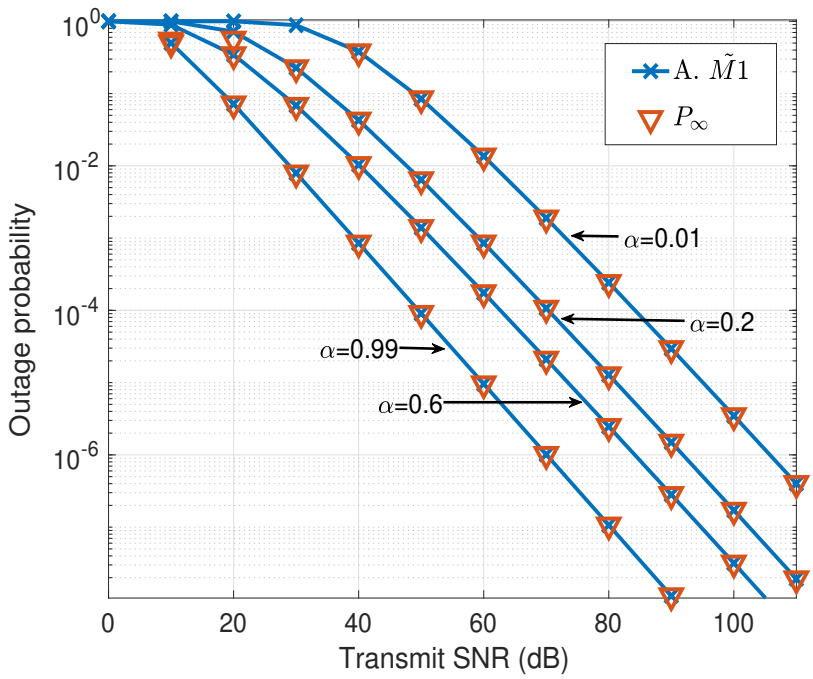

Figure 5.8: Validation of high SNR assumption. Outage probability for different α.

the increase of d_2 so that the difference between d_1 = 1.2 m and d_1 = 2 m is negligible to d_2, the maximum throughput is mainly affected by the path loss from the relay to destination. Thus, the difference of the maximum throughput reduces when d_2 is large.

Figs. 5.8 and 5.9 illustrate the impact of α on the outage probability and the system throughput as well as validating the high SNRs assumption. The derived analytical expressions of the approximation of Method 1 and the asymptotic line of outage probability against the transmit SNR, are denoted as "A.$M1$" and "P_∞" respectively. Fig. 5.8 shows that the increase of the EH duration always improves the outage probability. Also, when SNRs are higher than 40 dB, the asymptotic line which uses the series expansion at $u = 0$ matches the approximation of Method 1. According to Figs. 5.1 and 5.8, we can conclude that, at high SNRs, the outage probability of the FD EH relaying system can be accurately modeled using any of the theoretical Method 1, Method 1 approximation, series expansion, and Method 2. (cf. in (5.20), (5.23), (5.24) and (5.28), respectively). However, the theoretical Method 2 is preferred since it also matches the practice better at low SNRs. As shown in Fig. 5.9, the asymptotic line of throughput with a high transmit SNR assumption is defined in the figure as "R_{up}", which is the upper-bound of the system throughput. Note that the SNR in Figs. 5.6 and 5.9 is the transmit SNR, which is proportional to the trans-

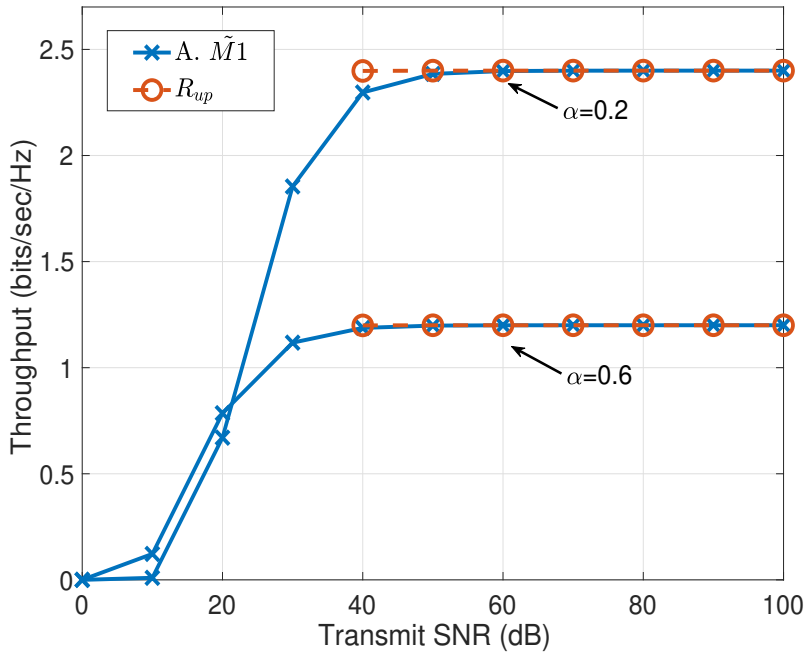

Figure 5.9: Validation of high SNR assumption. Throughput for different α.

mit power, thus a high SNR regime is a reasonable range to be considered. Fig. 5.9 also shows that an increase of the EH duration slightly improves system throughput if SNRs are low. However, at high SNRs, the system throughput for the case $\alpha = 0.2$ outperforms the case $\alpha = 0.6$ since the relay harvests enough energy from the transmitted signal and more time is spent on information transmission.

5.4 Chapter Summary

This chapter investigates an OFDM FD relaying system with no direct link from the source to the destination. An FD time switching-based relaying protocol is used to implement EH from the RF signals in the first phase as well as simultaneously receive and amplify-and-forward information in the second phase at the relay node. The performances of outage probability and throughput are evaluated for our FD system, in which the multipath propagated SI signals at the relay are eliminated by the PDC scheme. Specifically, the analytical expressions of the outage probability are derived in two different approaches over the Rayleigh frequency-selective fading channels, in which the approach considers product distribution of the source-relay channel and relay-destination channel is more ac-

curate. Based on the mathematical expression of the system throughput, the optimal time split has also been derived to obtain the largest system throughput. In addition, comparing FD with HD relaying systems, the results show that the throughput of the former is nearly doubled than the latter at high transmit SNRs. For simplification, the asymptotic lines of outage probability and throughput are researched and validated at high SNRs.

The next chapter will consider a PDC-based FD relaying system with WPT from the relay to the source in single-carrier Rayleigh flat fading channels.

Chapter 6

Throughput Analysis of Full-Duplex Transmission Networks with Wireless Energy Harvesting Enabled Sources

6.1 Introduction

In this chapter, we propose a two-hop PDC-based FD communication system in which the source harvests from the RF signal for the transmission of information signal to the relay. As reviewed in Chapter 2, the relay-assisted EH techniques can be classified into WPT from the source to the relay [14], [16], [27], [45] and WPT from the relay to the source [47]–[50]. It is worth noting that Chapter 5 considers a relaying system with an EH-capable relay while this chapter examines a relaying system with an EH-enabled source. WPT from the relay to the source is practical in many cases as introduced in Section 2.3.3 and attracts the attention of researchers. For example, the HD transmission and out-of-band FD transmission with WPT from the relay to the source are considered in [47]–[50] and [16] respectively. In [46], [52], [53], multiple-antenna technologies and FD transmission are studied. The SIC scheme in [46] requires the instantaneous channel state information (CSI) of the SI channel. In [52], [53], it is possible to use the information of direction-of-arrival (DOA) and direction-of-departure (DOD) of the SI channel for interference mitigation. Clearly, the estimations of DOA/DOD or the instantaneous CSI of the SI channels are usually required, thus the computational complexity and overhead are significant.

Motivated by literature, we propose an emerging system model where the PDC scheme is adopted at the relay to cancel the SI. This system does not require the instantaneous CSI of the SI channels. In particular, we consider an FD system as shown in Fig. 6.1 where the harvested energy at the source in the first phase is used to transmit data to the relay in the second phase. Besides, the relay works in the FD mode, receiving data from the source and simultaneously transmitting data to the destination. The purpose of this chapter is to analyze the throughput of the two-hop FD relaying system with the EH-capable sources using the PDC scheme for SI cancellation. Unlike our previous work [27] in Chapter 5, which considers the polarization state of the transmitter at the source to be orthogonal with that at the relay, this chapter not only considers orthogonal polarization states as a special case but also considers the effect of non-orthogonal polarization states on the FD EH-relaying system. Besides, the two-hop FD system with an EH relay in Chapter 5 shows that its outage probability is worse than that of the HD EH system. In contrast, the outage probability of the FD relaying system comprising an EH source can be as small as the outage probability of the HD_1 EH system and superior to that of the HD_2 one.

To the best of our knowledge, there is no existing work that has the similar system model, which constitutes one of the novelties of this chapter. Therefore, two HD transmission systems both of which have the WPT capability from the relay to the source are examined as benchmarks. The reason is that the performance of the HD systems can be considered as the boundary of the FD system. The numbers of nodes and antennas of the HD systems are the same as those in the FD system. The first HD system, denoted as HD_1, has the same EH duration as the FD system, and the second HD system, HD_2, has the same transmitting power at the source as the FD system. The detailed descriptions of HD systems will be illustrated in Section 6.2.3.

The main contributions of this chapter are summarized as follows.

- The analytical expressions of the system outage probability and throughput are presented and validated by simulations for both FD EH and HD EH relaying systems.
- The optimal time splits for FD and HD relaying systems are obtained numerically.

- In FD relaying systems, we find that the dissimilarity ρ between the polarization states of the relay antennas influences the PDC cancellation effect in terms of noise power. When $\rho > 0.5$, the output noise power of the PDC scheme is suppressed. When $\rho < 0.5$, its output noise power is amplified. The system throughput is more sensitive to ρ when the background noise power is higher.

- When the dissimilarity factor is $\rho = 1$ (i.e., their polarization states are orthogonal), the PDC scheme performs the best in suppressing the interference and noise. Thus, the polarization states should be selected as close to orthogonal as possible to maximizes the FD system throughput.

- The PDC scheme is adopted for the SI cancellation at the relay because this technique does not require the knowledge of the instantaneous CSI of the SI channels. Thereby, the complexity and overhead of the FD system are reduced.

- Comparisons of the FD and HD relaying architectures show that, at the cost of dual-polarized antennas and self-interference cancellation module, the outage probability of the FD system with the optimal ρ can be as small as that of the HD_1 system and superior to that of the HD_2 system. Besides, with the optimal time split and a proper transmit power of the relay node, the FD system can double the system throughput of the HD_1 counterpart and nearly double that of the HD_2 counterpart.

The content of this chapter has been published in [41].

The rest of chapter is organized as follows. Section 6.2 provides the system description and signal modeling of both FD EH systems and HD EH systems. Section 6.3 and Section 6.4 are the throughput analyses and numerical results, respectively. Section 6.5 concludes this chapter.

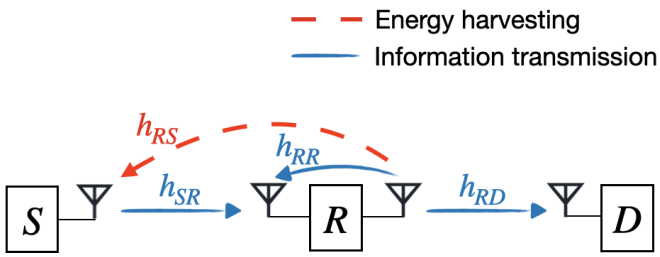

Figure 6.1: System model comprised of an EH source (S), a relay (R) and a destination (D).

6.2 System Model

6.2.1 FD System Description

In Chapter 5, we consider an FD OFDM relaying system with an an EH relay. This chapter considers an AF single-carrier relaying system which is comprised of an EH source (S), a relay (R), and a destination (D) as shown in Fig. 6.1. S and D are equipped with one dual-polarized antenna each while R is equipped with two sets of dual-polarized antennas, i.e., one for transmission and the other for reception. The direct link between S and D is not available because of the long-distance or heavy shadowing effects (i.e., obstructions, such as skyscrapers). h_{RS}, h_{SR}, h_{RR} and h_{RD} denote the channel coefficients of the Rayleigh block fading channels between R and S, S and R, the transmit and receive antennas at R, and R and D, respectively. We assume their expectation values satisfy $E\{|h_{RS}|^2\} = E\{|h_{SR}|^2\} = E\{|h_{RR}|^2\} = E\{|h_{RD}|^2\} = 1$. A "harvest-then-transmit" FD time switching-based relaying (TSR) protocol is considered in this chapter as shown in Fig. 6.2. The overall block time is T seconds in which energy is harvested at the source and then information is transmitted from S to D through R. The time split factor for EH is α, where $0 < \alpha < 1$. Phase I is the EH phase with the duration of αT. In this phase, the antenna in S works in the receiving mode and S harvests energy from the RF signal transmitted from R. Phase II is the information transmission phase, which occupies the remaining time $(1-\alpha)T$. It is assumed that D can estimate the S-R and R-D channels at the start of this phase in each block by using the pilots signal sent from S. It is worth noting that, the channel estimation of the SI channels at the relay is not needed because the PDC

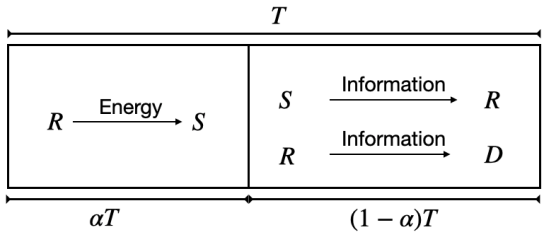

Figure 6.2: The FD TSR protocol for energy transfer and information transmission.

scheme does not require the knowledge of the instantaneous CSI of the SI channels. We assume the overhead for pilot transmission is negligible, which is in line with the works in [55], [114]. The antenna in S works in the transmitting mode and R works in the FD mode. R receives information from S and at the same time forwards information to D in the same frequency band. The PDC scheme proposed in [85], including polarization and digital signal processing technology, is adopted in this chapter to enable FD transmission. Detailed explanations of the working concepts of the PDC scheme can be found in Section 3.3. This digital SIC module is placed at the relay and is powered by the fixed power supply of the relay node. It is assumed that the power consumed by the SIC module is negligible compared to the signal power. In the information transmission process during Phase II, the polarization state used in the transmitter of S and the transmitter of R are denoted as **S** and **I** respectively. The selection of polarization states and the theory of SI signal cancellation have been discussed in Section 3.3.

6.2.2 Signal Modeling of FD EH System

Energy Harvesting

In Phase I of the FD TSR protocol, the RF signal x_e is sent from the relay to the EH receiver at the source node. During this EH phase, the received energy signal at the source can be expressed as

$$y_s[i] = \sqrt{\frac{P_r}{d_1^m}} h_{RS} x_e[i] + n_s[i], \tag{6.1}$$

where h_{RS} is the channel coefficient of the relay-to-source (R-S) channel and d_1 is the distance between the source and relay. P_r is the constant transmitted power of the relay node, x_e is the energy symbol transmitted from the relay at the time instant i with the expectation value $E\{|x_e[i]|^2\} = 1$ and $n_s[i]$ is the AWGN. Hence, if noise power is significantly smaller than $\frac{P_r}{d_1^m}$, the harvested energy at the source during the time αT is

$$E_s = \alpha T \Big(\frac{\eta P_r |h_{RS}|^2}{d_1^m} \Big), \tag{6.2}$$

where $0 < \eta < 1$ is the energy conversion efficiency. We assume all the harvested energy E_s at the source is used in Phase II for transmitting information signals. The transmission power of the source is

$$P_s = \frac{E_s}{(1-\alpha)T} = \frac{\alpha \eta P_r |h_{RS}|^2}{d_1^m (1-\alpha)}. \tag{6.3}$$

Information Transmission

In Phase II of the FD TSR protocol, the duration $(1-\alpha)T$ is used for transmitting information from the source to the relay and, at the same time, transmitting information from the relay to the destination. The polarization state of the desired information signal is $\mathbf{S}$ and the polarization state of the SI signal is $\mathbf{I}$, which are illustrated in Section 3.3.

We introduce ρ as the polarization dissimilarity factor of $\mathbf{S}$ and $\mathbf{I}$. The expression of ρ can be defined as

$$\begin{aligned} \rho &= 1 - \|\mathbf{I}^{\mathrm{H}}\mathbf{S}\|^2 = 1 - \mathbf{S}^{\mathrm{H}}\mathbf{I}\mathbf{I}^{\mathrm{H}}\mathbf{S} \\ &= \mathbf{S}^{\mathrm{H}}\mathbf{P}_{\mathrm{I}}^{\perp}\mathbf{S}, \end{aligned} \tag{6.4}$$

where $\|\cdot\|$ denotes the Euclidean norm and $(.)^{\mathrm{H}}$ denotes the Hermitian transposition. From (6.4), it is clear that when the vectors $\mathbf{S}$ and $\mathbf{I}$ are orthogonal, i.e., $\mathbf{I}^{\mathrm{H}}\mathbf{S} = 0$, ρ gets the maximum value 1. The value $\rho = 0$ occurs when $\mathbf{I}^{\mathrm{H}}\mathbf{S} = 1$. However, $\mathbf{S} \neq \mathbf{I}$ leads to $\rho \neq 0$. Thus, the range of ρ is $\rho \in (0, 1]$.

The received signal at the relay can be expressed as

$$y_r[i] = \sqrt{\frac{P_s}{d_1^m}} h_{SR}\mathbf{S}x_s[i] + \sqrt{P_i}\, h_{RR}\mathbf{I}x_r[i] + \mathbf{N}_r[i], \tag{6.5}$$

where $x_s[i]$ is the information signal transmitted by the source and $x_r[i]$ is the loopback interference due to the full-duplex transmission at the relay with $E\{|x_s[i]|^2\} = 1$ and $E\{|x_r[i]|^2\} = 1$. h_{SR} is the channel coefficient of the S$-$R channel and h_{RR} is the loopback interference channel gain. P_i is the power of the loopback interference signal, which is assumed to be less than the transmitting power of the relay P_r, due to some passive SIC technologies used at the relay, such as absorptive shielding [62], and the difference in polarization of the transmit and receive antennas at the relay. In the later simulation, for illustration and without loss of generality, we assume P_i is 25 dB smaller than P_r. $\mathbf{N}_r[i]$ is the AWGN at the relay node, which can be represented as

$$\mathbf{N}_r[i] = \begin{bmatrix} \mathrm{n}_H[i] \\ \mathrm{n}_V[i] \end{bmatrix}, \tag{6.6}$$

where $\mathrm{n}_H[i]$ represents the horizontal polarized component and $\mathrm{n}_V[i]$ represents the vertical polarized component. $\mathrm{n}_H[i]$ and $\mathrm{n}_V[i]$ obey the Gaussian distribution with a zero mean and a variance of $\frac{N_0}{2}$. From (6.5), the relay not only receives the information signal $x_s[i]$ from the source but also receives the SI signal from its own transmitter. A cancellation scheme as shown in Section 3.3, i.e., an oblique projection, is needed to maintain the desired signal with the polarization state $\mathbf{S}$ while canceling the SI signal with the polarization state $\mathbf{I}$. Equations (3.10) and (3.11) indicate the oblique projection $\mathbf{Q}_{\mathrm{SI}}$ has the range $\langle\mathbf{S}\rangle$ and null space $\langle\mathbf{I}\rangle$. From (6.4), if $\rho = \mathbf{S}^{\mathrm{H}}\mathbf{P}_{\mathrm{I}}^{\perp}\mathbf{S} = 1$, the oblique projection $\mathbf{Q}_{\mathrm{SI}}$ is simplified to the orthogonal projection whose range and null space are orthogonal. These equations are the key of the PDC scheme to protect the information and cancel the SI in

the FD transmission. After the PDC scheme, the post cancellation signal at the relay is

$$\begin{aligned} y_{out}[i] &= \mathbf{S}^{\mathrm{H}}\mathbf{Q}_{\mathrm{SI}}\, y_r[i] \\ &= \sqrt{\frac{P_s}{d_1^m}} h_{SR} x_s[i] + \mathbf{S}^{\mathrm{H}}\mathbf{Q}_{\mathrm{SI}}\mathbf{N}_r[i], \end{aligned} \tag{6.7}$$

where $\mathbf{S}^{\mathrm{H}}\mathbf{Q}_{\mathrm{SI}}\mathbf{N}_r$ is the residual noise because of the imperfect cancellation of the PDC scheme. If the input noise power of the PDC scheme is denoted as P_{ni} and its output noise power as P_{no}, we have [85]

$$\frac{P_{no}}{P_{ni}} = \frac{E\left[\|\mathbf{S}^{\mathrm{H}}\mathbf{Q}_{\mathrm{SI}}\mathbf{N}_r\|^2\right]}{N_0} = \frac{1}{2\rho}. \tag{6.8}$$

Since $P_{ni} = N_0$, the power of the residual noise is $\frac{N_0}{2\rho}$. From (6.7), the relay amplifies the input signal by a factor β in the AF protocol, which is given by

$$\beta^2 = \frac{P_r}{\frac{|h_{SR}|^2 P_s}{d_1^m} + \frac{N_0}{2\rho}}. \tag{6.9}$$

Hence, the transmitted signal from the relay can be expressed as

$$x_r[i] = \beta y_{out}[i-\tau], \tag{6.10}$$

where τ is the time delay caused by the relay processing. The received signal at the destination is

$$\begin{aligned} y_d[i] &= \frac{h_{RD}}{\sqrt{d_2^m}} x_r[i] + n_d[i] \\ &= \underbrace{\frac{h_{SR}h_{RD}\beta\sqrt{P_s}}{\sqrt{d_1^m d_2^m}} x_s[i-\tau]}_{\text{signal part}} + \underbrace{\frac{h_{RD}\beta}{\sqrt{d_2^m}} \mathbf{S}^H\mathbf{Q}_{\mathrm{SI}}\mathbf{N}_r[i-\tau] + n_d[i]}_{\text{noise part}}, \end{aligned} \tag{6.11}$$

where h_{RD} and d_2 are the channel coefficient of the R$-$D channel and the distance between the relay and destination, respectively. $n_d[i]$ is the AWGN at the destination. It can be seen from (6.7) and (6.11) that the cancellation scheme can eliminate the effect of SI channel h_{RR} and maintains the information signal with the same power. However, the oblique projection also causes the residual noise at the relay $\mathbf{S}^{\mathrm{H}}\mathbf{Q}_{\mathrm{SI}}\mathbf{N}_r$ with the variance $\frac{N_0}{2\rho}$ (cf.

(6.8)). This output noise power is regarded as the side-effect of the PDC scheme. From (6.9) and (6.11), the instantaneous end-to-end SNR can be expressed as

$$\gamma = \frac{\frac{P_s\beta^2|h_{SR}|^2|h_{RD}|^2}{d_1^m d_2^m}}{\frac{|h_{RD}|^2\beta^2 N_0}{2d_2^m\rho} + N_0} = \frac{\frac{P_r P_s|h_{SR}|^2|h_{RD}|^2}{d_1^m d_2^m\left(\frac{N_0}{2\rho}+\frac{P_s|h_{SR}|^2}{d_1^m}\right)}}{\frac{N_0 P_r|h_{RD}|^2}{2d_2^m\rho\left(\frac{N_0}{2\rho}+\frac{P_s|h_{SR}|^2}{d_1^m}\right)} + N_0}. \tag{6.12}$$

6.2.3 HD System Description

For comparison, we consider two HD EH relaying systems, denoted as HD_1 and HD_2, as benchmarks. This is because that the performance of the HD systems can be considered as the boundary of the FD system. More specifically, in theory, the throughput in FD systems can be twice the HD systems. Similar to the FD system, these two HD systems are comprised of an EH source (S), a relay (R), and a destination (D). S and D are equipped with one dual-polarized antenna each while R is equipped with two sets of dual-polarized antennas, i.e., one for transmission and the other for reception. The number of RF chains of HD_1, HD_2 and FD systems is the same. The direct link between S and D is not available. We also assume the CSI of S$-$R and R$-$D channels is available at the destination and the overhead of the channel estimation is negligible. Besides, the PDC scheme does not require the knowledge of the instantaneous CSI of the SI channel at the relay, thus the overhead complexity is the same as that in the HD systems. So, from the overhead complexity perspective, this allows a fair comparison between our system and the HD counterparts. In addition, the FD system and HD systems are equipped with the same number of antennas at the source and destination nodes for a fair comparison in terms of the system diversity. Both throughput and outage probability comparisons between our FD system and the HD counterparts have been included.

For the HD_1 TSR protocol shown in Fig. 6.3, the RF signal $\hat{x}_e$ is sent from the relay to the EH-enabled receiver at the source node in Phase I during the time αT. The remaining time $(1-\alpha)T$ is divided into two time slots where Phase II with duration $\frac{(1-\alpha)T}{2}$ is used for transmitting information from the source to the relay and Phase III with the remaining duration $\frac{(1-\alpha)T}{2}$ is used for transmitting information from the relay to the destination.

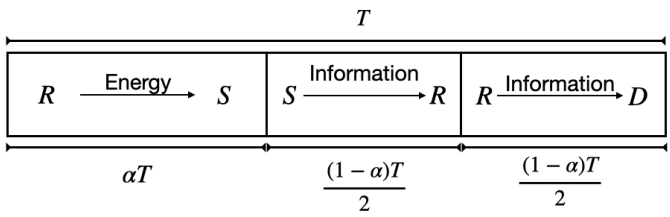

Figure 6.3: The HD_1 TSR protocol for energy transfer and information transmission.

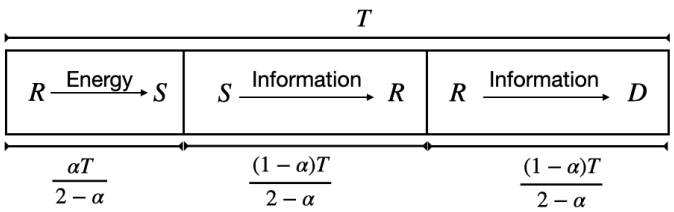

Figure 6.4: The HD_2 TSR protocol for energy transfer and information transmission.

This HD_1 system has the same total frame duration and EH duration as the FD system considered in Section 6.2.1. However, given that the duration of EH is the same but the duration of transmission is half of the FD system, the transmit power per symbol is larger in this scheme than the FD. For the HD_2 TSR protocol shown in Fig. 6.4, the EH duration in Phase I is reduced to $\alpha' T$ to ensure the transmitting power per symbol in the HD_2 system to be the same as that of the FD system. Then, Phase II and Phase III have the duration of $\frac{(1-\alpha')T}{2}$ each for information transmission. From (6.3), the time split factor α' is calculated as

$$\frac{\alpha \eta P_r |h_{RS}|^2}{d_1^m (1-\alpha)} = \frac{2\alpha' \eta P_r |h_{RS}|^2}{d_1^m (1-\alpha')}. \tag{6.13}$$

Hence,

$$\alpha' = \frac{\alpha}{2-\alpha}. \tag{6.14}$$

As a result, the duration $\frac{(1-\alpha')T}{2} = \frac{(1-\alpha)T}{2-\alpha}$.

6.2.4 Signal Modeling of HD EH System

Energy Harvesting

In the EH phase of the HD_1 system, the RF energy harvested during the duration αT at the source is the same as that in the FD system with $E_s = \alpha T \left(\frac{\eta P_r |h_{RS}|^2}{d_1^m}\right)$, which is used by

the source to transmit information to the relay (cf. Eq. (6.2)). The transmitting power of the source node is given by

$$\hat{P}_s = \frac{E_s}{\frac{(1-\alpha)T}{2}} = \frac{2\alpha\eta P_r |h_{RS}|^2}{d_1^m(1-\alpha)}. \tag{6.15}$$

From (6.3) and (6.15), it can be seen that the transmitting power of the source in HD_1 is doubled, compared to that in FD because the source in HD_1 only transmits half the amount of information in the FD counterpart.

In the HD_2 system, the EH phase is reduced from αT to $\alpha' T$. The transmitting power of the source node is

$$P'_s = \frac{E_s}{\frac{(1-\alpha')T}{2}} = \frac{\alpha' T\left(\frac{\eta P_r |h_{RS}|^2}{d_1^m}\right)}{\frac{(1-\alpha')T}{2}} = \frac{\alpha\eta P_r |h_{RS}|^2}{d_1^m(1-\alpha)}. \tag{6.16}$$

From (6.3) and (6.16), it can be seen that the transmitting power per symbol in the FD and HD_2 is the same.

Information Transmission

In the HD_1 system, the first time slot $\frac{(1-\alpha)T}{2}$ is used for the information transmission from the source to the relay. The received signal at the relay node is given by

$$\hat{y}_r[i] = \sqrt{\frac{\hat{P}_s}{d_1^m}} h_{SR}\hat{x}_s[i] + \hat{n}_r[i], \tag{6.17}$$

where $\hat{x}_s[i]$ is the information signal transmitted by the source and $\hat{n}_r[i]$ is the AWGN. In the AF protocol, the relay amplifies the received signal and forwards the signal to the destination. The second time slot $\frac{(1-\alpha)T}{2}$ is used for the information transmission from the relay to the destination. The transmitted signal $\hat{x}_r[i]$ at the relay is

$$\hat{x}_r[i] = \frac{\sqrt{P_r}\hat{y}_r[i-\tau]}{\sqrt{\frac{|h_{SR}|^2\hat{P}_s}{d_1^m} + N_0}}. \tag{6.18}$$

The received signal at the destination can be expressed as

$$\hat{y}_d[i] = \frac{h_{RD}}{\sqrt{d_2^m}}\hat{x}_r[i] + \hat{n}_d[i], \tag{6.19}$$

where $\hat{n}_d[i]$ is the AWGN. Substituting (6.17) and (6.18) into (6.19), $\hat{y}_d[i]$ is given by

$$\hat{y}_d[i] = \underbrace{\frac{\sqrt{P_r}\sqrt{\hat{P}_s}h_{SR}h_{RD}x_s[i-\tau]}{\sqrt{d_1^m}\sqrt{d_2^m}\left(\sqrt{\frac{|h_{SR}|^2\hat{P}_s}{d_1^m}+N_0}\right)}}_{\text{signal part}} + \underbrace{\frac{\sqrt{P_r}h_{RD}\hat{n}_r[i-\tau]}{\sqrt{d_2^m}\left(\sqrt{\frac{|h_{SR}|^2\hat{P}_s}{d_1^m}+N_0}\right)}}_{\text{noise part}} + \hat{n}_d[i]. \tag{6.20}$$

The SNR at the destination in the HD_1 system is

$$\hat{\gamma} = \frac{\frac{P_r\hat{P}_s|h_{SR}|^2|h_{RD}|^2}{d_1^m d_2^m\left(\frac{|h_{SR}|^2\hat{P}_s}{d_1^m}+N_0\right)}}{\frac{P_r|h_{RD}|^2N_0}{d_2^m\left(\frac{|h_{SR}|^2\hat{P}_s}{d_1^m}+N_0\right)}+N_0}. \tag{6.21}$$

Similarly, the SNR at the destination in the HD_2 system is

$$\gamma' = \frac{\frac{P_rP_s'|h_{SR}|^2|h_{RD}|^2}{d_1^m d_2^m\left(\frac{|h_{SR}|^2P_s'}{d_1^m}+N_0\right)}}{\frac{P_r|h_{RD}|^2N_0}{d_2^m\left(\frac{|h_{SR}|^2P_s'}{d_1^m}+N_0\right)}+N_0}. \tag{6.22}$$

In the following, the outage probability and throughput at the destination node of the FD system, the HD_1 system, and the HD_2 system are determined based on the received SNR, namely γ, $\hat{\gamma}$, and γ' respectively.

6.3 Throughput Analyses

6.3.1 FD EH Relaying

It is assumed that all channel coefficients h_{SR}, h_{RS}, h_{RR} and h_{RD} are independently and identically distributed (i.i.d.) random variables (RVs). Further we assume that $|h_{SR}|^2$ and $|h_{RS}|^2$ are i.i.d. exponential RVs with the mean λ_s while $|h_{RD}|^2$ is an i.i.d. exponential RV with the mean λ_d.

The system outage probability p_{out} is defined as the probability that the received power value falls below the threshold. In the FD system, the outage probability is given by

$$p_{out} \triangleq p\{\gamma < \gamma_{\text{th}}\}, \tag{6.23}$$

where $\gamma_{\text{th}} = 2^{R_c} - 1$ is the required threshold SNR and R_c is the fixed transmission rate at

the source. Invoking the received SNR at the destination in (6.12), we have

$$p_{out} = p\left\{ \frac{\frac{P_r P_s |h_{SR}|^2 |h_{RD}|^2}{d_1^m d_2^m \left(\frac{N_0}{2\rho} + \frac{P_s |h_{SR}|^2}{d_1^m}\right)}}{\frac{N_0 P_r |h_{RD}|^2}{2 d_2^m \rho \left(\frac{N_0}{2\rho} + \frac{P_s |h_{SR}|^2}{d_1^m}\right)} + N_0} < \gamma_{\text{th}} \right\}. \tag{6.24}$$

The result (6.25) can be obtained after some simple algebraic manipulations. Denote $a = 2\eta\alpha\rho P_r^2$, $b = 2\gamma_{\text{th}}\rho\eta\alpha P_r d_2^m N_0$, $c = \gamma_{\text{th}} N_0 P_r (d_1^m)^2 (1-\alpha)$, and $d = \gamma_{\text{th}} N_0^2 (d_1^m)^2 d_2^m (1-\alpha)$. The outage probability p_{out} can be rewritten as

$$\begin{aligned} p_{out} &= p\Big(\frac{a|h_{SR}|^2|h_{RS}|^2|h_{RD}|^2}{b|h_{SR}|^2|h_{RS}|^2 + c|h_{RD}|^2 + d} < 1\Big) \\ &= p\Big((a|h_{RD}|^2 - b)|h_{SR}|^2|h_{RS}|^2 < c|h_{RD}|^2 + d\Big) \\ &= \begin{cases} p\Big(X < \frac{cY+d}{aY-b}\Big), & Y > b/a \\ 1, & Y \le b/a, \end{cases} \end{aligned} \tag{6.26}$$

where $X \triangleq |h_{SR}|^2|h_{RS}|^2$, $Y \triangleq |h_{RD}|^2$. Following (6.26), p_{out} is given by

$$p_{out} = \int_0^{b/a} f_Y(z)dz + \int_{b/a}^{\infty} f_Y(z) p\Big(X < \frac{cz+d}{az-b}\Big)dz, \tag{6.27}$$

where

$$f_Y(z) = \frac{1}{\lambda_d} e^{-z/\lambda_d}, \tag{6.28}$$

and

$$\begin{aligned} p\Big(X < \frac{cz+d}{az-b}\Big) &= F_X\left(\frac{cz+d}{az-b}\right) \\ &= 1 - 2\sqrt{\frac{cz+d}{\lambda_s^2(az-b)}} K_1\left(2\sqrt{\frac{cz+d}{\lambda_s^2(az-b)}}\right), \end{aligned} \tag{6.29}$$

$$p_{out} = p\left(\frac{2\eta\alpha\rho Pr^2|h_{SR}|^2|h_{RS}|^2|h_{RD}|^2}{2\eta\alpha\rho P_r d_2^m N_0|h_{SR}|^2|h_{RS}|^2 + N_0 Pr(d_1^m)^2(1-\alpha)|h_{RD}|^2 + N_0^2(d_1^m)^2 d_2^m(1-\alpha)} < \gamma_{\text{th}}\right). \tag{6.25}$$

where z is the integration variable, $f_Y(z)$ in (6.28) is the probability density function (PDF) of the exponential random variable Y and λ_d is the mean value of Y, $F_X\left(\frac{cz+d}{az-b}\right)$ in (6.29) is the cumulative distribution function (CDF) of the exponential RV X and λ_s is the mean value of the exponential RVs $|h_{SR}|^2$ and $|h_{RS}|^2$[23], and $K_1(.)$ is the first-order modified Bessel function of the second kind [68]. Substituting $f_Y(z)$ and $F_X(z)$ into (6.27), we have

$$\begin{aligned} p_{out} &= \int_0^{b/a} \frac{1}{\lambda_d} e^{-z/\lambda_d} dz + \int_{b/a}^{\infty} \frac{1}{\lambda_d} e^{-z/\lambda_d} \Big(1 - uK_1(u)\Big) dz \\ &= 1 - \int_{b/a}^{\infty} uK_1(u) \frac{1}{\lambda_d} e^{-\frac{z}{\lambda_d}} dz, \end{aligned} \tag{6.30}$$

where $u \triangleq 2\sqrt{\frac{cz+d}{(az-b)\lambda_s^2}}$.

The system throughput can be computed as

$$\begin{aligned} R(\alpha) &= (1 - p_{out}) R_c (1-\alpha) \\ &= R_c(1-\alpha) \int_{b/a}^{\infty} uK_1(u) \frac{1}{\lambda_d} e^{-\frac{z}{\lambda_d}} dz, \end{aligned} \tag{6.31}$$

The throughput $R(\alpha)$ is a function of system parameters and its optimization in terms of ρ and α will be illustrated below.

From (6.8) and (6.25), it is clear that the polarization dissimilarity factor ρ of **S** and **I** affects the output noise power of the PDC scheme and the system outage probability. When **S** and **I** are orthogonal, the corresponding ρ is 1, which minimizes the residual noise power output of the PDC scheme as well as the system outage probability. Thus, the throughput in (6.31) is maximized when ρ is 1.

It can also be seen from (6.25) and (6.31) that the time split factor, α, of the TSR protocol affects the system throughput. The optimal α can be obtained by solving the following optimization problem

$$\begin{aligned} \alpha^* &= \arg\max_{\alpha} R(\alpha) \\ &\text{subject to } 0 < \alpha < 1. \end{aligned} \tag{6.32}$$

$R(\alpha)$ is a concave function of α. The optimal value α^* is obtained by solving the equation $\frac{dR(\alpha)}{d\alpha} = 0$. Due to the involvement of Bessel function in the expression of $R(\alpha)$, finding

the closed-form solution of α^* is difficult. Thus, the value α^* is numerically calculated using the built-in function "solve" of Matlab.

6.3.2 HD EH Relaying

In the HD_1 system, using the definition of the outage probability in (6.23) and invoking (6.21), the outage probability is

$$\begin{aligned}\hat{p}_{out} &\triangleq p\{\hat{\gamma} < \gamma_{\text{th}}\} \\ &= p\left\{\frac{\frac{P_r\hat{P}_s|h_{SR}|^2|h_{RD}|^2}{d_1^m d_2^m\left(\frac{|h_{SR}|^2\hat{P}_s}{d_1^m}+N_0\right)}}{\frac{P_r|h_{RD}|^2N_0}{d_2^m\left(\frac{|h_{SR}|^2\hat{P}_s}{d_1^m}+N_0\right)}+N_0} < \gamma_{\text{th}}\right\}. \end{aligned} \tag{6.33}$$

Equation (6.34) is derived by substituting $\hat{P}_s$ in (6.15) into (6.33). Set $\hat{a} = 2\eta\alpha Pr^2$, $\hat{b} = 2\gamma_{\text{th}}\eta\alpha P_r d_2^m N_0$, $\hat{c} = \gamma_{\text{th}}N_0 Pr(d_1^m)^2(1-\alpha)$, and $\hat{d} = \gamma_{\text{th}}N_0^2(d_1^m)^2 d_2^m(1-\alpha)$. The outage probability is given by

$$\hat{p}_{out} = \begin{cases} p\left(X < \frac{\hat{c}Y+\hat{d}}{\hat{a}Y-\hat{b}}\right), & Y > \hat{b}/\hat{a} \\ 1, & Y \le \hat{b}/\hat{a}. \end{cases} \tag{6.35}$$

where $X \triangleq |h_{SR}|^2|h_{RS}|^2$, $Y \triangleq |h_{RD}|^2$. After substituting the PDF and CDF of the exponential RVs into (6.35), we have

$$\begin{aligned}\hat{p}_{out} &= \int_0^{\hat{b}/\hat{a}} f_Y(z)dz + \int_{\hat{b}/\hat{a}}^{\infty} f_Y(z)F_X\left(\frac{\hat{c}z+\hat{d}}{\hat{a}z-\hat{b}}\right)dz \\ &= 1 - \int_{\hat{b}/\hat{a}}^{\infty} \hat{u}K_1(\hat{u})\frac{1}{\lambda_d}e^{-\frac{z}{\lambda_d}}dz, \end{aligned} \tag{6.36}$$

$$\hat{p}_{out} = p\left(\frac{2\eta\alpha Pr^2|h_{SR}|^2|h_{RS}|^2|h_{RD}|^2}{2\eta\alpha P_r d_2^m N_0|h_{SR}|^2|h_{RS}|^2 + N_0 Pr(d_1^m)^2(1-\alpha)|h_{RD}|^2 + N_0^2(d_1^m)^2 d_2^m(1-\alpha)} < \gamma_{\text{th}}\right). \tag{6.34}$$

where $\hat{u} \triangleq 2\sqrt{\frac{\hat{c}z+\hat{d}}{(\hat{a}z-\hat{b})\lambda_s^2}}$. Thus, the system throughput is

$$\begin{aligned}\hat{R}(\alpha) &= \frac{1-\alpha}{2}R_c(1-\hat{p}_{out}) \\ &= \frac{R_c(1-\alpha)}{2}\int_{\hat{b}/\hat{a}}^{\infty}\hat{u}K_1(\hat{u})\frac{1}{\lambda_d}e^{-\frac{z}{\lambda_d}}dz,\end{aligned} \tag{6.37}$$

The optimal α can be obtained by solving the following optimization problem

$$\begin{aligned}\hat{\alpha}^* &= \arg\max_{\alpha}\hat{R}(\alpha) \\ &\text{subject to } 0<\alpha<1.\end{aligned} \tag{6.38}$$

The value $\hat{\alpha}^*$ depends on many parameters, such as efficiency η, distances d_1 and d_2, powers P_r and $\hat{P}_s$, noise variance N_0, threshold γ_{th} and transmission rate R_c. The computational complexity of $\hat{R}(\alpha)$ makes the closed-form expression of the optimal α difficult. Thus, the value $\hat{\alpha}^*$ is numerically calculated using the built-in function "solve" of Matlab.

Similarly, by the definition of the outage probability in (6.23) and invoking (6.22), the outage probability in the HD_2 system is

$$\begin{aligned}p'_{out} &\triangleq p\{\gamma' < \gamma_{\text{th}}\} \\ &= p\left\{\frac{\frac{P_rP_s'|h_{SR}|^2|h_{RD}|^2}{d_1^m d_2^m(\frac{|h_{SR}|^2P_s'}{d_1^m}+N_0)}}{\frac{P_r|h_{RD}|^2N_0}{d_2^m(\frac{|h_{SR}|^2P_s'}{d_1^m}+N_0)}+N_0} < \gamma_{\text{th}}\right\}.\end{aligned} \tag{6.39}$$

Equation (6.40) is derived by substituting P_s' in (6.16) into (6.39). Set $a' = \eta\alpha Pr^2$, $b' = \gamma_{\text{th}}\eta\alpha P_r d_2^m N_0$, $c' = \gamma_{\text{th}}N_0 Pr(d_1^m)^2(1-\alpha)$, and $d' = \gamma_{\text{th}}N_0^2(d_1^m)^2 d_2^m(1-\alpha)$. Hence,

---

$$p'_{out} = p\left(\frac{\eta\alpha Pr^2|h_{SR}|^2|h_{RS}|^2|h_{RD}|^2}{\eta\alpha P_r d_2^m N_0|h_{SR}|^2|h_{RS}|^2 + N_0 Pr(d_1^m)^2(1-\alpha)|h_{RD}|^2 + N_0^2(d_1^m)^2 d_2^m(1-\alpha)} < \gamma_{\text{th}}\right). \tag{6.40}$$

the outage probability is given by

$$\begin{aligned} p'_{out} &= \int_0^{b'/a'} f_Y(z)dz + \int_{b'/a'}^{\infty} f_Y(z)F_X\left(\frac{c'z+d'}{a'z-b'}\right)dz \\ &= 1 - \int_{b'/a'}^{\infty} u'K_1(u')\frac{1}{\lambda_d}e^{-\frac{z}{\lambda_d}}dz, \end{aligned} \tag{6.41}$$

where $u' \triangleq 2\sqrt{\frac{c'z+d'}{(a'z-b')\lambda_s^2}}$. Thus, the system throughput is

$$\begin{aligned} R'(\alpha) &= \frac{1-\alpha}{2-\alpha}R_c(1-p'_{out}) \\ &= \frac{R_c(1-\alpha)}{2-\alpha}\int_{b'/a'}^{\infty} u'K_1(u')\frac{1}{\lambda_d}e^{-\frac{z}{\lambda_d}}dz, \end{aligned} \tag{6.42}$$

The optimal α can be obtained by solving the following optimization problem

$$\begin{aligned} \alpha'^* &= \arg\max_{\alpha} R'(\alpha) \\ &\text{subject to } 0 < \alpha < 1. \end{aligned} \tag{6.43}$$

The value α'^* is numerically calculated using the built-in function "solve" of Matlab.

6.4 Numerical Results

We assume the path loss exponent $m = 3$, $d_{SR} = 20$ m, $d_{RD} = 200$ m, the EH efficiency $\eta = 0.8$, and the carrier frequency is 2.4 GHz. The noise power N_0 is assumed to be either -90 dBm or -80 dBm for system bandwidth $B = 160$ MHz [111], and the transmission power of the relay is assumed to be $P_r = 1$ Watt [14]. The transmission rate of the source is 8 bits/sec/Hz. The throughputs derived in this chapter are in bits/sec/Hz. The considered range of the time split factor α and polarization dissimilarity factor ρ are $0 < \alpha < 1$ and $0 < \rho \leq 1$, respectively. To calculate the throughput in bits per seconds, $R(\alpha)$, $\hat{R}(\alpha)$, and $R'(\alpha)$ need to be multiplied with the system bandwidth B.

Fig. 6.5 illustrates the FD analytical result based on (6.31) with respect to ρ ranging from 10^{-5} to 1 since $\rho \in (0,1]$ as shown in Section II. The figure illustrates that the polarization dissimilarity factor ρ and the time split factor α affect the throughput performances. In this simulation, the relay transmission power is $P_r = 1$ Watt and AWGN

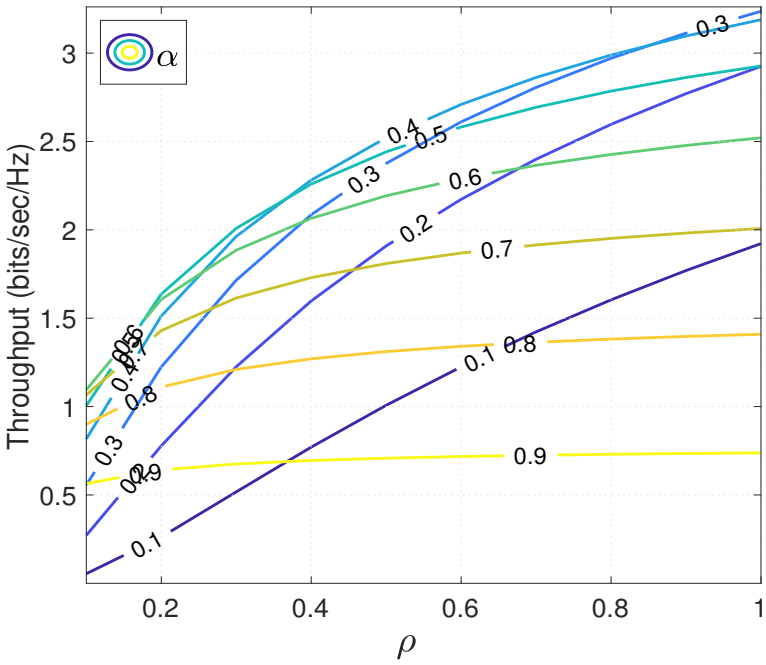

Figure 6.5: Throughput vs. the dissimilarity ρ of polarization states with different time splits α in the FD EH system. $P_r = 1$ Watt and $N_0 = -80$ dBm.

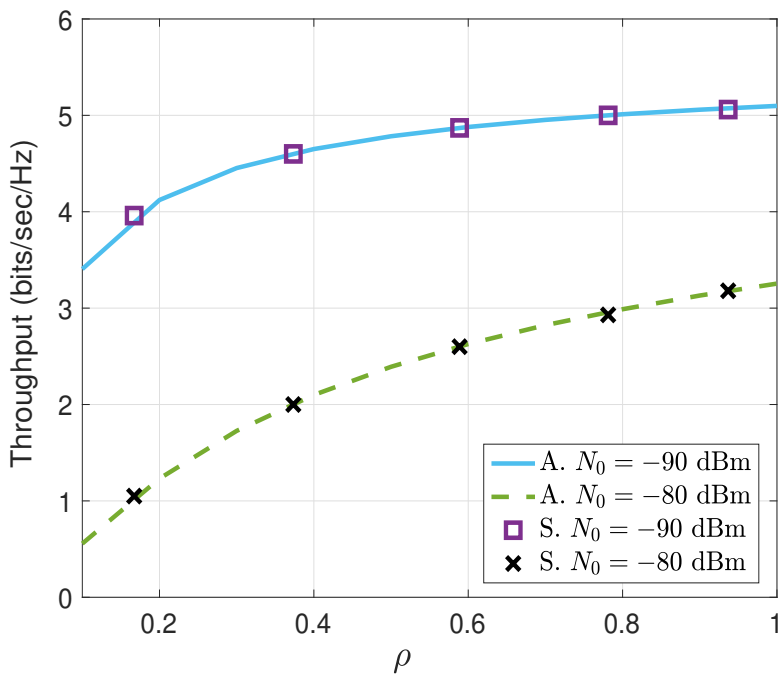

Figure 6.6: Analytical and simulation results for $N_0 = -80$ and -90 dBm in the FD EH system. $\alpha = 0.3$ and $P_r = 1$ Watt.

Table 6.1: Data collected from the simulation result where R is the FD throughput. $\alpha = 0.3$ and $P_r = 1$ Watt.

ρ	**S**	**I**	R
0.1672	$\begin{bmatrix} 0.7174+0.0000i \\ -0.6850-0.1268i \end{bmatrix}$	$\begin{bmatrix} 0.8279+0.0000i \\ -0.4613+0.3189i \end{bmatrix}$	3.96(-90 dBm) 1.05(-80 dBm)
0.3734	$\begin{bmatrix} 0.9703+0.0000i \\ -0.0197-0.2410i \end{bmatrix}$	$\begin{bmatrix} 0.8907+0.0000i \\ -0.2990+0.3425i \end{bmatrix}$	4.60(-90 dBm) 2.00(-80 dBm)
0.5888	$\begin{bmatrix} 0.9287+0.0000i \\ -0.0750-0.3632i \end{bmatrix}$	$\begin{bmatrix} 0.4166+0.0000i \\ 0.6291-0.6563i \end{bmatrix}$	4.87(-90 dBm) 2.60(-80 dBm)
0.7813	$\begin{bmatrix} 0.3050+0.0000i \\ 0.5023-0.8091i \end{bmatrix}$	$\begin{bmatrix} 0.9832+0.0000i \\ 0.0406-0.1778i \end{bmatrix}$	5.00(-90 dBm) 2.93(-80 dBm)
0.9368	$\begin{bmatrix} 0.8436+0.0000i \\ 0.5252+0.1115i \end{bmatrix}$	$\begin{bmatrix} 0.6649+0.0000i \\ -0.7316+0.1503i \end{bmatrix}$	5.06(-90 dBm) 3.18(-80 dBm)

is $N_0 = -80$ dBm. As shown in the figure, for all α values, the throughput increases with the increase of ρ and the throughput is maximized when ρ approaches to 1, i.e., the polarization states of the transmitters at the source and the relay are orthogonal. The throughput is sensitive to the dissimilarity, especially for the α close to its optimal value, as the throughput decreases significantly if ρ decreases. This means that the polarization states of the transmitters of the source and the relay are required to be orthogonal with each other to achieve the maximum system throughput for any particular value of α. Besides, it is also shown that the throughput is reduced in both the lower and higher range of the α values. For the increment of α in the figure being 0.1, the maximum throughput occurs at $\alpha = 0.3$ for $\rho = 1$.

Fig. 6.6 illustrates the influence of dissimilarity on the throughput R by plotting both analytical results (cf. (6.4) and (6.31)) and simulation results. The FD analytical results are denoted by the letter A and the FD simulation results are denoted by the letter S. In this simulation, the time split factor is 0.3 and transmission power of the relay is 1 Watt. The five specific polarization states randomly chosen for this simulation and the corresponding values of ρ and R are presented in Table 6.1. Fig. 6.6 shows that the maximum throughput is about 3.2 bits/sec/Hz when $N_0 = -80$ dBm while that is about 5.1 bits/sec/Hz when $N_0 = -90$ dBm. Fig. 6.6 also indicates that the throughput is more

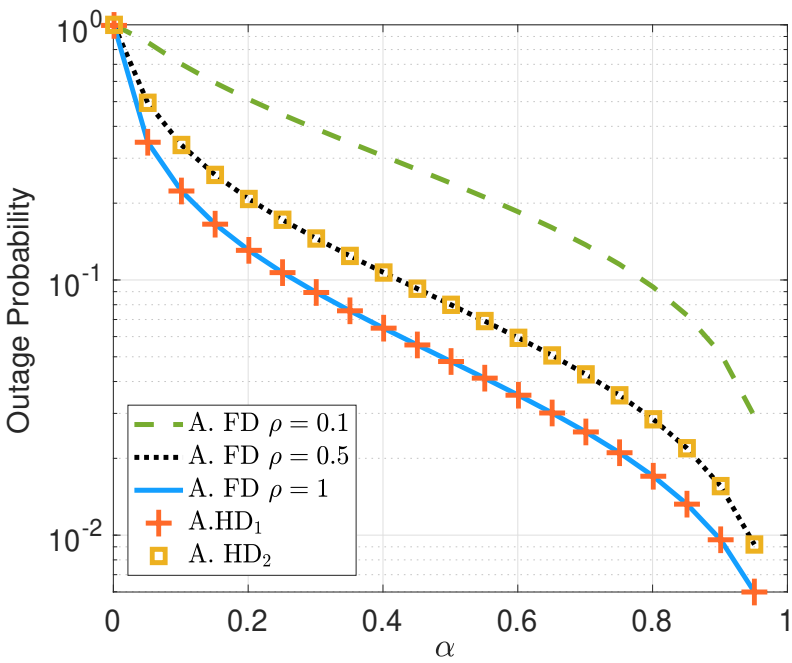

Figure 6.7: Outage probability vs. time split factor α for the HD EH and FD EH systems. $N_0 = -90$ dBm and $P_r = 1$ Watt.

sensitive to ρ in more noisy environments. The throughput increases 1.10 bits/sec/Hz when $N_0 = -90$ dBm while it increases 2.13 bits/sec/Hz when $N_0 = -80$ dBm for the researched ρ range. Besides, it can be seen that the analytical and simulation results match for both scenarios, which verifies the accuracy of the expression in (6.31).

Fig. 6.7 plots the analytical results of the outage probabilities of the HD EH relaying systems, i.e., HD$_1$ and HD$_2$, and the FD EH relaying system with respect to $0 < \alpha < 1$. The noise and transmitting power of the relay are set to be -90 dBm and 1 Watt, respectively. The HD$_1$ and HD$_2$ systems are considered as two benchmarks. In the FD case, the effects of different polarization dissimilarity factors on the outage probability are researched. It is clear that for all cases the outage probabilities decline with the increase of α, i.e., with the increase of the EH time. In comparison, the FD system has the same EH duration as the HD$_1$ system. The source of the FD EH system uses the same total energy as the HD$_1$ EH system to transmit the double amount of information. Thus, the transmitting power per symbol $\hat{P}_s$ in the HD$_1$ case is twice as much as the P_s in the FD case. At the cost of antenna polarization and the digital cancellation scheme, the FD EH system can achieve the same outage probability as the HD$_1$ EH system when $\rho = 1$

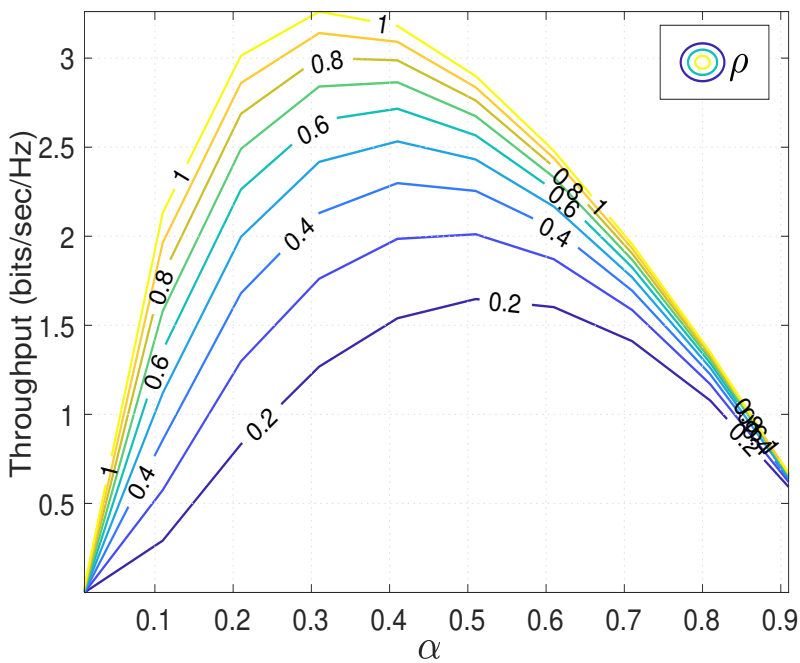

Figure 6.8: Throughput vs. time split factor α for different values of $\log(\rho)$ in the FD EH system. $P_r = 1$ Watt and $N_0 = -80$ dBm.

as shown in Fig. 6.7. Unlike the HD_1 system, the EH duration in the HD_2 system is reduced compared to the HD_1 and FD systems to keep the transmitting power per symbol P_s' in the HD_2 system is the same as P_s in the FD system. The results show that the outage probability of "A. FD $\rho = 1$" is lower than that of "A. HD_2". It is because the PDC scheme can suppress the noise power at the relay by the factor 2ρ as shown in (6.8). Moreover, "A. FD $\rho = 0.5$" matches "A. HD_2" as the outage probabilities of the FD system and the HD_2 system are the same when the polarization dissimilarity factor $\rho = 0.5$ as illustrated in (6.25) and (6.40). In addition, consistent with Figs. 6.5 and 6.6, the decrease of the dissimilarity increases the outage probability as the performance for the case $\rho = 0.1$ is inferior to that for $\rho = 1$.

Fig. 6.8 plots the change of throughput performance along with the time split factor α in the FD EH system when $P_r = 1$ Watt and $N_0 = -80$ dBm. The results are obtained from the analytical expression of throughput in (6.31). The curves with different colors represent different values of ρ, where the lighter colors stand for the larger values of ρ. Fig. 6.8 clearly shows that $R(\alpha)$ in (6.31) is a concave function and the optimal α exists and is unique for each specific ρ value. It is observed that the optimal α value increases

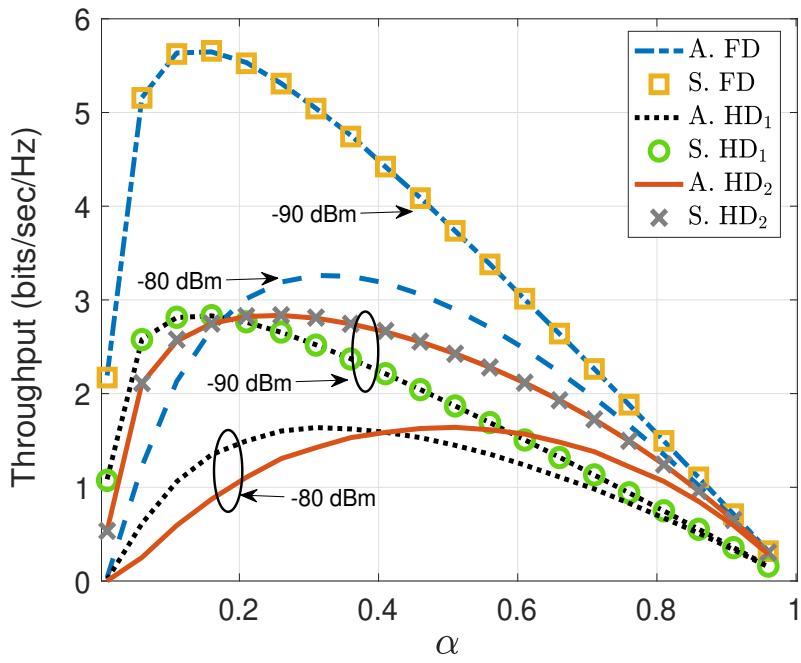

Figure 6.9: Throughput vs. time split factor α for different noise variance N_0. $\rho = 1$ and $P_r = 1$ Watt.

along with the decrease of the maximum throughput and the decrease of ρ. For example, the throughput is maximized at 3.2 bits/sec/Hz with the corresponding $\alpha = 0.3$ and $\rho = 1$. Whereas, the throughput is maximized at 1.6 bits/sec/Hz when $\alpha = 0.5$ and $\rho = 0.2$.

Fig. 6.9 plots the analytical and simulation results of the system throughput with respect to α in the FD EH relaying system, HD_1 EH system, and HD_2 EH system with different noise variances. We can see that the noise variance has a significant influence on the maximum system throughput. For example, in the FD system, the peak value of the throughput is 5.6 bits/sec/Hz with $N_0 = -90$ dBm while that is 3.2 bits/sec/Hz with $N_0 = -80$ dBm. Similarly to Fig. 6.8, the optimal α increases along with the decrease of the maximum throughput even though the reduction of the maximum throughput in Fig. 6.9 is caused by the increase of the noise variance, rather than by the decrease of ρ. Also, in all cases, the maximum throughput of the FD system is almost twice of the HD counterpart. The HD_1 system and HD_2 system have almost the same maximum throughput but different optimal α values. In Fig. 6.9, the optimal α numerically evaluated with $N_0 = -90$ dBm in the FD system by (6.32) is 0.16, in the HD_1 system by (6.38) is also 0.16, and in the HD_2 system by (6.43) is 0.26. The simulation results match the analytical results, which verifies the

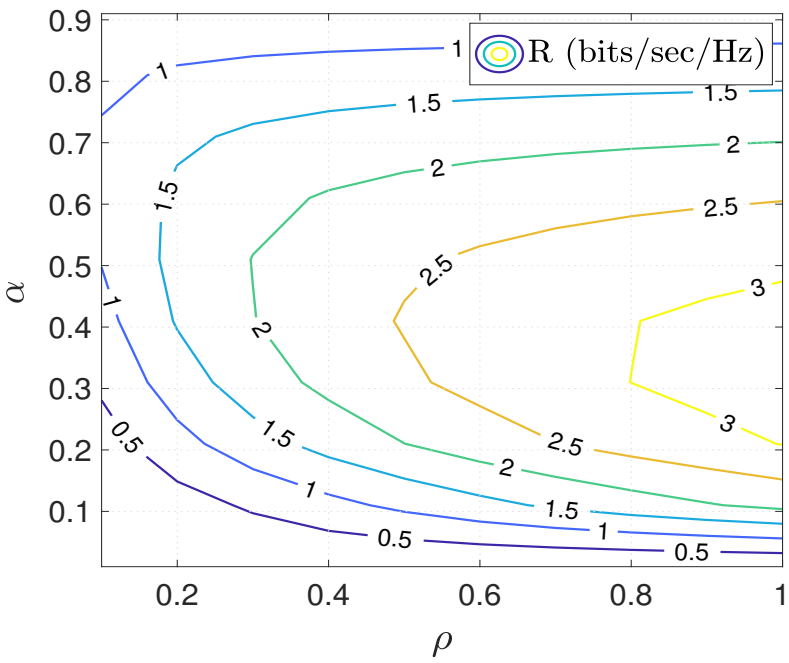

Figure 6.10: A contour plot of the FD throughput performance R. $P_r = 1$ Watt and $N_0 = -80$ dBm.

correctness of the theoretical analyses. This means that the optimal time split values for the FD EH relaying system and the HD EH relaying systems can be obtained accurately by solving numerically the optimization problem in (6.32), (6.38) and (6.43).

Fig. 6.10 plots the contours of the analytical throughput in the FD EH system with the x-coordinates representing the dissimilarity and the y-coordinates representing the time split factor. The line with a lighter color, i.e., yellow color, represents a greater throughput. From this figure, the pairs of values α and ρ to achieve a specific throughput value can be found. For example, when $\alpha = 0.3$ and $\rho = 0.8$ or $\alpha = 0.2$ and $\rho = 1$, the throughput is 3 bits/sec/Hz. Recall that these analytical values ($\alpha = 0.2$, $\rho = 1$, $R = 3$ bits/sec/Hz) are consistent with those values numerically evaluated in Fig. 6.9.

Fig. 6.11 illustrates the analytical and simulation results of throughput with respect to P_r/N_0 in dB for the HD EH and FD EH systems. It is worth noting that P_r/N_0 is the transmit SNR at the source, thus its value is in a high dB range. We assume the time split is 0.2 and the polarization dissimilarity factor is 1. The throughputs of HD and FD systems have a small difference when P_r/N_0 is less than 100 dB. Then, for both systems, throughput increases significantly within the range 100 dB $< P_r/N_0 <$ 130 dB and tends

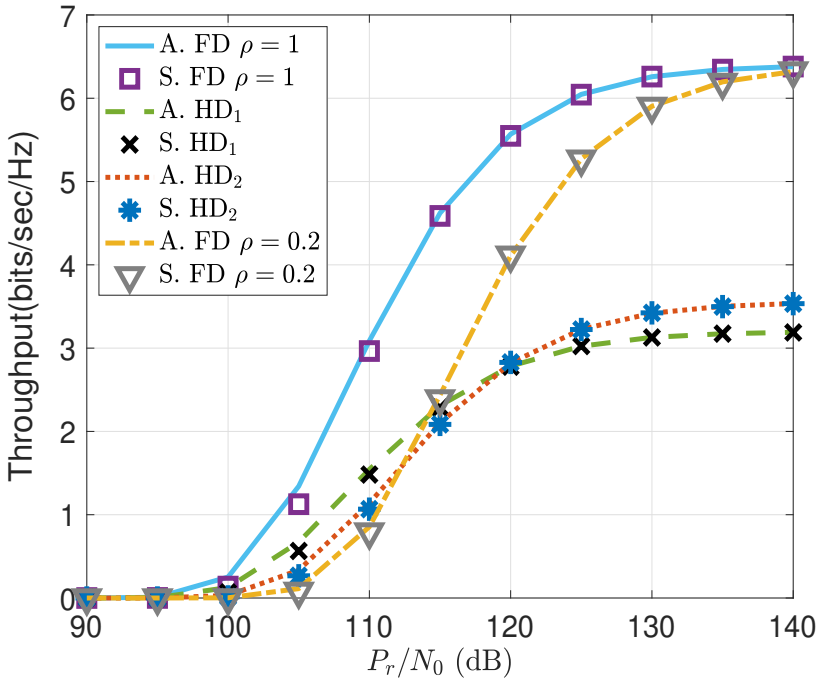

Figure 6.11: Throughput vs. P_r/N_0 in dB for the HD EH and FD EH systems. $\alpha = 0.2$.

to maintain the same value after 130 dB. For different polarization dissimilarity factors of the FD system, the throughput of $\rho = 1$ is higher than that of $\rho = 0.2$ within certain P_r/N_0 ranges and they gradually approach to the same maximum value. As for the HD$_1$ and HD$_2$ systems, the throughput of HD$_2$ is saturated at 3.5 bits/sec/Hz while HD$_1$ is saturated at 3.2 bits/sec/Hz, which illustrates that the former is 1.1 times than the latter. It is clear that, the FD system is saturated at 6.3 bits/sec/Hz. Thus, when the transmission power P_r at the relay is sufficiently large than the noise variance, the throughput in the FD system is nearly double that of the HD systems. This observation also implies that the PDC scheme in the FD system can cancel the SI signal effectively, resulting in the received SNR at the destination being well above the threshold value γ_{th}. Besides, the simulation results of HD and FD systems match the analytical results, which verifies the theoretical analyses shown in (6.31) and (6.37), respectively.

From Figs. 6.7 and 6.11, it is clear that, with the cost of the polarized antennas and the digital SIC module, the FD EH system can double the system throughput while achieving the system outage probability as low as that in the HD EH counterpart.

6.5 Chapter Summary

This chapter considers a two-hop FD system with the WPT from the relay to the source. We assume the direct link from the source to the destination is not available and the information transmission between these two nodes relies on the assistance of the intermediate relay. The EH-capable source is utilized to achieve the self-sustainability of the wireless network. The relay is used to facilitate a long-distance transmission even when the transmitting power at the source node is low. An FD TSR protocol is used in the system to facilitate the cooperation of EH and HD information transmission at the source as well as enable the FD transmission at the relay. The PDC scheme, consisting of antenna polarization and digital signal processing, is adopted at the relay to cancel the SI signal generated by its own transmitter. The results show that the system throughput is a concave function with respect to the time split factor and the optimal time split can be numerically calculated. Moreover, the results reveal that the polarization dissimilarity factor has an influence on the interference and output noise power of the PDC scheme. When polarization states are orthogonal, the output noise of the PDC scheme is suppressed significantly, which leads to its best cancellation effect. Besides, at the cost of the polarized antennas and the additional digital signal processing module, the FD EH system can achieve the same outage probability as the HD_1 EH system, while doubling the system throughput. With the PDC scheme, the outage probability of the FD EH system can be superior to that of the HD_2 EH system. Besides, the throughput of the former nearly doubles that of the latter.

The next chapter will consider the adaptation of the SER technique to a PDC-based FD relaying system with an EH-enabled source node and an EH-enabled relay node.

Chapter 7

Wireless Information and Power Transfer using Full-Duplex Self-Energy Recycling Relays

7.1 Introduction

This chapter proposes a PDC-based FD network with an energy-harvesting-enabled source and a self-energy recycling (SER)-enabled relay. The fixed power supply at the relay is only used in the first phase to broadcast energy signals to the source. During this process, the receive antenna of the relay also receives the energy signals, allowing the relay to recycle its own energy. In the remaining phase, the recycled power is used at the relay to forward signals from the source to the destination, using the PDC-based full-duplex technique. An in-depth analysis and comparison of the throughput of the proposed system with that of the non-recycling counterpart are presented. The power saving and throughput improvement capabilities of the SER enabled system is researched. In particular, the consumed power in the proposed system can be reduced by up to 80% to achieve the same throughput compared to the non-recycling system for a small-to-medium distance range between the relay and the destination. Alternatively, the proposed FD-SER system can boost the system throughput by 1.61 times the non-recycling counterpart with the same power consumption.

7.2 Motivation and Contributions

Inspired by the recent studies in the SER, we propose a full-duplex self-energy recycling relaying system with EH capabilities at both the source node and the relay node. For brevity, the proposed system is named as the FD-SER system here. The source and destination are equipped with a single antenna, while the relay has two antennas to facilitate FD transmission. The proposed two-phase time-splitting protocol lets the source and relay harvest energy in the first phase from the energy signal, which is broadcast from the relay powered by a fixed power supply. A portion of the energy of the transmitted signals is recycled at the relay via the SI channel. In the second phase, the relay receives information from the source, and simultaneously transmits information to the destination. The transmission of the source and relay depends solely on the harvested energy. The SI signal in this phase is canceled by a PDC scheme. The proposed system suits the wireless sensor networks, such as the body sensor networks [115] and the military sensor networks. For example, an energy-constrained sensor is placed within the human body or underground so that replacing the battery to prolong its lifetime is inconvenient. Instead, this sensor can harvest energy from the nearby relay. The relay node also can assist the source sensor to forward information to the destination when direct communication is not possible. The SER is enabled at the relay, which improves the system energy and power efficiencies as proved later in this chapter. The proposed FD-SER system will be compared with the FD non-energy-recycling (NER) EH relaying system with wireless power transfer from the relay to the source discussed in Chapter 6 [41]. For brevity, the non-recycling system is named as the FD-NER system, which is comprised of an EH source, a relay, and a destination. In [41], the relay uses a fixed power supply in the whole transmission process since the relay does not have the self-recycling capability. Thus, no loop-back SER channel nor SER power is considered in the FD-NER system in [41]. The differences of the system model and analytical expressions between this paper and [41] will be elaborated in Section 7.5. The impact of the EH duration, transmit SNR ratio, and S-R distances and R-D distances on the system throughput in both systems are then examined in this chapter.

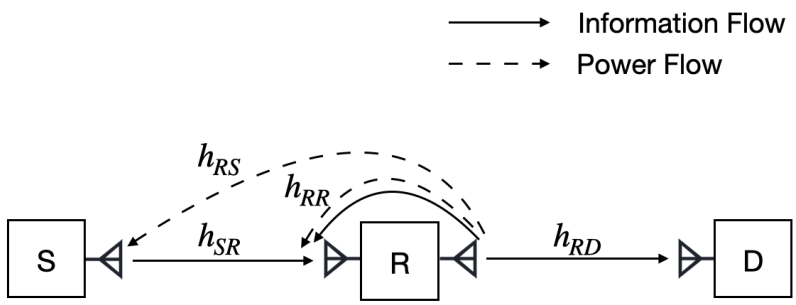

Figure 7.1: Schematic of the proposed FD-SER system.

The major contributions of this work are summarized as follows.

1. In this chapter, a PDC-based FD-SER system is proposed. We have proved that the throughput of the proposed system is comparable with the throughput of the FD-NER system in a small-to-medium R-D distance range while the total power consumption is significantly reduced.

2. The relation between the normalized power consumption and the normalized throughput has been investigated. It has been shown that the proposed recycling system can save up to 80% of the total consumed power while achieving almost the same throughput as the FD-NER one. Alternatively, with the same total power, the relay in our proposed FD-SER system can use a higher power to broadcast energy to the source (and to itself) in the first phase, compared to the FD-NER one, since the FD-SER system only uses the harvested power to forward the signals from the source to the destination in the remaining time. The throughput of the proposed system is revealed to be boosted by 1.61 times that of the FD-NER system.

3. The trade-off between the proposed system and the FD-NER one, with the same total power consumption, is examined. It is shown that the proposed system is very promising as it outperforms the FD-NER one in most cases.

The content of this chapter has been published in [105].

The rest of this chapter is organized as follows. Section 7.3 provides an overview of the system model and transmission protocol. Section 7.4 models the transmission of the

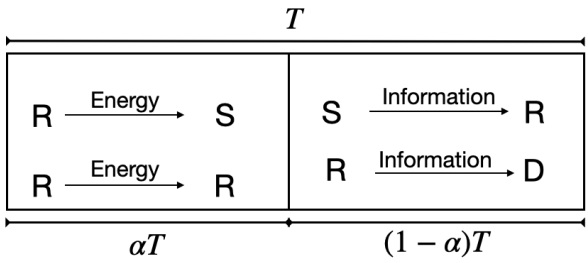

Figure 7.2: Illustration for the proposed two-phase protocol.

energy signal and the information signal in one block time. The analytical expressions for the proposed FD-SER system and the FD-NER system are derived in Section 7.5. Section 7.6 presents the simulation results and Section 7.7 concludes the chapter.

7.3 System Model

In this chapter, we consider an amplify-and-forward FD information transmission system with an EH source (S), a hybrid power-supplied-and-SER relay (R), and a destination (D) as shown in Fig. 7.1. S and D are equipped with one dual-polarized antenna each while R is equipped with two sets of dual-polarized antennas, i.e., one for transmission and the other for reception. The direct link between S and D is assumed to be unavailable due to, for example, heavy shadowing effects (i.e., obstructions). Denote h_{SR}, h_{RS},h_{RR}, and h_{RD} as the channel coefficients of the Rayleigh block fading channels between S and R; R and S; the transmit (Tx) and receive (Rx) antennas at R; and R and D, respectively. We assume their expectation values satisfy $E\{|h_{SR}|^2\} = E\{|h_{RS}|^2\} = E\{|h_{RR}|^2\} = E\{|h_{RD}|^2\} = 1$, where $E\{.\}$ denotes the expectation operation. Denote d_1 and d_2 as the distances between S $\rightarrow$ R and between R $\rightarrow$ D. Denote d_3 as the distance between the Tx and Rx antennas of the relay. The two-phase protocol used in our system is illustrated in Fig. 7.2. The total duration of one block is T. The first and second phases, namely the energy harvesting phase and the information transmission phase, occupy the duration αT and $(1-\alpha)T$, respectively, where $0 < \alpha < 1$.

7.4 Signal Model

7.4.1 Energy Harvesting Phase

During the energy harvesting phase, the antenna at S works in the receiving mode. R works in a HD mode and uses its fixed power supply P_r to broadcast the energy signal. S and R are equipped with linear EH modules. Thus, not only S harvests the energy from R, but also the EH circuitry at R recycles a portion of its own transmitted energy via a loop channel h_{RR}. The polarization of the Tx antenna at R matches the polarization of the Rx antennas at S and R for an optimal reception. The harvested power at S and R will be used for the information transmission in the next phase.

As mentioned in Chapter 6, the received energy signal at the source node S is

$$y_{ei} = \sqrt{\frac{P_r}{d_1^\beta}} h_{RS} x_e + n_s. \tag{7.1}$$

However, in this chapter, P_r is the fixed power supply at R, which is only used in the first phase as the energy source. d_1 is the distance from the source to the relay, h_{RS} is the channel coefficient of the $R \to S$ channel, x_e is the energy symbol with $E\{|x_e|^2\} = 1$, and n_s is the AWGN at S with variance of N_0.

Using (7.1), the total received RF energy E_s of the source node during the time αT is

$$E_s = \frac{\eta_1 P_r |h_{RS}|^2}{d_1^\beta} \alpha T, \tag{7.2}$$

where $0 < \eta_1 < 1$ is the energy conversion efficiency of the source node. Thus, the average RF power for transmission during the next phase at the source is given by

$$P_s = \frac{E_s}{(1-\alpha)T} = \frac{\eta_1 \alpha P_r |h_{RS}|^2}{(1-\alpha) d_1^\beta}. \tag{7.3}$$

In addition, the received energy signal at the relay node R from its own transmitter is

$$y_{er} = \sqrt{\frac{P_r}{d_3^\beta}} h_{RR} x_e + n_r, \tag{7.4}$$

where n_r is the AWGN at R with power N_0. The self-recycling power at the relay is

$$P_{er} = \frac{\eta_2 \alpha P_r |h_{RR}|^2}{(1-\alpha) d_3^{\beta}}, \tag{7.5}$$

where $0 < \eta_2 < 1$ is the energy conversion efficiency of the relay node. Generally, the system is appropriate for any values of $\eta_1, \eta_2 \in (0,1)$. In practice, we assume $\eta_2 > \eta_1$ since the receiver at R is closer to its own transmitter than the receiver at S, thus having a larger input power into the EH circuit [109], [110]. The harvested power P_s and P_{er} will be used in the second phase for information transmission as there is no fixed power supply at S and R in the information transmission phase.

7.4.2 Information Transmission Phase

In this phase, the antenna at S works in the transmitting mode. The source uses the harvested power P_s to transmit the information signal to the relay. The relay works in the FD mode to receive information and forward information at the same time on the same frequency. The power used by the relay to forward information is the recycled power P_{er}. The power supply P_r is switched off in this phase for saving energy. The polarization of the antenna at S and the antennas at R is different from the first phase. Specifically, the polarization of the Rx antenna at R matches that of the Tx antenna at S but differs from that of the Tx antenna at R. The aim is that R receives the maximum power of the desired information signal from S while receiving the minimum amount of the SI power from its own transmitter. Referring to Chapter 2, the polarization state of the desired information signal as $\mathbf{S}$ and the polarization state of the SI signal as $\mathbf{I}$. $\mathbf{S}$ and $\mathbf{I}$ are given as below

$$\begin{aligned} \mathbf{S} &= \begin{bmatrix} \cos(\varepsilon_s) & \sin(\varepsilon_s)\exp(j\delta_s) \end{bmatrix}^{\mathrm{T}}, \\ \mathbf{I} &= \begin{bmatrix} \cos(\varepsilon_i) & \sin(\varepsilon_i)\exp(j\delta_i) \end{bmatrix}^{\mathrm{T}}. \end{aligned} \tag{7.6}$$

where $\varepsilon_i, \varepsilon_s \in [0, \pi/2]$ are polarized angles of the dual-polarized antennas, $\delta_i, \delta_s \in [0, 2\pi]$ are phase differences between the vertical and horizontal polarized components of the dual-polarized antennas. $\mathbf{S}$ and $\mathbf{I}$ are unit vectors, i.e., $\mathbf{S}^{\mathrm{H}}\mathbf{S} = \mathbf{I}^{\mathrm{H}}\mathbf{I} = 1$ and $\mathbf{S} \neq \mathbf{I}$. The

received signal at R is

$$\mathbf{y}_r[i] = \sqrt{\frac{P_s}{d_1^\beta}} h_{SR}\mathbf{S}x_s[i] + \sqrt{\frac{P_{er}}{d_3^\beta}} h_{RR}\mathbf{I}x_r[i] + \mathbf{N}_r[i], \tag{7.7}$$

where $x_r[i]$ is the loop-back self-interference signal, i.e., a delayed version of $\hat{y}_r$ which will be mentioned later in (7.8), and $E\{|x_r[i]|^2\} = 1$. h_{RR} is the SI channel of the relay. The AWGN at R is $\mathbf{N}_r[i] = \begin{bmatrix} \mathrm{n}_H[i] \\ \mathrm{n}_V[i] \end{bmatrix}$, where n_H represents the horizontal polarized component and n_V represents the vertical polarized component. n_H and n_V obey the Gaussian distribution with a zero mean and a variance of $\frac{N_0}{2}$.

The desired received signal in $\mathbf{y}_r[i]$ is interfered by the SI signal $x_r[i]$. The signal $x_r[i]$ can be canceled by the PDC scheme utilizing the polarization states $\mathbf{S}$ and $\mathbf{I}$ and the oblique projection $\mathbf{Q}_{\mathrm{SI}}$ as discussed in Section 3.3 in Chapter 3. Thus, the post-processed signal at the output of the PDC scheme $\hat{y}_r[i]$ is expressed as

$$\begin{aligned} \hat{y}_r[i] &= \mathbf{S}^{\mathrm{H}}\mathbf{Q}_{\mathrm{SI}} \left(\sqrt{\frac{P_s}{d_1^\beta}} h_{SR}\mathbf{S}x_s[i] + \sqrt{\frac{P_{er}}{d_3^\beta}} h_{RR}\mathbf{I}x_r[i] + \mathbf{N}_r[i] \right) \\ &= \sqrt{\frac{P_s}{d_1^\beta}} h_{SR}x_s[i] + \hat{n}_r[i], \end{aligned} \tag{7.8}$$

where $\hat{n}_r[i] = \mathbf{S}^{\mathrm{H}}\mathbf{Q}_{\mathrm{SI}}\mathbf{N}_r[i]$. The polarization dissimilarity factor ρ of $\mathbf{S}$ and $\mathbf{I}$ is discussed in Section 6.2.2 in Chapter 6, which can be defined as $\rho = \mathbf{S}^{\mathrm{H}}\mathbf{P}_{\mathrm{I}}^{\perp}\mathbf{S}$. The power of $\hat{n}_r$ is $E\left[\|\mathbf{S}^{\mathrm{H}}\mathbf{Q}_{\mathrm{SI}}\mathbf{N}_r\|^2\right] = \frac{N_0}{2\rho}$. Eq. (7.8) shows that the PDC scheme can eliminate the effect of the SI channel. However, the oblique projection also causes the residual noise at the relay $\mathbf{S}^{\mathrm{H}}\mathbf{Q}_{\mathrm{SI}}\mathbf{N}_r$ with the variance $\frac{N_0}{2\rho}$. This output noise power is considered as the side-effect of the PDC scheme.

The received signal at the destination is

$$\begin{aligned} y_d[i] &= \sqrt{\frac{\xi^2}{d_2^\beta}} h_{RD}\hat{y}_r[i] + n_d[i] \\ &= \frac{\xi h_{RD} h_{SR}\sqrt{P_s}}{\sqrt{d_1^\beta d_2^\beta}} x_s[i] + \frac{\xi h_{RD}}{\sqrt{d_2^\beta}} \hat{n}_r[i] + n_d[i], \end{aligned} \tag{7.9}$$

where $\xi^2 = \frac{P_{er}}{\frac{|h_{SR}|^2 P_s}{d_1^\beta} + \frac{N_0}{2\rho}}$ denotes the amplifying factor at the relay in the AF protocol, and P_s and P_{er} follow Eqs. (7.3) and (7.5), respectively. It is reasonable to assume that the Rayleigh fading channels$|h_{SR}|^2$ and $|h_{RS}|^2$ are independent and identically distributed (i.i.d.) exponential random variables (RVs) with mean λ_s, $|h_{RD}|^2$ is an i.i.d. exponential RV with mean λ_d, and $|h_{RR}|^2$ is an i.i.d. exponential RV with mean λ_r.

7.5 Throughput Analysis

In this section, the throughput of the proposed FD-SER system is analyzed. From (7.9), the end-to-end SNR from the source to destination is

$$\gamma_{SD} = \frac{\frac{P_s \xi^2 |h_{SR}|^2 |h_{RD}|^2}{d_1^\beta d_2^\beta}}{\frac{\xi^2 |h_{RD}|^2 N_0}{2\rho d_2^\beta} + N_0} = \frac{\frac{P_s P_{er} |h_{SR}|^2 |h_{RD}|^2}{d_1^\beta d_2^\beta \left(\frac{|h_{SR}|^2 P_s}{d_1^\beta} + \frac{N_0}{2\rho} \right)}}{\frac{P_{er} |h_{RD}|^2 N_0}{2\rho d_2^\beta \left(\frac{|h_{SR}|^2 P_s}{d_1^\beta} + \frac{N_0}{2\rho} \right)} + N_0}. \tag{7.10}$$

Define $X_1 = |h_{SR}|^2$, $X_2 = |h_{RS}|^2$, $Y = |h_{RD}|^2$, and $Z = |h_{RR}|^2$. From (7.3), (7.5), and (7.10), the SNR γ_{SD} at the destination is given by

$$\gamma_{SD} = \frac{a X_1 X_2 Y Z}{b + cYZ + dX_1 X_2}, \tag{7.11}$$

where

$$\begin{aligned} a &= 2P_r^2 \alpha^2 \eta_1 \eta_2 \rho, \\ b &= d_1^{2\beta} d_2^\beta d_3^\beta N_0^2 (1-\alpha)^2, \\ c &= P_r \alpha \eta_2 d_1^{2\beta} N_0 (1-\alpha), \\ d &= 2\alpha \eta_1 \rho P_r d_2^\beta d_3^\beta N_0 (1-\alpha). \end{aligned} \tag{7.12}$$

The outage probability P_{out} is defined as the probability when the system SNR γ_{SD} is below the threshold SNR γ_{th}, where $\gamma_{th} = 2^{R_c} - 1$, and R_c is the source transmission rate

in $bits/sec/Hz$.

$$\begin{aligned} P_{out} &= \Pr\{\gamma_{SD} < \gamma_{th}\} \\ &= \Pr\left\{\frac{aX_1X_2YZ}{b+cYZ+dX_1X_2} < \gamma_{th}\right\} \\ &= \Pr\left\{aX_1X_2YZ < \gamma_{th}\left(b+cYZ+dX_1X_2\right)\right\} \\ &= \Pr\left\{YZ(aX_1X_2-\gamma_{th}c) < \gamma_{th}b+\gamma_{th}dX_1X_2\right\}. \end{aligned} \tag{7.13}$$

The probability density function (PDF) of X_1X_2 is given by [16], [116]

$$f_{X_1X_2}(z) = \frac{2}{\lambda_s^2}K_0\left(2\sqrt{\frac{z}{\lambda_s^2}}\right), \tag{7.14}$$

where $K_n(x)$ is the n-th order modified Bessel function of the second kind. The cumulative distribution function (CDF) of YZ is [16], [27]

$$F_{YZ}(z) = 1-2\sqrt{\frac{z}{\lambda_d\lambda_r}}K_1\left(2\sqrt{\frac{z}{\lambda_d\lambda_r}}\right). \tag{7.15}$$

From (7.13), the outage probability is

$$\begin{aligned} P_{out} &= \begin{cases} \Pr\left\{YZ < \frac{\gamma_{th}b+\gamma_{th}dX_1X_2}{aX_1X_2-c\gamma_{th}}\right\}, & X_1X_2 > \frac{c\gamma_{th}}{a} \\ 1, & X_1X_2 \leqslant \frac{c\gamma_{th}}{a} \end{cases} \\ &= \int_0^{\frac{c\gamma_{th}}{a}} f_{X_1X_2}(x)dx \\ &+ \int_{\frac{c\gamma_{th}}{a}}^{\infty} F_{YZ}\left(\frac{\gamma_{th}b+\gamma_{th}dX_1X_2}{aX_1X_2-c\gamma_{th}}\right) f_{X_1X_2}(x)dx. \end{aligned} \tag{7.16}$$

Substituting (7.14) and (7.15) into (7.16), we have

$$P_{out} = 1-\frac{2}{\lambda_s^2}\int_{\frac{c\gamma_{th}}{a}}^{\infty} K_0\left(2\sqrt{\frac{x}{\lambda_s^2}}\right) uK_1(u)\,dx, \tag{7.17}$$

where $u = 2\sqrt{\frac{\gamma_{th}b+x\gamma_{th}d}{\lambda_d\lambda_r(ax-c\gamma_{th})}}$.

Because the information is transmitted in the duration $(1-\alpha)T$ (seconds), the system

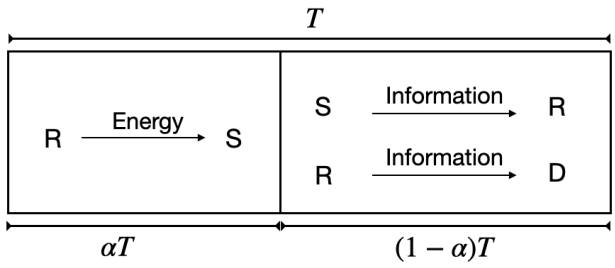

Figure 7.3: Two-phase protocol of the NER system.

throughput can be computed as

$$\begin{aligned} R_c(\alpha) &= (1-P_{out})R_c(1-\alpha) \\ &= R_c(1-\alpha)\frac{2}{\lambda_s^2}\int_{\frac{c\gamma_{th}}{a}}^{\infty} K_0\left(2\sqrt{\frac{x}{\lambda_s^2}}\right) uK_1(u)\,dx. \end{aligned} \tag{7.18}$$

Recall that R_c is the source transmission rate. The final expression of the throughput in (7.18) depends on the outage probability, which in turn depends on the self-recycling power at the relay, P_{er}, as shown in (7.10) and (7.13).

7.6 NER System

For comparison, the FD relaying system with an EH-enabled source and an ordinary relay without the energy-recycling capability in [41] is analyzed below. The system protocol is illustrated in Fig. 7.3 where there is no energy recycling at the relay. As a result, different from the proposed SER system which can switch from the fixed power to the self-recycled power and vice versa at the beginning of each phase, in the NER system, the relay must use the fixed power supply P_r during the whole block time T. In the EH phase, the RF signal is sent from the relay to the EH receiver at the source node. In the information transmission phase, the harvested energy at the source is used for transmitting information to the relay and, at the same time, the fixed power supply at the relay is used for transmitting information to the destination.

Recall the equation (7.1), it is also the received energy signal at S in the NER system. The harvested power at S is P_s as illustrated in (7.3). The received signal at the destination

of the NER system is similar to (7.9), except that the amplifying factor at R is

$$\xi_n^2 = \frac{P_r}{\frac{|h_{SR}|^2 P_s}{d_1^\beta} + \frac{N_0}{2\rho}}. \tag{7.19}$$

Thus, the end-to-end SNR and the outage probability as illustrated in [41] are

$$\gamma_n = \frac{\frac{P_r P_s |h_{SR}|^2 |h_{RD}|^2}{d_1^m d_2^m \left(\frac{N_0}{2\rho} + \frac{P_s |h_{SR}|^2}{d_1^m}\right)}}{\frac{N_0 P_r |h_{RD}|^2}{2 d_2^m \rho \left(\frac{N_0}{2\rho} + \frac{P_s |h_{SR}|^2}{d_1^m}\right)} + N_0}, \tag{7.20}$$

where P_s follows (7.3). The outage probability, P_n, in the NER system is

$$P_n = \Pr\left\{\frac{a'\gamma_{th} X^2 Y}{b' X^2 + c' Y + d'} < \gamma_{th}\right\}, \tag{7.21}$$

where

$$\begin{aligned} a' &= 2\eta_1 \alpha \rho P_r^2, \\ b' &= 2\gamma_{th} \rho \eta_1 \alpha P_r d_2^\beta N_0, \\ c' &= \gamma_{th} N_0 P_r (d_1^\beta)^2 (1-\alpha), \\ d' &= \gamma_{th} N_0^2 (d_1^\beta)^2 d_2^\beta (1-\alpha). \end{aligned} \tag{7.22}$$

and $X \triangleq |h_{SR}|^2 |h_{RS}|^2$, $Y \triangleq |h_{RD}|^2$.

The system throughput is computed as [41, Eq. (35)]

$$R_n(\alpha) = R_c(1-\alpha) \int_{b'/a'}^{\infty} u' K_1(u') \frac{1}{\lambda_d} e^{-\frac{z}{\lambda_d}} dz, \tag{7.23}$$

where

$$u' = 2\sqrt{\frac{c'z + d'}{\lambda_s^2 (a'z - b')}}. \tag{7.24}$$

The outage probability of the SER system proposed in this paper depends on four random variables, $|h_{SR}|^2$, $|h_{RS}|^2$, $|h_{RD}|^2$, and $|h_{RR}|^2$ where h_{RR} is the channel gain of the loop-back channel at the relay, while that of the NER system in [41] depends on three random variables, $|h_{SR}|^2, |h_{RS}|^2$, and $|h_{RD}|^2$. As a result, the derivation of the outage probability

and the throughput in the two systems are considerably different. This can be seen clearly from (7.13), where four variables X_1, X_2, Y, and Z are involved (unlike (7.21) in the NER system where three variables $|h_{SR}|^2, |h_{RS}|^2$, and $|h_{RD}|^2$ are involved). Besides, in (7.18), the integration is taken over the product of the two modified-Bessel functions of the second kind (rather than the integration of the single modified-Bessel function of the second kind in (7.23) in the NER system).

7.7 Numerical Results

We assume the path loss exponent is $\beta = 3$. Since the efficiency is proportional to the average signal power at the input of the rectifier [110], we assume that the EH efficiency at S is $\eta_1 = 0.4$ and at R is $\eta_2 = 0.8$ (except Fig. 7.13 where we consider the whole possible range of η_2). The noise power N_0 is assumed to be -90 dBm, and the transmission rate of the source is 8 bits/sec/Hz. The polarization dissimilarity factor is $\rho = 1$, i.e., the polarization states of the desired signal and the SI signal are orthogonal, except Fig. 7.12 where we consider the whole possible range of ρ. The carrier frequency of 300 MHz is considered and the distance between the Rx antenna of the relay and its Tx antenna is $d_3 = 1$ m to make sure the two antennas experience independent fading. In this paper, we aim to quantify the power saving and the throughput improvement when adopting SER. The protocols of the SER and NER systems are illustrated in Figs. 7.2 and 7.3, respectively. For a fair comparison, the EH fraction, α, of the SER and NER systems is set to be the same in each comparison to keep the harvested energy at the source to be the same.

Fig. 7.4 illustrates the throughput comparison between the proposed FD-SER system $R_c(\alpha)$ (cf. Eq. (7.18)) and the FD-NER system $R_n(\alpha)$ (cf. Eq. (7.23)). The notations A.SER and S.SER stand for the analytical results and the simulation results of the SER system, respectively. A.NER represents the analytical results of the non-energy-recycling system in [23]. The results show that the throughput of the proposed FD-SER system almost reaches that of the FD-NER system within the whole range $0 < \alpha < 1$ when the R-D distance is $d_2 = 50$ m. Recall that the relay only uses the power αP_r in the whole

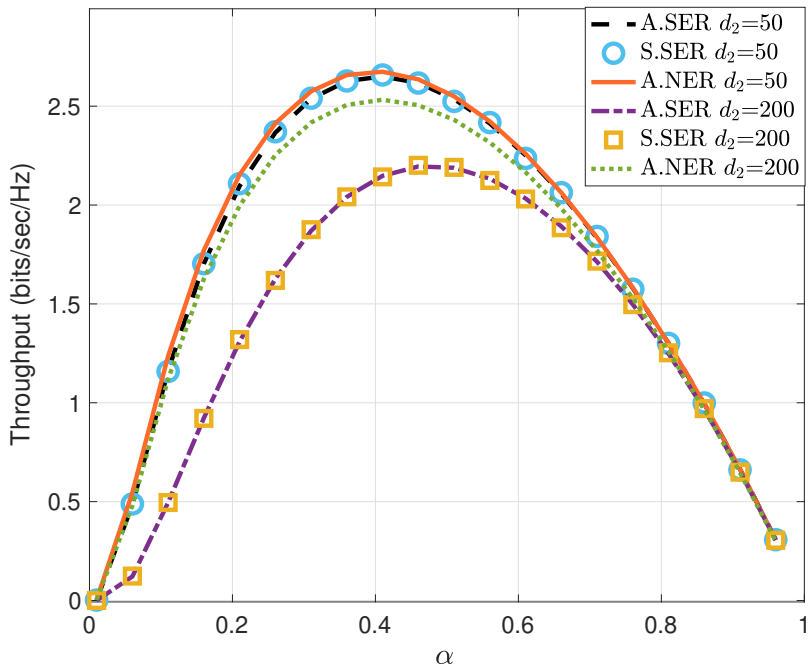

Figure 7.4: Throughput v.s. α when $P_r = 0.1$ Watts and $d_1 = 20$ m.

block T in the proposed system, while it uses the power P_r in the FD-NER system. Thus, we define the normalized power consumption as the ratio of the consumed power at the relay of the FD-SER system to that of the FD-NER system, i.e., $\frac{P_c}{P_n} = \frac{\alpha P_r}{P_r} = \alpha$. Note that $0 < \alpha < 1$. This means that the FD-SER system can save the power consumption by $(1-\alpha)P_n$ Watts while having almost the same throughput as the FD-NER one for the small-to-medium R-D distance range (some tens of meters). With the increase of d_2, the throughput of the FD-SER system is getting worse than that of the FD-NER system as expected, because the self-recycled energy at the relay is limited.

Fig. 7.5 compares the throughputs of the two systems versus the transmit SNR for different R-D distances, d_2. The transmit SNR at the relay is defined as $\frac{P_r}{N_0}$. The throughputs of the two systems are almost the same for the whole considered transmit SNR range, if the R-D distance is in a small-to-medium range. For a long-distance range, the throughput of the FD-SER system is slightly worse than that of the FD-NER system unless the transmit SNR is large enough.

Fig. 7.6 plots the effect of α on the harvested energy at the source node and the self-recycled energy at the relay node in our proposed SER system when $P_r = 1$ Watt and $T = 4.256$ ms [117]. The S-R distance is $d_1 = 20$ m and the distance between the antennas

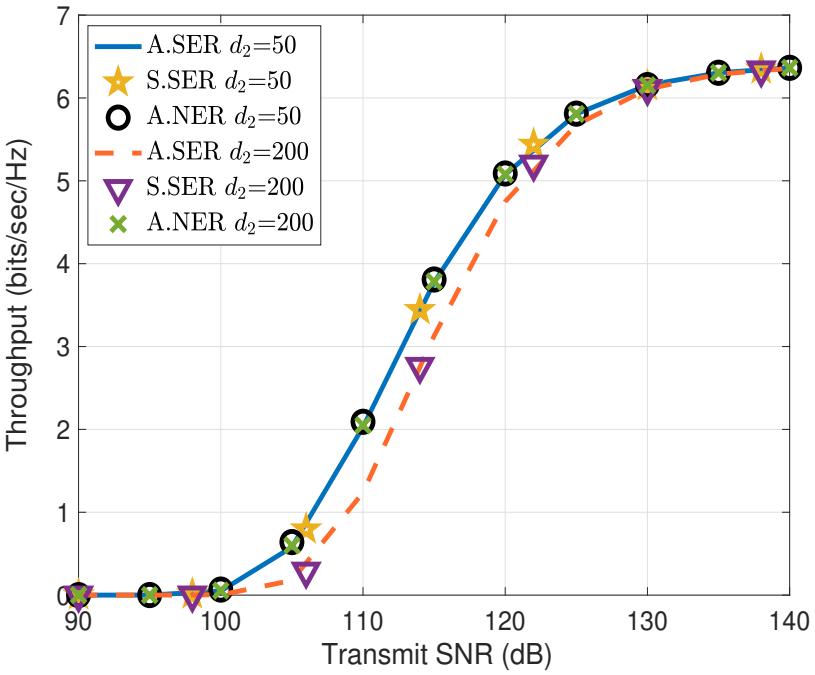

Figure 7.5: Throughput v.s. transmit SNR when $\alpha = 0.2$ and $d_1 = 20$ m.

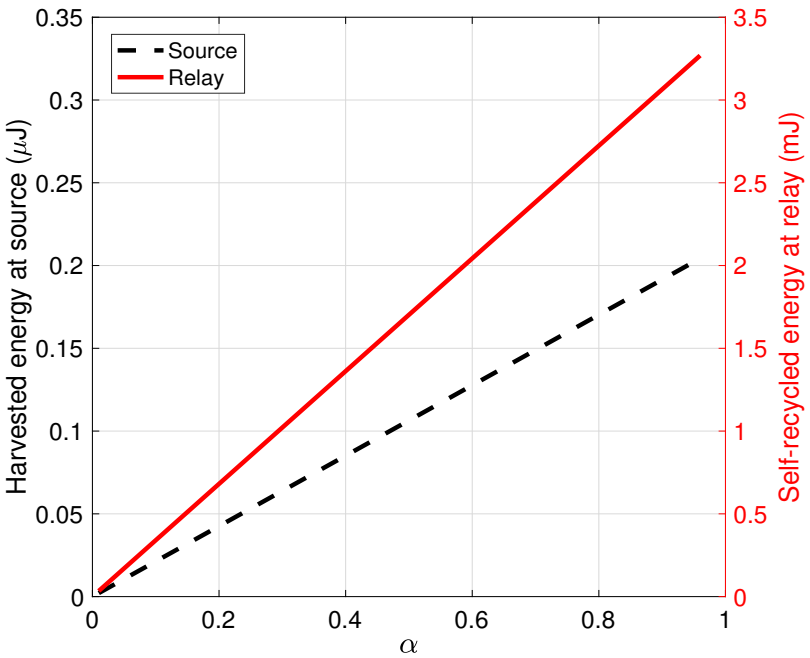

Figure 7.6: Harvested energy v.s. α when $P_r = 1$ Watt and $T = 4.256$ ms.

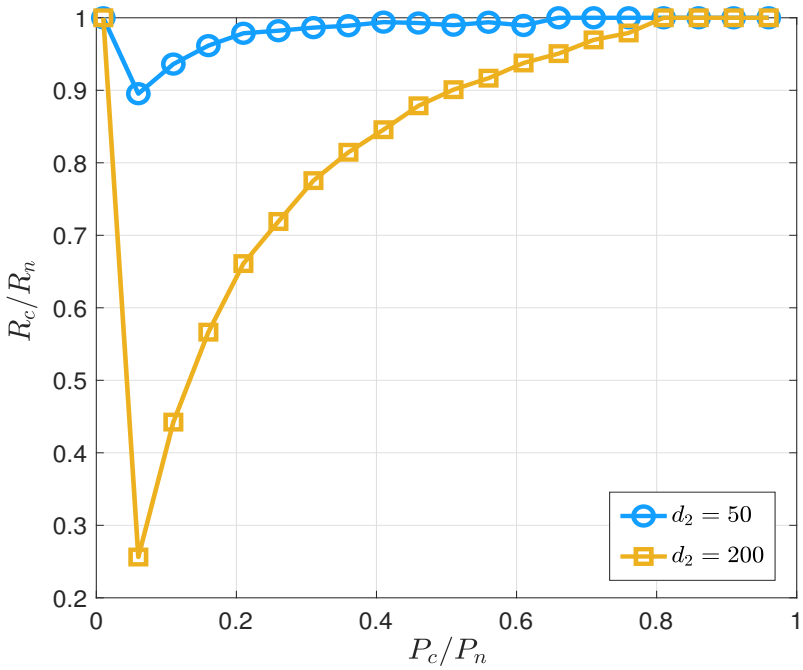

Figure 7.7: Normalized throughput v.s. normalized power consumption when $P_r = 1$ Watt and $d_1 = 20$ m.

at the relay is $d_3 = 1$ m. The results show that the recycled energy at R is around sixteen thousand times the harvested energy at S due to the influence of path loss and energy conversion efficiencies. The results also reveal that adopting the SER technique at the relay can reuse a significant amount of energy.

Fig. 7.7 plots the normalized throughput of the FD-SER system $\frac{R_c}{R_n}$ for different values of the normalized power consumption $\frac{P_c}{P_n}$ (a.k.a. α) for $P_r = 1$ Watt. The result shows that, when $P_c = 0.2P_n$, the throughput is $R_c = 0.97R_n$ for $d_2 = 50$ m and $R_c = 0.66R_n$ for $d_2 = 200$ m. This means that the FD-SER system can save 80% of energy to achieve 97% of the throughput achieved in the FD-NER counterpart for $d_2 = 50$ m, and 66% of the throughput for $d_2 = 200$ m. The worst point is $P_c = 0.06P_n$ for both $d_2 = 50$ m and $d_2 = 200$ m. At this point, 94% energy is saved to have 90% of the throughput achieved in the FD-NER system for $d_2 = 50$ m, and 25% of the throughput for $d_2 = 200$ m. These observations indicate that our FD-SER system can save a large amount of energy, while still being able to achieve a relatively high throughput in a small-to-medium R-D distance range.

Fig. 7.8 illustrates the optimal EH fraction, α, for different relay transmit powers when

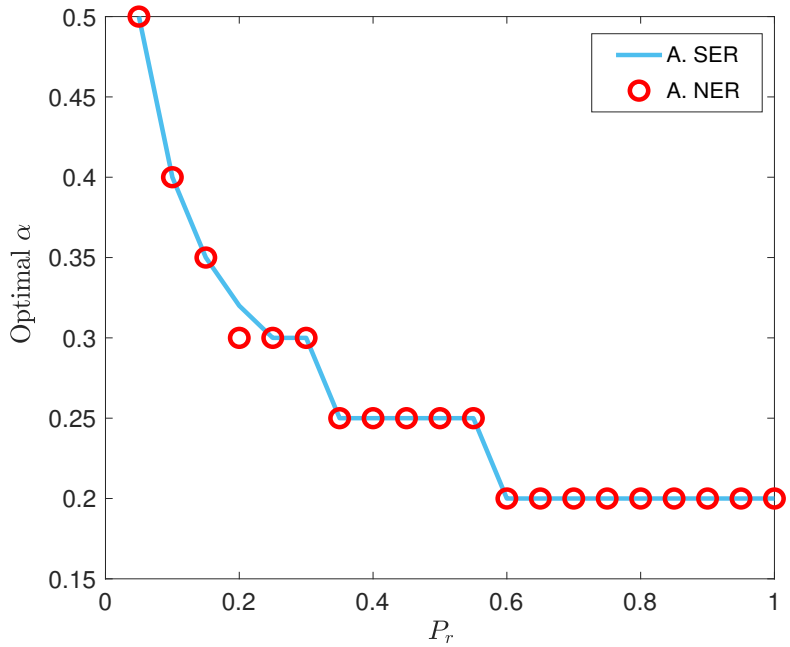

Figure 7.8: Optimal EH fraction v.s. relay transmit power P_r when $d_1 = 20$ m and $d_2 = 50$ m.

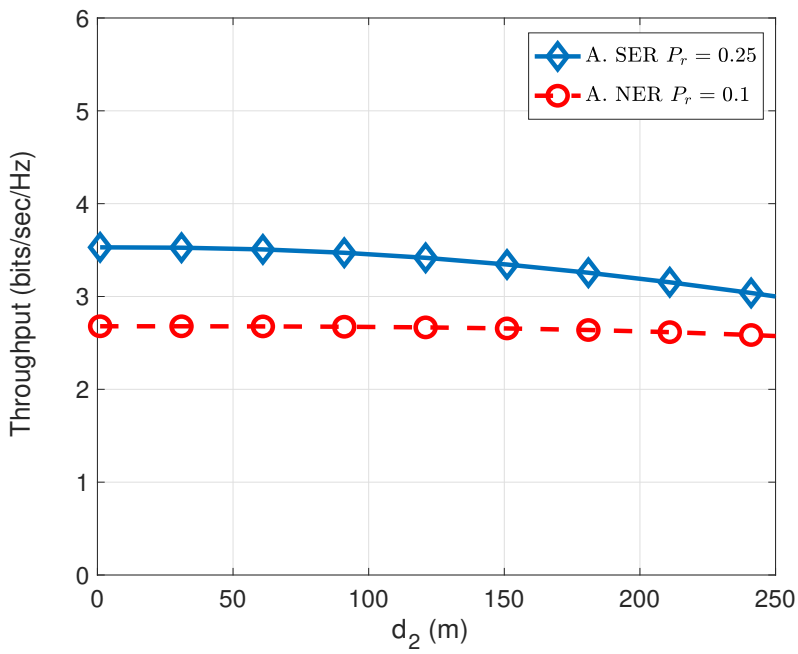

Figure 7.9: Throughput v.s. the R-D distance d_2 when $\alpha = 0.4$ and $d_1 = 20$ m.

$d_1 = 20$ m and $d_2 = 50$ m in both the SER and NER systems. Fig. 7.8 shows that the optimal α decreases with the increase of P_r and the optimal α is almost the same in these two systems for the considered distances of S-R and R-D.

Fig. 7.9 illustrates the throughput performance in both the SER and NER systems when $\alpha = 0.4$ and $d_1 = 20$ m. In this figure, P_r is selected as 0.25 Watts and 0.1 Watts for the SER and NER systems, respectively, to guarantee the same total consumed power in the two system for a fair comparison. Recall Figs. 7.4 and 7.8, it is clear that $\alpha = 0.4$ will optimize the throughput of the NER system for a wide range of d_2 from 50 m to 200 m when $P_r = 0.1$ Watts. However, $\alpha = 0.4$ is not the optimal value of the SER system when $P_r = 0.25$ Watts. This means Fig. 7.9 compares the throughput of the SER system with the optimal throughput of the NER one, given that the total power consumption of the two systems is the same. Thus, this figure shows the minimum throughput improvement that could be achieved by the proposed SER system, compared to the NER counterpart, for the considered set of parameters.

Fig. 7.10 examines the impact of the R-D distance, d_2, and the transmit power at the relay, P_r, on the throughput of the FD-SER and FD-NER systems. Our analyses are derived for generic α values. As we need to make sure that α is the same in both the SER and NER systems for a fair comparison, the parameter $\alpha = 0.2$ is chosen in both system as an example for illustration. Besides, the EH fraction α is set to be 0.2 as it is the optimal value for $P_r = 1$ Watt as shown in Fig. 7.8. Thus, the following figures (Figs. 7.10-7.13) show the upper bound of the throughput improvement that could by achieved by the SER system, compared to the NER counterpart. Fig. 7.10a compares the throughput of the SER and NER systems when the same transmit power is used at the relay and $\alpha = 0.2$ in both systems. From Fig. 7.10a, the throughputs of these two systems are almost the same when d_2 is less than 90 m for $P_r = 1$ Watt and when d_2 is less than 50 m for $P_r = 0.1$ Watts. These observations prove that the consumed power in the proposed system can be reduced by up to 80%to achieve the same throughput compared to the non-recycling system for a small-to-medium range of d_2. Fig. 7.10b shows that the throughput of the FD-SER system is 5.08 bits/sec/Hz when $d_2 = 20$ m and 4.75 bits/sec/Hz when $d_2 = 200$ m. Meanwhile,

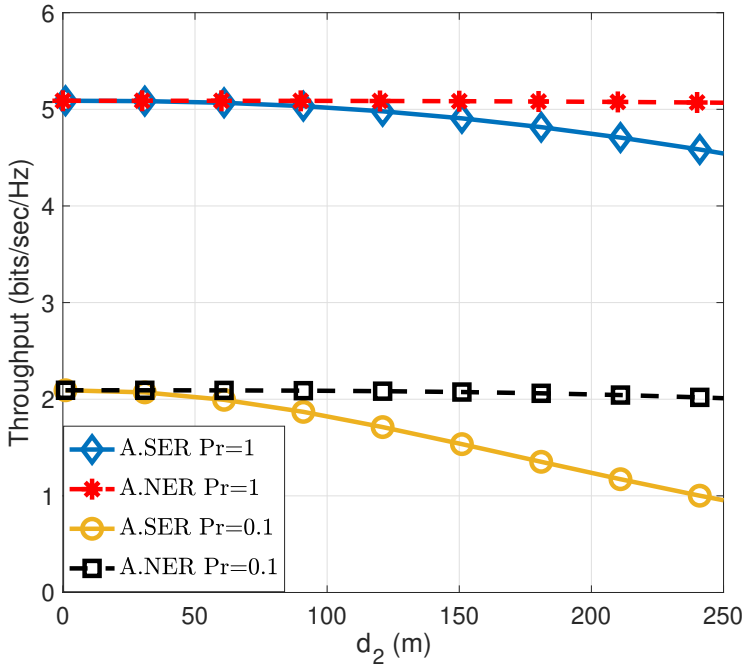

(a)

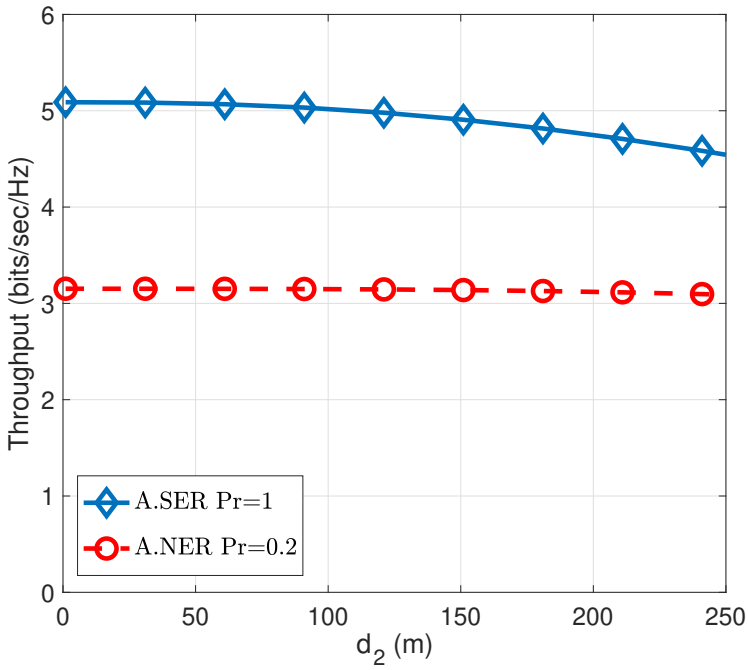

(b)

Figure 7.10: Throughput v.s. the R-D distance d_2 when $\alpha = 0.2$ and $d_1 = 20$ m.

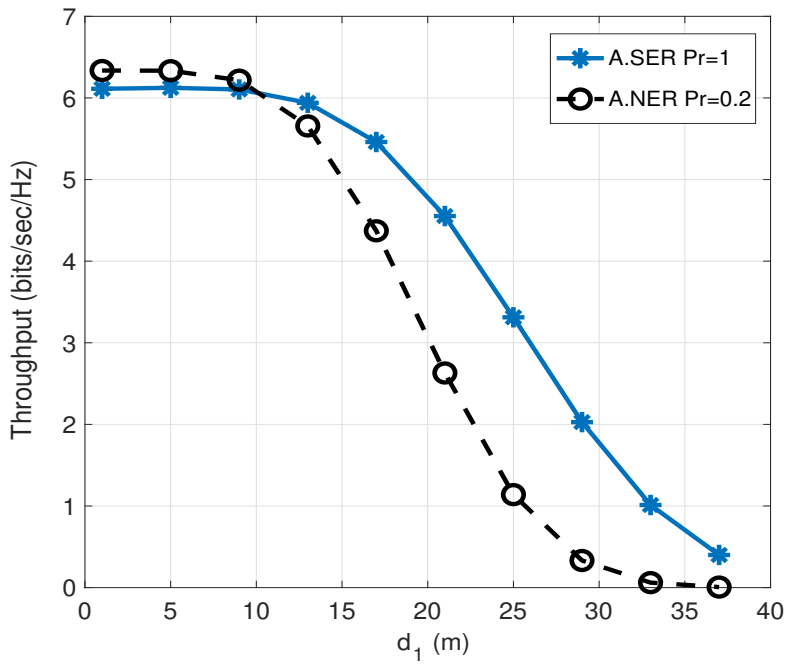

Figure 7.11: Throughput v.s. d_1 when $\alpha = 0.2$ and $d_1 = 200 - d_2$ m.

the throughput of the FD-NER system reduces slowly from 3.15 bits/sec/Hz at $d_2 = 20$ m to 3.12 bits/sec/Hz at $d_2 = 200$ m. Note that the power consumed at the relay of the proposed FD-SER system is 0.2 Watts when $\alpha = 0.2$ and $P_r = 1$ Watt, which is exactly the same as the power consumed at the relay of the FD-NER system with $P_r = 0.2$ Watts. This result shows that, with the same consumed power, the throughput in our FD-SER system can be up to 1.61 times higher than that in the FD-NER system. This is because the FD-SER system saves the energy consumed in the second phase by adopting the SER technique. The relay in the FD-SER system uses a higher power, compared to the FD-NER one, to transmit energy signal to the source and itself in the first phase. Thus, the FD-SER system achieves a higher throughput in a small-to-medium R-D range.

Fig. 7.11 plots the throughput performance of the proposed FD-SER system versus the S-R distance d_1 when $\alpha = 0.2$, with the non-cycling system serving as a benchmark. As mentioned above, when $\alpha = 0.2$ and $P_r = 1$ Watt, the total consumed power of the FD-SER system is exactly the same as that of the FD-NER system with $P_r = 0.2$ Watts. The relay-transmitting power in the second phase of the FD-SER system depends on the harvested energy while the FD-NER system relay has the fix power supply. The total source-to-destination (S-D) distance is set to be 200 m and the S-R distance is $d_1 =$

$200-d_2$ m. Fig. 7.11 aims to explore the effect of relay location on the system throughput in comparison with the NER counterpart. As a result, the same total S-D distance of 200 m is considered in both systems. The results show that the throughput in both systems decreases as d_1 increases due to a larger path loss in the S-D link. Consequently, the received signal strength at the relay is poorer and the throughput decreases. However, the proposed system still outperforms the FD-NER system, unless d_1 is under 10 m, where the former is slightly inferior than the latter. This is because, when d_1 is too small, the relay is too far from the destination. Due to the limited recycled energy at the relay, the system throughput will be reduced. Fig. 7.11 thus shows the trade-off between the two systems. For this simulation scenario, if the relay has to be put more than 10 m away from the source due to, for example, the unavailability of the physical place for the installation of the relay (like in mining tunnels), the proposed FD-SER system is a better choice than the counterpart. This demonstrates the usefulness of our proposed system in a realistic scenario. Clearly, the optimal relay location in the proposed system is approaching the source node, rather than the middle point between the source and the destination which is a well-known observation for a conventional half-duplex, non-energy harvesting system reported in the literature.

Fig. 7.12 plots the throughput of the FD-SER and FD-NER systems versus the polarization dissimilarity factor, ρ, when $\alpha = 0.2$. The comparison of the two systems is based on the same total energy consumption, so $P_r = 1$ in the SER system and $P_r = 0.2$ in the SER system. The analytical results show that the throughput increases with the increase of ρ. Since $0 < \rho \leqslant 1$, the maximum throughput is obtained when $\rho = 1$, i.e., the polarization states of the desired signal and the SI signal are orthogonal. Fig. 7.12 indicates clearly that our proposed system still outperforms the FD-NER one even when the polarization states of the antennas are not orthogonal.

Fig. 7.13 illustrates the impact of the energy efficiency at S, η_1, on the system throughput. We set $\alpha = 0.2$, $d_1 = 20$ m, $d_2 = 200$ m, and $P_r = 1$ Watt in the FD-SER system and $P_r = 0.2$ Watts in the FD-NER system. Note that usually $\eta_2 > \eta_1$ as the distance between the transmit-end and the receive-end of the energy signal at R is closer than that at S.

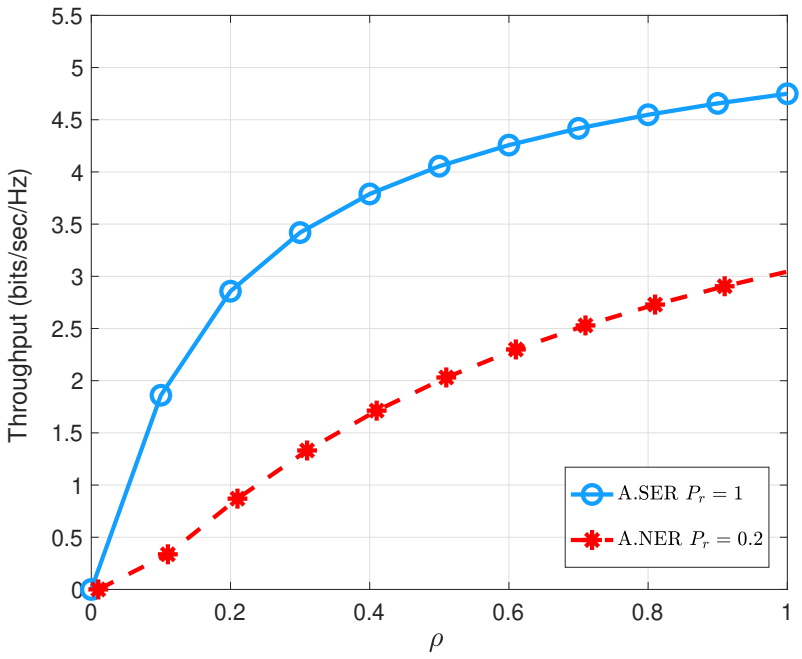

Figure 7.12: Throughput v.s. polarization dissimilarity factor, ρ, when $\alpha = 0.2$.

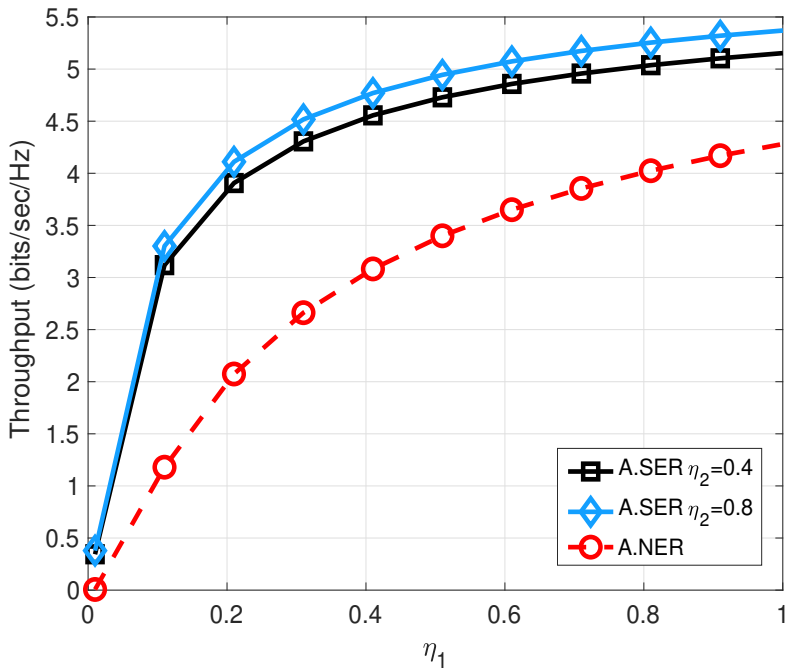

Figure 7.13: Throughput v.s. efficiency at S, η_1, when $P_r = 1$ Watt in the FD-SER system and $P_r = 0.2$ Watts in the FD-NER system.

Fig. 7.13 reveals that throughput is proportional to η_1 in both systems. The increase of the efficiency at R, η_2, in the FD-SER system will improve further the system throughput. In addition, if η_1 increases by 0.4, the throughput increases by about 0.4 bits/sec/Hz to 4.8 bits/sec/Hz. This figure also shows the variation of η_2 in terms of $\eta_2 = 0.4$ and $\eta_2 = 0.8$. If η_2 increases by 0.4, the throughput increases by about 0.2 bits/sec/Hz. Thus, it is clear that the throughput depends more on η_1 rather than η_2.

7.8 Conclusion

In this chapter, we have proposed a PDC-based FD relaying network with an EH-enabled source and a SER-enabled relay. The relay only uses its fixed power supply in the first phase to broadcast energy signals to the sources. During this process, it also recycles part of its own transmitted energy. In the remaining phase, the relay uses the recycled power to forward signals from the source to the destination in a PDC-based FD communication mode. Analytical expressions have been derived for the outage probability and throughput of the system, confirmed by our simulations. This chapter reveals that, compared to the FD-NER system, our proposed system can save significantly the total consumed power while achieving almost the same system throughput for a small-to-medium R-D distance range. Alternatively, with the same power consumption, our system outperforms the counterpart in most cases. Therefore, it is a promising solution to save power or boost the system throughput in FD EH relaying systems. Our future works include extending the two-antenna relay to a multi-antenna structure, considering other SIC techniques, such as the analog least mean square loop [118], and examining the correlated fading channels between antennas [119].

Chapter 8

Conclusions and Future Works

8.1 Conclusions

This thesis has investigated the outage probability, throughout, and BER of different two-hop FD WPT systems. The scope of the research includes SIC schemes, WPT from the source to the relay and from the relay to the source, SER technique, single-carrier Rayleigh flat fading channels, and OFDM multipath frequency selective fading channels. With respect to the research objectives presented in Chapter 1, this thesis is summarized as follows.

1. The adaptations of the PDC scheme to the FD-EH relaying systems for both the single-carrier Rayleigh flat fading channels and the OFDM frequency selective fading channels are investigated. It has been found that the PDC scheme does not require the instantaneous CSI of the SI channels. The simulation results in the single-carrier system with WET from the source to the relay show that the FD EH relaying system almost doubles the system throughput, compared to the HD EH relaying system, at the cost of about 5 dB inferior error performance. The throughput and BER in the OFDM system with WET from the source to the relay are researched. The results show that for a given time splitting factor, the number of sub-bands should be chosen small enough, provided that each sub-band still experiences a flat fading channel, to achieve both high system throughput and a good BER performance. The FD system substantially improves the system throughput, while maintaining the same BER by a modest increase in SNR compared to the HD

system. In both the single-carrier system and the OFDM system, to achieve a high throughput along with a good error performance, a combined selection of a high transmit SNR and a suitable EH time is required.

2. A PDC-enabled OFDM FD relaying system with WET from the source to the relay is investigated. The mathematical expressions of the throughput for an OFDM sub-band are derived in two different approaches over the Rayleigh frequency-selective fading channels. The first method considers the distributions of the two exponential random variables independently. The second method considers product distribution of the S-R channel and R-D channel, which is more accurate. Comparing FD with HD relaying systems shows that the throughput of the former is nearly doubled than the latter at high transmit SNRs. For simplification, the asymptotic lines of outage probability and throughput are researched and validated at high SNRs.

3. A PDC-enabled FD relaying system in single-carrier Rayleigh flat fading channels and with WET from the relay to the source is proposed. The EH-capable source is utilized to achieve the self-sustainability of the wireless network. The relay is used to facilitate a long-distance transmission even when the transmitting power at the source node is low. The system throughput is a concave function for the time split factor and the optimal time split can be numerically calculated. Moreover, the polarization dissimilarity factor influences the interference and output noise power of the PDC scheme. When polarization states are orthogonal, the output noise of the PDC scheme is suppressed significantly, which leads to its best cancellation effect. We provide the analysis of outage probability and throughput of an FD relaying system and two HD relaying systems. The HD_1 system has the same EH duration as the FD system while the HD_2 system has the same transmitting power at the source as the FD one. At the cost of the polarized antennas and the additional digital signal processing module, the FD system can achieve the same outage probability as the HD_1 system, while doubling the system throughput. With the PDC scheme, the outage probability of the FD system can be superior to that of the HD_2 system and the throughput of the former is nearly double that of the latter.

4. We have proposed a PDC-based FD relaying network with an EH-enabled source and an SER-enabled relay in the single-carrier Rayleigh flat fading channels. The relay only uses its fixed power supply in the first phase to broadcast energy signals to the sources. During this process, it also recycles part of its own transmitted energy. In the remaining phase, the relay uses recycled power to forward signals from the source to the destination, using the PDC-based FD technique. Analytical expressions have been derived for the outage probability and throughput of the system, confirmed by our simulations. The paper reveals that, compared to the FD-NER system, our proposed system can save 80% of the total consumed power while achieving almost the same system throughput for a small-to-medium R-D distance range. Alternatively, with the same power consumption, our system outperforms the counterpart in most cases. Therefore, it is a promising solution to save power or boost the system throughput in FD EH relaying systems.

8.2 Future Works

The possible research directions in the future include.

- The consideration of a high-speed multi-antenna (i.e., MIMO-OFDM) EH relaying system which transmits quasi-orthogonal or differential space-time-frequency codes in an FD mode [120]–[122]. A comprehensive analysis of the multi-antenna FD EH relaying system in a correlated fading channel can be provided.

- The extension of our proposed system to the case of multiple users [123], multiple sources, or multiple relays [124], [125]. It might also consider non-linear RF EH models and examine other promising SIC techniques, such as the analog least mean square loops, to cancel the SI at the relay.

- The consideration of other channel fading models, such as the Nakagami fading, Log-normal shadow fading, and Rician fading. Besides, providing analytical evaluations of spectral efficiency and energy efficiency.

Bibliography

[1] Y. Li and S. Kishore, "Asymptotic analysis of amplify-and-forward relaying in nakagami-fading environments," *IEEE Trans. Wireless Commun.*, vol. 6, no. 12, pp. 4256–4262, Dec. 2007.

[2] Z. Lin, L. C. Tran, and F. Safaei, "Performance evaluation of cooperative communications for STFC MB-OFDM UWB," in *Proc. ISCI*, HSurat Thani, Thailand, Sep. 2013, pp. 46–51.

[3] Q. Zhang, J. Jia, and J. Zhang, "Cooperative relay to improve diversity in cognitive radio networks," *IEEE Commun. Mag.*, vol. 47, no. 2, pp. 111–117, Feb. 2009.

[4] P. Herhold, E. Zimmermann, and G. Fettweis, "Cooperative multi-hop transmission in wireless networks," *Comput. Networks*, vol. 49, no. 3, pp. 299–324, Jun. 2005.

[5] Z. Lin, L. C. Tran, and F. Safaei, "Order-4 orthogonal cooperative communication in space-time-frequency coded MB-OFDM UWB," in *Proc. ISCIT*, Gold Coast, QLD, Australia, Oct. 2012, pp. 920–925.

[6] T. Le Chung, Z. Lin, F. Safaei, A. Mertins, and D. T. Ngo, "Exact error performance analysis of binary space-time block coded cooperative communications systems in rayleigh fading channels," in *Proc. ATC*, Ho Chi Minh City, Vietnam, Oct. 2015, pp. 567–571.

[7] T. N. Do and B. An, "Cooperative spectrum sensing schemes with the interference constraint in cognitive radio networks," *Sensors*, vol. 14, no. 5, pp. 8037–8056, May 2014.

[8] V. N. Q. Bao, N. Linh-Trung, and M. Debbah, "Relay selection schemes for dual-hop networks under security constraints with multiple eavesdroppers," *IEEE Trans. Wireless Commun.*, vol. 12, no. 12, pp. 6076–6085, Dec. 2013.

[9] D. Mishra and S. De, "Optimal time allocation for RF-powered DF relay-assisted cooperative communication," *Electr. Lett.*, vol. 52, no. 14, pp. 1274–1276, Jul. 2016.

[10] Y. Liu, "Wireless information and power transfer for multirelay-assisted cooperative communication," *IEEE Commun. Lett.*, vol. 20, no. 4, pp. 784–787, Feb. 2016.

[11] N. T. Do, V. N. Q. Bao, and B. An, "A relay selection protocol for wireless energy harvesting relay networks," in *Proc. ATC*, Ho Chi Minh City, Vietnam, Oct. 2015, pp. 243–247.

[12] Y. Chen, "Energy-harvesting AF relaying in the presence of interference and Nakagami-*m* fading," *IEEE Trans. Wireless Commun.*, vol. 15, no. 2, pp. 1008–1017, Feb. 2016.

[13] K. Xiong, P. Fan, C. Zhang, and K. B. Letaief, "Wireless information and energy transfer for two-hop non-regenerative MIMO-OFDM relay networks," *IEEE J. Sel. Areas Commun.*, vol. 33, no. 8, pp. 1595–1611, Aug. 2015.

[14] A. A. Nasir, X. Zhou, S. Durrani, and R. A. Kennedy, "Relaying protocols for wireless energy harvesting and information processing," *IEEE Trans. Wireless Commun.*, vol. 12, no. 7, pp. 3622–3636, Jul. 2013.

[15] Y. Hu, N. Cao, and Y. Chen, "Analysis of wireless energy harvesting relay throughput in rician channel," *Mobile Inform. Syst.*, vol. 2016, pp. 1–9, Oct. 2016.

[16] C. Zhong, H. A. Suraweera, G. Zheng, I. Krikidis, and Z. Zhang, "Wireless information and power transfer with full duplex relaying," *IEEE Trans. Commun.*, vol. 62, no. 10, pp. 3447–3461, Oct. 2014.

[17] Q. N. Le, V. N. Q. Bao, and B. An, "Full-duplex distributed switch-and-stay energy harvesting selection relaying networks with imperfect CSI: Design and outage analysis," *J. Commun. Networks*, vol. 20, no. 1, pp. 29–46, Feb. 2018.

[18] Y. Dong, M. J. Hossain, and J. Cheng, "Performance of wireless powered amplify and forward relaying over Nakagami-*m* fading channels with nonlinear energy harvester," *IEEE Commun. Lett.*, vol. 20, no. 4, pp. 672–675, Apr. 2016.

[19] P. N. Son, H. Y. Kong, and A. Anpalagan, "Exact outage analysis of a decode-and-forward cooperative communication network with Nth-best energy harvesting relay selection," *Ann. Telecommun.*, vol. 71, no. 5, pp. 251–263, Jun. 2016.

[20] S. S. Ikki and M. H. Ahmed, "Performance analysis of adaptive decode-and-forward cooperative diversity networks with best-relay selection," *IEEE Trans. Commun.*, vol. 58, no. 1, pp. 68–72, Jan. 2010.

[21] K. R. Liu, A. K. Sadek, W. Su, and A. Kwasinski, *Cooperative communications and networking*. Cambridge Uni. Press, 2009.

[22] K. M. Rabie, A. Salem, E. Alsusa, and M.-S. Alouini, "Energy-harvesting in cooperative AF relaying networks over log-normal fading channels," in *Proc. IEEE ICC*, Kuala Lumpur, Malaysia, May 2016, pp. 1–7.

[23] A. Sabharwal *et al.*, "In-band full-duplex wireless: Challenges and opportunities," *IEEE J. Sel. Areas Commun.*, vol. 32, no. 9, pp. 1637–1652, Sep. 2014.

[24] S. Li and R. D. Murch, "Full-duplex wireless communication using transmitter output based echo cancellation," in *Proc. GLOBECOM*, Houston, TX, USA, Dec. 2011, pp. 1–5.

[25] H. Ju, S. Lim, D. Kim, H. V. Poor, and D. Hong, "Full duplexity in beamforming-based multi-hop relay networks," *IEEE J. Sel. Areas Commun.*, vol. 30, no. 8, pp. 1554–1565, Sep. 2012.

[26] J. Li, L. C. Tran, and F. Safaei, "Performance evaluation of full-duplex energy harvesting relaying networks using PDC self-interference cancellation," in *Proc. IEEE ICSPCS*, Cairns, QLD, Australia, Dec. 2018, pp. 1–6.

[27] ——, "Outage probability and throughput analyses in full-duplex relaying systems with energy transfer," *IEEE Access*, vol. 8, pp. 150 150–150 161, Aug. 2020.

[28] K. Yang, H. Cui, L. Song, and Y. Li, "Joint relay and antenna selection for full-duplex AF relay networks," in *Proc. IEEE ICC*, Sydney, NSW, Australia, Jun. 2014, pp. 4454–4459.

[29] A. T. Le, L. C. Tran, and X. Huang, "Cyclostationary analysis of analog least mean square loop for self-interference cancellation in in-band full-duplex systems," *IEEE Commun. Lett.*, vol. 21, no. 12, pp. 2738–2741, Dec. 2017.

[30] A. T. Le, L. C. Tran, and X. Huang, "On performance of analog least mean square loop for self-interference cancellation in in-band full-duplex OFDM systems," in *Proc. IEEE VTC*, Sydney, NSW, Australia, Jun. 2017, pp. 1–5.

[31] L. C. Tran and A. Mertins, "Error performance and energy efficiency analyses of fully cooperative OFDM communication in frequency selective fading," *IET Commun.*, vol. 10, no. 18, pp. 2525–2533, Dec. 2016.

[32] O. Ozel, K. Tutuncuoglu, J. Yang, S. Ulukus, and A. Yener, "Transmission with energy harvesting nodes in fading wireless channels: Optimal policies," *IEEE J. Sel. Areas Commun.*, vol. 29, no. 8, pp. 1732–1743, Sep. 2011.

[33] J. Yang and S. Ulukus, "Optimal packet scheduling in an energy harvesting communication system," *IEEE Trans. Commun.*, vol. 60, no. 1, pp. 220–230, Jan. 2012.

[34] K. Tutuncuoglu and A. Yener, "Optimum transmission policies for battery limited energy harvesting nodes," *IEEE Trans. Wireless Commun.*, vol. 11, no. 3, pp. 1180–1189, Mar. 2012.

[35] D. Altinel and G. K. Kurt, "Diversity combining for RF energy harvesting," in *Proc. IEEE VTC Spring*, Sydney, NSW, Australia, Jun. 2017, pp. 1–5.

[36] Z. Wang *et al.*, "A novel magnetic energy harvester using spinning magnetoelectric transducer," *IEEE Trans. Magn.*, vol. 52, no. 7, pp. 1–4, Jul. 2016.

[37] J. Cannarella *et al.*, "Coupling factor between the magnetic and mechanical energy domains in electromagnetic power harvesting applications," *IEEE Trans. Magn.*, vol. 47, no. 8, pp. 2076–2080, Aug. 2011.

[38] Q. Zhang and E. S. Kim, "Micromachined energy-harvester stack with enhanced electromagnetic induction through vertical integration of magnets," *J. Microelectromech. Syst.*, vol. 24, no. 2, pp. 384–394, Apr. 2015.

[39] R. Zhang and C. K. Ho, "MIMO broadcasting for simultaneous wireless information and power transfer," *IEEE Trans. Wireless Commun.*, vol. 12, no. 5, pp. 1989–2001, May 2013.

[40] J. Li, L. C. Tran, and F. Safaei, "Full-duplex OFDM relaying systems with energy harvesting in multipath fading channels," in *Proc. IEEE VTC2019-Fall*, Honolulu, HI, USA, Sep. 2019, pp. 1–5.

[41] J. Li, L. C. Tran, and F. Safaei, "Throughput analysis of in-band full-duplex transmission networks with wireless energy harvesting enabled sources," *IEEE Access*, vol. 9, pp. 74 989–75 002, May 2021.

[42] M. Dong, W. Li, and F. Amirnavaei, "Online joint power control for two-hop wireless relay networks with energy harvesting," *IEEE Trans. Signal Process.*, vol. 66, no. 2, pp. 463–478, Jan. 2018.

[43] K. M. Rabie, B. Adebisi, and M.-S. Alouini, "Half-duplex and full-duplex AF and DF relaying with energy-harvesting in log-normal fading," *IEEE Transa. Green Commun. Networking*, vol. 1, no. 4, pp. 468–480, Dec. 2017.

[44] D. Cassioli, M. Win, and A. Molisch, "The ultra-wide bandwidth indoor channel: From statistical model to simulations," *IEEE J. Sel. Areas Commun.*, vol. 20, no. 6, pp. 1247–1257, Aug. 2002.

[45] Z. Zhou, M. Peng, Z. Zhao, and Y. Li, "Joint power splitting and antenna selection in energy harvesting relay channels," *IEEE Signal Process. Lett.*, vol. 22, no. 7, pp. 823–827, Jul. 2015.

[46] M. Mohammadi *et al.*, "Throughput analysis and optimization of wireless-powered multiple antenna full-duplex relay systems," *IEEE Trans. Commun.*, vol. 64, no. 4, pp. 1769–1785, Apr. 2016.

[47] Z. Hadzi-Velkov, N. Zlatanov, T. Q. Duong, and R. Schober, "Rate maximization of decode-and-forward relaying systems with RF energy harvesting," *IEEE Commun. Lett.*, vol. 19, no. 12, pp. 2290–2293, Dec. 2015.

[48] M. Tian, W. Sun, L. Huang, S. Zhao, and Q. Li, "Joint beamforming and relay selection in AF two-way relay networks with energy transfer," *IEEE Syst. J.*, vol. 14, no. 2, pp. 2597–2600, Jun. 2020.

[49] X. Huang and N. Ansari, "Optimal cooperative power allocation for energy-harvesting-enabled relay networks," *IEEE Trans. Veh. Technol.*, vol. 65, no. 4, pp. 2424–2434, Apr. 2016.

[50] S. Luo, G. Yang, and K. C. Teh, "Throughput of wireless-powered relaying systems with buffer-aided hybrid relay," *IEEE Trans. Wireless Commun.*, vol. 15, no. 7, pp. 4790–4801, Jul. 2016.

[51] N. Zlatanov, D. W. K. Ng, and R. Schober, "Capacity of the two-hop relay channel with wireless energy transfer from relay to source and energy transmission cost," *IEEE Trans. Wireless Commun.*, vol. 16, no. 1, pp. 647–662, Jan. 2017.

[52] K. Xu, Z. Shen, Y. Wang, X. Xia, and D. Zhang, "Hybrid time-switching and power splitting SWIPT for full-duplex massive MIMO systems: A beam-domain approach," *IEEE Trans. Veh. Technol.*, vol. 67, no. 8, pp. 7257–7274, Aug. 2018.

[53] X. Xia, K. Xu, Y. Wang, and Y. Xu, "A 5G-enabling technology: Benefits, feasibility, and limitations of in-band full-duplex mMIMO," *IEEE Veh. Technol. Mag.*, vol. 13, no. 3, pp. 81–90, Sep. 2018.

[54] A. M. Fouladgar and O. Simeone, "On the transfer of information and energy in multi-user systems," *IEEE Commun. Lett.*, vol. 16, no. 11, pp. 1733–1736, Nov. 2012.

[55] B. Medepally and N. B. Mehta, "Voluntary energy harvesting relays and selection in cooperative wireless networks," *IEEE Trans. Wireless Commun.*, vol. 9, no. 11, pp. 3543–3553, Nov. 2010.

[56] Z. Ding *et al.*, "Application of smart antenna technologies in simultaneous wireless information and power transfer," *IEEE Commun. Mag.*, vol. 53, no. 4, pp. 86–93, Apr. 2015.

[57] S. Bi, C. K. Ho, and R. Zhang, "Wireless powered communication: Opportunities and challenges," *IEEE Commun. Mag.*, vol. 53, no. 4, pp. 117–125, Apr. 2015.

[58] D. Mishra and S. De, "Achievable throughput in relay-powered RF harvesting cooperative sensor networks," in *Proc. NCC*, Guwahati, India, Sep. 2016, pp. 1–6.

[59] H. Zhao, J. Liu, J. Wang, W. Guo, and Y. Tang, "Impacts of attenuators on analog self-interference cancellation in full duplex radios," in *Proc. IEEE GC Wkshps*, Dec. 2016, pp. 1–5.

[60] D. Kim, H. Lee, and D. Hong, "A survey of in-band full-duplex transmission: From the perspective of PHY and MAC layers," *IEEE Commun. Surveys Tut.*, vol. 17, no. 4, pp. 2017–2046, Feb. 2015.

[61] M. Heino *et al.*, "Recent advances in antenna design and interference cancellation algorithms for in-band full duplex relays," *IEEE Commun. Mag.*, vol. 53, no. 5, pp. 91–101, May 2015.

[62] E. Everett, A. Sahai, and A. Sabharwal, "Passive self-interference suppression for full-duplex infrastructure nodes," *IEEE Trans. Wireless Commun.*, vol. 13, no. 2, pp. 680–694, Feb. 2014.

[63] M. Duarte and A. Sabharwal, "Full-duplex wireless communications using off-the-shelf radios: Feasibility and first results," in *Proc. ASILOMAR*, Pacific Grove, CA, USA, Nov. 2010, pp. 1558–1562.

[64] M. Mikhael *et al.*, "An in-band full-duplex transceiver prototype with an in-system automated tuning for RF self-interference cancellation," in *Proc. 5GU*, Akaslompolo, Finland, Nov. 2014, pp. 110–115.

[65] H. Zhuang *et al.*, "Duplexer design and implementation for self-interference cancellation in full-duplex communications," in *Proc. EUSIPCO*, Budapest, Hungary, Aug. 2016, pp. 125–129.

[66] A. Masmoudi and T. Le-Ngoc, "Channel estimation and self-interference cancellation in full-duplex communication systems," *IEEE Trans. Veh. Technol.*, vol. 66, no. 1, pp. 321–334, Jan. 2016.

[67] J. R. Krier and I. F. Akyildiz, "Active self-interference cancellation of passband signals using gradient descent," in *Proc. IEEE PIMRC*, BLondon, UK, Aug. 2013, pp. 1212–1216.

[68] D. Korpi *et al.*, "Full-duplex mobile device: Pushing the limits," *IEEE Commun. Mag.*, vol. 54, no. 9, pp. 80–87, Sep. 2016.

[69] V. Tapio, M. Juntti, A. Pärssinen, and K. Rikkinen, "Real time adaptive RF and digital self-interference cancellation for full-duplex transceivers," in *Proc. ASILOMAR*, Pacific Grove, CA, USA, Nov. 2016, pp. 1558–1562.

[70] D. Liu, Y. Shen, S. Shao, Y. Tang, and Y. Gong, "On the analog self-interference cancellation for full-duplex communications with imperfect channel state information," *IEEE Access*, vol. 5, pp. 9277–9290, Jun. 2017.

[71] B. King, J. Xia, and S. Boumaiza, "Digitally assisted RF-analog self interference cancellation for wideband full-duplex radios," *IEEE Trans. Circuits Syst. II: Express Briefs*, vol. 65, no. 3, pp. 336–340, Mar. 2018.

[72] J. Tamminen *et al.*, "Digitally-controlled RF self-interference canceller for full-duplex radios," in *Proc. EUSIPCO*, Budapest, Hungary, Aug. 2016.

[73] T. Huusari *et al.*, "Wideband self-adaptive RF cancellation circuit for full-duplex radio: Operating principle and measurements," in *Proc. VTC Spring*, Glasgow, UK, May 2015, pp. 1–7.

[74] A. T. Le, L. C. Tran, X. Huang, and Y. J. Guo, "Analog least mean square loop with I/Q imbalance for self-interference cancellation in full-duplex radios," *IEEE Trans. Veh. Technol.*, vol. 68, no. 10, pp. 9848–9860, Oct. 2019.

[75] A. T. Le, L. C. Tran, X. Huang, Y. J. Guo, and L. Hanzo, "Analog least mean square adaptive filtering for self-interference cancellation in full duplex radios," *IEEE Wireless Commun.*, vol. 28, no. 1, pp. 12–18, Feb. 2021.

[76] D. Korpi, L. Anttila, V. Syrjälä, and M. Valkama, "Widely linear digital self-interference cancellation in direct-conversion full-duplex transceiver," *IEEE J. Sel. Areas Commun.*, vol. 32, no. 9, pp. 1674–1687, Sep. 2014.

[77] D. Korpi *et al.*, "Adaptive nonlinear digital self-interference cancellation for mobile inband full-duplex radio: Algorithms and RF measurements," in *Proc. GLOBECOM*, San Diego, CA, USA, Dec. 2015, pp. 1–7.

[78] V. Tapio and M. Sonkki, "Analog and digital self-interference cancellation for full-duplex transceivers," in *Proc.EW*, Oulu, Finland, May 2016, pp. 1–5.

[79] N. Li, W. Zhu, and H. Han, "Digital interference cancellation in single channel, full duplex wireless communication," in *Proc. WiCom*, Shanghai, China, Sep. 2012, pp. 1–4.

[80] D. Korpi, M. AghababaeeTafreshi, M. Piilila, L. Anttila, and M. Valkama, "Advanced architectures for self-interference cancellation in full-duplex radios: Algorithms and measurements," in *Proc. ASILOMAR*, Pacific Grove, CA, USA, Nov. 2016, pp. 1553–1557.

[81] L. Anttila, D. Korpi, V. Syrjälä, and M. Valkama, "Cancellation of power amplifier induced nonlinear self-interference in full-duplex transceivers," in *Proc. ASILOMAR*, Pacific Grove, CA, USA, Nov. 2013, pp. 1193–1198.

[82] M. S. Sim, M. Chung, D. K. Kim, and C.-B. Chae, "Low-complexity nonlinear self-interference cancellation for full-duplex radios," in *Proc. GC Wkshps*, Washington, DC, USA, Dec. 2016, pp. 1–6.

[83] D. Korpi *et al.*, "Digital self-interference cancellation under nonideal RF components: Advanced algorithms and measured performance," in *Proc. IEEE SPAWC*, Stockholm, Sweden, Jun. 2015, pp. 286–290.

[84] E. Ahmed, A. M. Eltawil, and A. Sabharwal, "Self-interference cancellation with phase noise induced ICI suppression for full-duplex systems," in *Proc. GLOBECOM*, Atlanta, GA, USA, Dec. 2013, pp. 3384–3388.

[85] Y. Liu, C. Guo, Z. Zeng, and D. Li, "The polarization-enabled digital self-interference cancellation scheme for the full duplex communication," in *Proc. WPMC*, Sydney, NSW, Australia, Sep. 2014, pp. 414–418.

[86] N. Phungamngern, P. Uthansakul, and M. Uthansakul, "Digital and RF interference cancellation for single-channel full-duplex transceiver using a single antenna," in *Proc. ECTI-CON*, Krabi, Thailand, May 2013, pp. 1–5.

[87] M. E. Knox, "Single antenna full duplex communications using a common carrier," in *Proc. WAMICON*, Cocoa Beach, FL, USA, Apr. 2012, pp. 1–6.

[88] D. Bharadia, E. McMilin, and S. Katti, "Full duplex radios," *SIGCOMM Comput. Commun. Rev.*, vol. 43, no. 4, pp. 375–386, Aug. 2013.

[89] K. Kwon, D. Hwang, H.-K. Song, and S. S. Nam, "Full-duplex with self-energy recycling in the RF powered multi-antenna relay channels," *IEEE Signal Process. Lett.*, vol. 26, no. 10, pp. 1516–1520, Oct. 2019.

[90] Y. Zeng and R. Zhang, "Full-duplex wireless-powered relay with self-energy recycling," *IEEE Wireless Commun. Lett.*, vol. 4, no. 2, pp. 201–204, Apr. 2015.

[91] Ö. T. Demir and T. E. Tuncer, "Optimum QoS-aware beamformer design for full-duplex relay with self-energy recycling," *IEEE Wireless Commun. Lett.*, vol. 7, no. 1, pp. 122–125, Feb. 2018.

[92] S. Xu, X. Song, Z. Xie, J. Cao, and J. Wang, "Secrecy transmission for self-energy recycling untrusted relay networks with imperfect channel state information," *IEEE Access*, vol. 7, pp. 169 724–169 733, Dec. 2019.

[93] D. Hwang, K. C. Hwang, D. I. Kim, and T.-J. Lee, "Self-energy recycling for RF powered multi-antenna relay channels," *IEEE Trans. Wireless Commun.*, vol. 16, no. 2, pp. 812–824, Feb. 2017.

[94] J. Qiao, H. Zhang, F. Zhao, and D. Yuan, "Secure transmission and self-energy recycling with partial eavesdropper CSI," *IEEE J. Sel. Areas Commun.*, vol. 36, no. 7, pp. 1531–1543, Jul. 2018.

[95] Z. Wang, X. Yue, and Z. Peng, "Full-duplex user relaying for NOMA system with self-energy recycling," *IEEE Access*, vol. 6, pp. 67 057–67 069, Dec. 2018.

[96] L. Zhang, Y. Cai, M. Zhao, B. Champagne, and L. Hanzo, "Nonlinear MIMO transceivers improve wireless-powered and self-interference-aided relaying," *IEEE Trans. Wireless Commun.*, vol. 16, no. 10, pp. 6953–6966, Oct. 2017.

[97] S. Yang, Y. Ren, G. Lu, and J. Wang, "Optimal resource allocation for full-duplex wireless-powered relaying with self-energy recycling," in *Proc. WCSP*, Xi'an, China, Oct. 2019, pp. 1–6.

[98] Ö. T. Demir and T. E. Tuncer, "Robust optimum and near-optimum beamformers for decode-and-forward full-duplex multi-antenna relay with self-energy recycling," *IEEE Trans. Wireless Commun.*, vol. 18, no. 3, pp. 1566–1580, Mar. 2019.

[99] H. Liu, K. J. Kim, K. S. Kwak, and H. Vincent Poor, "Power splitting-based SWIPT with decode-and-forward full-duplex relaying," *IEEE Trans. Wireless Commun.*, vol. 15, no. 11, pp. 7561–7577, Nov. 2016.

[100] M. H. N. Shaikh, V. A. Bohara, and A. Srivastava, "Performance analysis of a full-duplex MIMO decode-and-forward relay system with self-energy recycling," *IEEE Access*, vol. 8, pp. 226 248–226 266, Dec. 2020.

[101] A. El Shafie and N. Al-Dhahir, "Secure communications in the presence of a buffer-aided wireless-powered relay with self-energy recycling," *IEEE Wireless Commun. Lett.*, vol. 5, no. 1, pp. 32–35, Feb. 2016.

[102] Z. Wei, X. Zhu, S. Sun, Y. Jiang, A. Al-Tahmeesschi, and M. Yue, "Research issues, challenges, and opportunities of wireless power transfer-aided full-duplex relay systems," *IEEE Access*, vol. 6, pp. 8870–8881, Mar. 2018.

[103] V.-D. Nguyen, T. Q. Duong, H. D. Tuan, O.-S. Shin, and H. V. Poor, "Spectral and energy efficiencies in full-duplex wireless information and power transfer," *IEEE Trans. Commun.*, vol. 65, no. 5, pp. 2220–2233, Feb. 2017.

[104] X. Zhou, R. Zhang, and C. K. Ho, "Wireless information and power transfer: Architecture design and rate-energy tradeoff," *IEEE Trans. Commun.*, vol. 61, no. 11, pp. 4754–4767, Nov. 2013.

[105] J. Li, L. C. Tran, and F. Safaei, "Wireless information and power transfer using full-duplex self-energy recycling relays," *IEEE Access*, vol. 9, pp. 158 808–158 819, Nov. 2021.

[106] R. T. Behrens and L. L. Scharf, "Signal processing applications of oblique projection operators," *IEEE Trans. Signal Process.*, vol. 42, no. 6, pp. 1413–1424, Jun. 1994.

[107] D. W. K. Ng, E. S. Lo, and R. Schober, "Energy-efficient resource allocation in OFDMA systems with hybrid energy harvesting base station," *IEEE Trans. Wireless Commun.*, vol. 12, no. 7, pp. 3412–3427, Jul. 2013.

[108] T. Riihonen, S. Werner, and R. Wichman, "Hybrid full-duplex/half-duplex relaying with transmit power adaptation," *IEEE Trans. Wireless Commun.*, vol. 10, no. 9, pp. 3074–3085, Sep. 2011.

[109] E. Boshkovska, D. W. K. Ng, N. Zlatanov, and R. Schober, "Practical non-linear energy harvesting model and resource allocation for SWIPT systems," *IEEE Commun. Lett.*, vol. 19, no. 12, pp. 2082–2085, Dec. 2015.

[110] B. Clerckx *et al.*, "Fundamentals of wireless information and power transfer: From RF energy harvester models to signal and system designs," *IEEE J. Sel. Areas Commun.*, vol. 37, no. 1, pp. 4–33, Jan. 2019.

[111] E. Khorov, A. Kiryanov, A. Lyakhov, and G. Bianchi, "A tutorial on IEEE 802.11ax high efficiency WLANs," *IEEE Commun. Surveys Tuts.*, vol. 21, no. 1, pp. 197–216, 1st Quart. 2019.

[112] S. S. Das, E. D. Carvalho, and R. Prasad, "Variable sub-carrier bandwidths in OFDM systems," in *Proc. IEEE VTC*, Dublin, Leinster, Ireland, Apr. 2007, pp. 1866–1870.

[113] S. Kurt and B. Tavli, "Path-loss modeling for wireless sensor networks: A review of models and comparative evaluations.," *IEEE Antennas Propag. Mag.*, vol. 59, no. 1, pp. 18–37, Feb. 2017.

[114] C. K. Ho and R. Zhang, "Optimal energy allocation for wireless communications with energy harvesting constraints," *IEEE Trans. Signal Process.*, vol. 60, no. 9, pp. 4808–4818, Sep. 2012.

[115] C. C. Y. Poon, B. P. L. Lo, M. R. Yuce, A. Alomainy, and Y. Hao, "Body sensor networks: In the era of big data and beyond," *IEEE Reviews Biomedical Eng.*, vol. 8, pp. 4–16, Aug. 2015.

[116] I. S. Gradshteyn and I. M. Ryzhik, *Table of integrals, series, and products*, 5th ed. Academic press, Inc., 1996.

[117] B. Varghese, N. E. John, S. Sreelal, and K. Gopal, "Design and development of an RF energy harvesting wireless sensor node (EH-WSN) for aerospace applications," *Procedia Comput. Sci.*, vol. 93, pp. 230–237, Aug. 2016.

[118] A. T. Le, L. C. Tran, X. Huang, Y. J. Guo, and J. Y. C. Vardaxoglou, "Frequency-domain characterization and performance bounds of ALMS loop for RF self-interference cancellation," *IEEE Trans. Commun.*, vol. 67, no. 1, pp. 682–692, Jan. 2019.

[119] L. C. Tran, T. A. Wysocki, A. Mertins, and J. Seberry, "A generalized algorithm for the generation of correlated rayleigh fading envelopes in wireless channels," *EURASIP J. Wireless Commun. Networking*, vol. 2005, no. 5, pp. 801–815, Oct. 2005.

[120] N. P. Le, L. C. Tran, and F. Safaei, "Energy-efficiency analysis of per-subcarrier antenna selection with peak-power reduction in MIMO-OFDM wireless systems," *Int. J. Antennas Propag.*, vol. 2014, pp. 1–13, Jun. 2014.

[121] L. C. Tran, A. Mertins, and T. A. Wysocki, "Quasi-orthogonal space-time-frequency codes in MB-OFDM UWB," *Comput. Electr. Eng.*, vol. 36, no. 4, pp. 766–774, Jul. 2010.

[122] L. C. Tran, A. Mertins, and T. A. Wysocki, "Unitary differential space-time-frequency codes for MB-OFDM UWB wireless communications," *IEEE Trans. Wireless Commun.*, vol. 12, no. 2, pp. 862–876, Feb. 2013.

[123] Z. Ding and H. V. Poor, "Cooperative energy harvesting networks with spatially random users," *IEEE Signal Process. Lett.*, vol. 20, no. 12, pp. 1211–1214, Dec. 2013.

[124] J. Men and J. Ge, "Non-orthogonal multiple access for multiple-antenna relaying networks," *IEEE Commun. Lett.*, vol. 19, no. 10, pp. 1686–1689, Aug. 2015.

[125] J. Lee and N. Al-Dhahir, "Exploiting sparsity for multiple relay selection with relay gain control in large AF relay networks," *IEEE Wireless Commun. Lett.*, vol. 2, no. 3, pp. 347–350, Apr. 2013.